BACTERIAL CULTIVATION IN MICROSCALE DROPS AND CAPSULES TO RESOLVE SINGLE-CELL GROWTH PHYSIOLOGY

by

Shawna Leigh Pratt

A dissertation submitted in partial fulfillment
of the requirements for the degree

of

Doctor of Philosophy

in

Chemical Engineering

MONTANA STATE UNIVERSITY
Bozeman, Montana

May 2023

DEDICATION

Dedicated to Matthias, Elsa, Harper, and Heidi. You make my world so bright!

ACKNOWLEDGEMENTS

George, thank you for all of it. You are the light at the end of the tunnel, every single day. Thanks for letting me share my science with you. Mom and Dad, thank you for supporting me. Thank you for always answering the phone, for filling our fridge and freezers, and for showing up to do a year's worth of housework in a weekend. Connie, thank you for believing in me, challenging me, and giving me room to grow. Thank you for helping me find this path, and for never leaving my cheering section. I will miss having you be such a big part of my life.

Hannah and Calvin, thank you for being our Bozeman family. Jake, Carter, Humberto, Mallory, Travis, Emma, and Dimitri; I am so lucky to have been part of such a close-knit lab. Thank you to Tats, Mike, and Kerry, for including me as an honorary lab-mate. Thank you to the in-law lab: Isaak Thornton, Reha Abassi, Barkan Sidar, and Jim Wilking. I enjoyed working with you all so much! I am so grateful that we all ended up here, on this path, all at the same time.

Thank you to my mentors and not-yet mentioned members of my committee: Christine, Abbie, Jeff, Sweeney, Ross, Matthew and Ryan. Thank you for helping teaching me how to do this sometimes very hard thing, and for encouraging and supporting me along the way. Thank you for always lending me your ear and treating me with grace.

Thank you to the CBE and to the CBE family. Kristen, Heidi, and Betsey, I admire the way you carry yourselves in this type of work and am thankful for the opportunity to learn from and work with you. Sarah (Huth) and Kristen (Griffin), thank you for being helpful and encouraging resources. To all the of the CBE faculty: thank you for keeping open doors, sharing your work and ideas, and generating a sense of camaraderie and family. I learned so much from being here. And finally, thank you to Marilyn Delger. You rock. Go P.E.O.!

TABLE OF CONTENTS

TABLE OF CONTENTS CONTINUED

TABLE OF CONTENTS CONTINUED

TABLE OF CONTENTS CONTINUED

LIST OF TABLES

Table Page

LIST OF FIGURES

Figure Page

LIST OF FIGURES CONTINUED

Figure Page

ABSTRACT

Single-cell heterogeneity contributes to the complex population dynamics of infectious microbial communities. Improving our understanding of single-cell physiology and heterogeneity may aid in mitigating microbial infections; however, assaying large populations of single cells can be challenging. Despite recent developments in single-cell assaying, tracking the physiology of large numbers of individual cells and their lineages over time is difficult to achieve using current technologies. Here, I apply drop-based microfluidics to develop microscale tools for improving high-throughput single-cell microbial growth assays. Drop-based microfluidics is a technology that generates and manipulates microscale drops. In this work, I create water-in-oil drops and hydrogel-shelled microcapsules using drop-based microfluidics to study the growth of *P. aeruginosa* bacteria, a key pathogen implicated in chronic lung infections and wounds. The growth of single bacterial cells inside drop microcompartments is observed via time-lapse confocal microscopy. Bacteria were cultured in water-in-oil drops and prepared for long-term storage in a novel microfluidic device environment, which we call a DropSOAC (Drop Stabilization on a Chip) chamber. The DropSOAC method prevents drop destabilization by saturating microfluidic devices with equilibrated water and oil, maintaining phase equilibrium in the drop emulsion. Using DropSOAC, the single-cell growth of starved *P. aeruginosa* wildtype and hibernation promotion factor mutants were characterized, revealing significant growth heterogeneity in the mutant strain. Finally, we present a method for generating hydrogel-shelled microcapsules that enables the culturing of single cells in microscale environments where nutrients and waste can diffuse in and out of the microculture environment. A 3-D microfluidic device and capsule generation protocol are designed, resulting in an optimized approach for capsule production using phase-separating polymer systems and rapid hydrogel crosslinking. The growth of hundreds of individual *P. aeruginosa* cells is observed over time with the hydrogel-shelled microcapsules. Due to the permeability of the microcapsules, antibiotics can be introduced at various times during growth to investigate single and biofilm *P. aeruginosa* physiology. Overall, this work introduces novel approaches for high-throughput, single-cell microbial growth characterization that enables a deeper understanding of the role of heterogeneity in bacterial populations.

CHAPTER ONE

INTRODUCTION

Single-cell heterogeneity contributes fitness advantages to bacterial populations, which, in the case of chronic infections, can decrease treatment efficacy. Understanding single-cell physiology and heterogeneity requires assaying large populations of single cells. Recently, the application of single-cell resolved assays has increased. However, high-throughput, single-cell growth assays remain underdeveloped, primarily because understanding growth dynamics requires the ability to track cells over time. The presented body of work adapts drop-based microfluidic approaches to establish and improve high-throughput single-cell microbial growth assays using microscale drops and capsules. These advancements were applied to study *Pseudomonas aeruginosa,* a key pathogen in chronic lung infections.

Funding and Collaborations

Research funding was supplied by NSF-EPSCOR 1736255 (Dr. Connie Chang, Co-I), NSF-CAREER 1753352 (Connie Chang, PI), and the Montana State University Thermal Biology Institute. Personal financial support for Shawna Pratt was provided by Montana IDeA Networks of Biomedical Research Excellence (INBRE), a Norm Asbjornson College of Engineering (NACOE) Raymond E. and Erin S. Schultz Emerging Fellows Award, and a Philanthropic Educational Organization (PEO) Scholars Fellowship. Work was done in collaboration with Dr. Michael Franklin's lab group in Microbiology and Cell Biology at Montana State University. Specific collaborators from Dr. Franklin's lab were Dr. Tatsuya Akiyama and Kerry Williamson. Research was conducted in Montana State University's Chemical and Biological Engineering

Department, the Center for Biofilm Engineering (CBE), and Montana Nanotechnology Facilities. The Murdoch Charitable Fund financially supports the CBE microscopy resources used in this work. Assistance was provided by Dr. Heidi Smith, the CBE Microscopy Facilities Manager, Betsey Pitts, the retired CBE Microscopy Facilities Manager, and Dr. Kristen Brileya, the CBE operations manager.

Dissertation Outline

Four chapters and a series of appendices comprise the remainder of this dissertation. Chapter 2 discusses the importance of single-cell research in the chronic infection problem, and the potential for drop-based microfluidics as a tool for single-cell research. Chapter 3 presents a method for stabilizing microfluidic drops for time-lapse microbial incubation and its application to characterizing heterogeneity in starved *P. aeruginosa* populations. Chapter 4 presents a method for generating hydrogel-shelled capsules for bacterial cultivation, and the application of these capsules to study the effect of antibiotic dosage timing. Chapter 5 summarizes these research products in the broad scope of single-cell microbial assays. The body of this dissertation is followed by an appendix comprised of four sections labeled A-D. These sections include (A) a co-author publication [1] that used the method described in Chapter 3 to investigate the role of hibernation promotion factor in *P. aeruginosa* dormancy; (B) the evolution of the incubation chamber designed initially in Chapter 3; (C) supporting information for Chapter 4; and, (D) an unpublished investigation into electrophoretic alginate disintegration.

Chapter 2: "Drop-Based Microfluidic Approaches for Chronic Infection Research"

Chapter overview: "My dissertation encompasses the development of microscale microbial cultivation tools using drop-based microfluidics. These tools aim to resolve single-cell growth physiology and population heterogeneity. The presented advancements to single-cell cultivation were motivated by the study of pathogens in chronic infections, focusing on *Pseudomonas aeruginosa*. Here [in Chapter 2], I provide context for the chronic infection problem, single-cell studies, and the application of drop-based microfluidics to single-cell microbial research."

Chapter 3 "DropSOAC: Stabilizing Microfluidic Drops for Time-Lapse Quantification of Single-Cell Bacterial Physiology

Chapter abstract: "The physiological heterogeneity of cells within a microbial population imparts resilience to stresses such as antimicrobial treatments and nutrient limitation. This resilience is partially due to a subpopulation of cells that can survive such stresses and regenerate the community. Microfluidic approaches now provide a means to study microbial physiology and bacterial heterogeneity at the single-cell level, improving our ability to isolate and examine these subpopulations. Drop-based microfluidics provides a high-throughput approach to study individual cell physiology within bacterial populations. Using this approach, single cells are isolated from the population and encapsulated in growth medium dispersed in oil using a 15 μm diameter drop making microfluidic device. The drops are arranged as a packed monolayer inside a polydimethylsiloxane (PDMS) microfluidic device. Growth of thousands of individual cells in identical microenvironments can then be imaged using confocal laser scanning microscopy (CLSM). A challenge for this approach has been the maintenance of drop stability during

extended time-lapse imaging. In particular, the drops do not maintain their volume over time during incubation in PDMS devices, due to fluid transport into the porous PDMS surroundings. Here [in Chapter 3], we present a strategy for PDMS device preparation that stabilizes drop position and volume within a drop array on a microfluidic chip for over 20 h. The stability of water-in-oil drops is maintained by soaking the device in a reservoir containing both water and oil in thermodynamic equilibrium. This ensures that phase equilibrium of the drop emulsion fluids within the porous PDMS material is maintained during drop incubation and imaging. We demonstrate the utility of this approach, which we label DropSOAC (Drop Stabilization On A Chip), for time-lapse studies of bacterial growth. We characterize growth of *Pseudomonas aeruginosa* and its Δ*hpf* mutant derivative during resuscitation and growth following starvation. We demonstrate that growth rate and lag time heterogeneity of hundreds of individual bacterial cells can be determined starting from single isolated cells. The results show that the DropSOAC capsule provides a high-throughput approach toward studies of microbial physiology at the single cell level and can be used to characterize physiological differences of cells from within a larger population." [1]

Chapter 4: Hydrogel-shelled microcapsules enable permeable, single-cell bacterial culturing

Chapter abstract: Cell-level heterogeneity within microbial populations contributes to fitness advantages that make pathogenic microbial communities, like those involved in chronic infections, harder to treat. Identifying and understanding cell-level heterogeneity requires single-cell resolved studies. Drop-based microfluidics provides a powerful tool for high throughput single cells isolation and assay, but there is still room to improve this technology; One challenge is the difficulty of conducting multi-step assays in a drop format due to the fragility and aqueous

impermeability of a drop's oil/water interface. This limitation makes replicating chronic infection-relevant processes, like antibiotic dosing, challenging in a water-in-oil drop-based platform. Here, we introduce multi-step capabilities to microfluidic single-cell cultivation and growth characterization by generating hydrogel-shelled capsules (figure 1). This new capsule generation approach is summarized as the BioFlex method and relies on non-planar microfluidic device design, nanoemulsion-based crosslinker delivery, and manipulating an aqueous two-phase system. The Bioflex method produces permeable, biocompatible, and adjustable hydrogel-shelled microcapsules developed specifically for single-cell microbial isolation and cultivation. The resulting capsules enable longitudinal single-cell resolved microbial cultivation with transient chemical conditions, broadening single-cell studies to systems requiring complex, time-varied parameters, which is demonstrated here through an assay measuring changes in the effect of ciprofloxacin on *Pseudomonas aeruginosa* depending on ciprofloxacin dosage timing. By developing this method, we have provided microbiologists with a high-throughput single-cell cultivation platform compatible with multi-step cultivation processes. More broadly, we have generated an optimized capsule generation method primed for implementation throughout biology.

Chapter 5: Conclusion

Chapter introduction: "In this dissertation conclusion, the research aim addressed by this body of work is reintroduced and compared to the outcomes of the presented body of work. Next, the broader contributions of this work, categorized as tools, techniques, and the advancement of fundamental knowledge in microfluidics, are presented. A discussion of the limitations of the work, and suggestions for addressing these limitations, follows the contribution

section. Before concluding this dissertation, I present a broader challenge for the continued development of single-cell microfluidic assays, and discuss potential approaches for addressing this challenge. Finally, I conclude the dissertation by highlighting the overarching achievements of this work."

CHAPTER TWO

DROP-BASED MICROFLUIDIC APPROACHES FOR CHRONIC INFECTION RESEARCH

Overview

My dissertation encompasses the development of microscale microbial cultivation tools using drop-based microfluidics. These tools aim to resolve single-cell growth physiology and population heterogeneity. The presented advancements to single-cell cultivation were motivated by the study of pathogens in chronic infections, focusing on the *Pseudomonas aeruginosa.* Here, I provide context for the chronic infection problem, single-cell studies, and the application of drop-based microfluidics to single-cell microbial research.

Chronic Infections and *P. aeruginosa*

Costs of chronic infections

Chronic bacterial infections are long-term infections characterized by continuous inflammation, tissue damage, and unresponsiveness to host immunity and medical intervention [2]. Chronic infections encompass chronic wounds, including diabetic foot ulcers and venous leg ulcers [3]; infections in internal bodily systems, such as chronic lung infections [4] and chronic sinusitis [5]; and medical device-associated infections [6], such as periprosthetic joint infections [7].

Chronic infections significantly impact sufferers' quality of life and increase the likelihood of mortality and life-changing medical interventions such as amputation and long-term hospitalization [8-10]. These infections largely impact vulnerable subpopulations, including

older people, the immunocompromised, and those with chronic diseases [11, 12]. Recently, a meta-analysis synthesizing the impacts of chronic wounds identified reduced health-related quality of life (HRQoL) across functional, symptomatic, and mental health aspects. In fact, the degree of HRQoL loss associated with chronic wounds was comparable to chronic obstructive pulmonary disease (COPD) and cardiovascular disease [8], which are recognized as high-suffering diseases[13, 14]

Chronic wounds have tangible societal effects, accruing $18B in healthcare costs, 2M sufferers, and 200K deaths in the United States annually[15]. Like chronic wounds, other types of chronic microbial infections have reduced quality of life and increased economic burden and mortality [4, 16]. These characteristics are expected to increase with the continued rise of antimicrobial-resistant microorganisms [17].

Biofilms in chronic infections

The majority of chronic infections are the result of microbial biofilms[15, 18]. The term "biofilm" describes densely aggregated microbial communities bound by extracellular matrix [19]. Traditionally, biofilms were defined by surface association, for instance, biofilm infections on the surface of medical implants. However, many have recently included free-floating aggregates, like those that form in mucous, as a biofilm, expanding the definition to all instances of matrix-bound, aggregated cells [20]. A biofilm community is heterogeneous in structure, chemical environment, and physiology [19, 21]. The phenotypic heterogeneity observed in biofilms is understood to arise from stochastic and strategic variations in gene expression, genetic mutation, and response to spatio-chemical diversity within the biofilm [19] (Figure 1).

A biofilm's complex phenotypic portfolio and the protection of extracellular matrix confer significant fitness advantages. Biofilms have broadly enhanced resistance to factors including antimicrobial treatment[15] and environmental stresses such as oxidation and nutrient limitation[22]. These traits hinder the effective treatment of chronic infections caused by microbial biofilms. Additionally, competitive inter-cellular interactions in biofilms can increase the virulence of biofilm infections by producing antagonistic molecules [23, 24]. The mechanisms underlying these biofilm-associated advantages and virulence traits are of intense interest to researchers hoping to understand and effectively treat biofilm-based chronic infections.

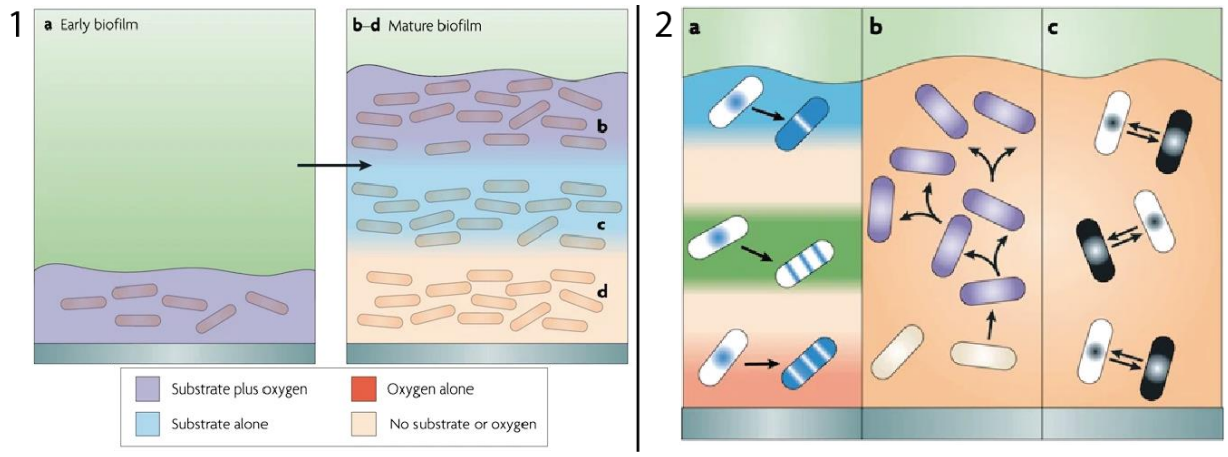

Figure 1: Chemical and physiological heterogeneity in biofilms, adapted from *Physiological heterogeneity in biofilms*, by Stewart and Franklin [19]. Panel 1: Biofilms and characteristic biofilm chemical gradients develop simultaneously as bacteria consume substrates and diffusion driven transport limits molecular movement. (1a) The early biofilm contains a homogenously oxygen- and substrate-rich environment. (1b) In the mature biofilm, an -oxic, nutrient-rich region exists near the biofilm surface. Deeper into the biofilm, oxygen is consumed, leaving just substrate. Even deeper in the biofilm (1c), there may be no remaining substrate or oxygen, just cells suspended in biofilm matrix. Panel2: Physiological heterogeneity can be the result of (2a) response to a heterogeneous chemical environment, (2b) genetic mutation giving rise to genetic variants, and (2c) stochastic, or random, phenotype expression.

Pseudomonas aeruginosa

Pseudomonas aeruginosa (P. aeruginosa) is an opportunistic pathogen prevalent in chronic lung infections, especially those with comorbid cystic fibrosis (CF) and chronic obstructive pulmonary disease (COPD)[25, 26]. *P. aeruginosa* is a gram-negative, rod-shaped, flagellated bacterium capable of producing biofilm-forming extracellular compounds [27, 28]. Additionally, *P. aeruginosa* possesses a diverse, adaptable metabolism as a facultative anaerobe capable of consuming both simple and complex carbon substrates [27, 29] and produces many virulence factors that impact the outcomes of human infections. Many of these factors were evolved for competition in the non-human environment; Examples include type VI secretion systems and the production of pyocyanin, rhamnolipids, and siderophores, which target other organisms found in *P. aeruginosa* compatible environments [30] (Figure 2).

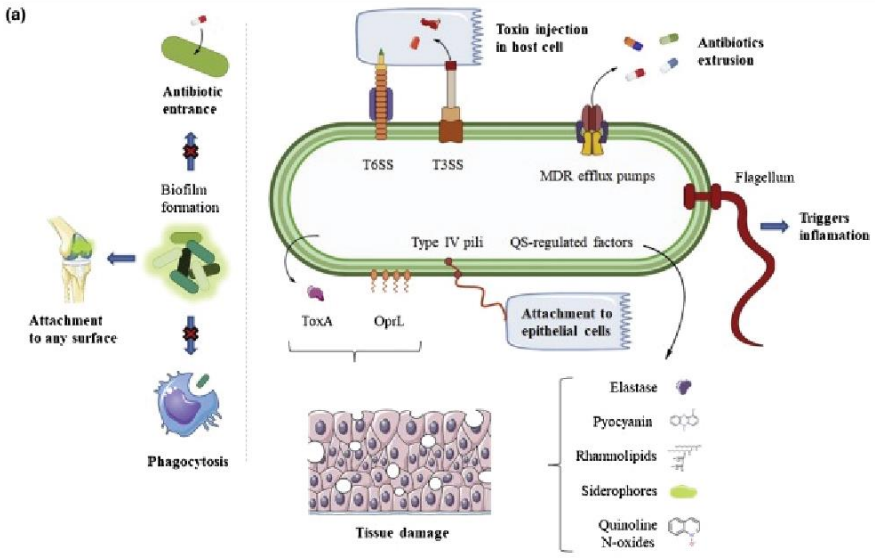

Figure 2: Diverse pathogenicity and virulence factors for *P. aeruginosa*, from *Pseudomonas aeruginosa*: an antibiotic resilient pathogen with an environmental origin, by Laborda et al.[30]. (a) Host immune response and treatment efficacy is reduced for *P. aeruginosa* biofilms, which readily form in the human body. (b) *P. aeruginosa* produces many antagonistic factors adapted for bacterial warfare that enhance the virulence of *P. aeruginosa* in the context of human infection. In addition to these factors, *P. aeruginosa* has other fitness advantages that increase chronicity, such as pili that enable surface attachment, initiating biofilm formation [31] and antibiotic efflux pumps, which are an adaptation related to multi-drug resistance[32].

P. aeruginosa's ability to acquire multidrug resistance exacerbates *P. aeruginosa* infection risks. Antibiotic resistance in *P. aeruginosa* is linked to the production of antibiotic degrading enzymes, ability to incorporate new genetic material, cell surface structure, topoisomerase modification, and the ability to upregulate efflux pumps [32]. The Centers for Disease Control (CDC) estimates that multidrug-resistant *P. aeruginosa* infections resulted in 32,600 hospitalizations, 2,700 deaths, and $767 M in healthcare costs in 2017 alone [25]. These traits have earned *P. aeruginosa* a "serious threat" designation by the CDC [25] and a "critical priority" designation by the World Health Organization [33]. Together, the demonstrated

healthcare costs, biofilm-forming capabilities, and multidrug resistance acquisition make the study of *P. aeruginosa* an essential aspect of infectious disease research [25, 33].

Single-cell studies

The proposed role of heterogeneity in biofilm fitness [19] and the ubiquity of biofilms in chronic infections [15] highlights the importance of understanding the subgroups present in biofilm populations. Single-cell studies, which can observe and characterize physiology and phenotype at the cell level, allows subpopulation identification and characterization, which are steps towards understanding subpopulation roles [34]. The scientific community is already aware of several single cell phenomena that enhance virulence or chronicity, such as persister phenotypes [35], metabolic cooperativity [36], bet-hedging [37], and strain differentiation [38, 39]. This realization poses important questions: How many more phenomena might we find with additional single-cell methods and the broader application of single cell studies, and how might understanding these phenomena change our ability to treat chronic infections, especially in the face of increasing antibiotic resistance.

Drop-based Microfluidics in Single-Cell Research

Drop-based microfluidics

Drop-based microfluidics is a useful technology for exploring microbial populations with single-cell resolution[40-42]. Drop-based microfluidics allows users to produce microscale liquid drops that are the same length scale as the microorganisms themselves, approximately 10-100 μm in diameter, that can be used to encapsulate the microorganisms for assaying. The application of drop-based microfluidics to single-cell biology research includes cultivation and

evolution [1, 43, 44], sorting and selection [45, 46], and RNA- or DNA-sequencing [47]. Drop-based microfluidic workflows rely on effective microfluidic device design and fabrication, device operation, and fluid formulations, all of which are tunable over a wide parameter space for per-application optimization. Drop-based microfluidic devices are built from microscale channels and junctions. More complex devices incorporate features such as valves and chambers [48]. Microfluidic devices are commonly fabricated using polydimethylsiloxane (PDMS) or, less commonly, glass, resins, and thermoplastics [49]. Hydrophobic or hydrophilic treatments can be applied to microfluidic device channel surfaces to control surface wettability and fine-tune fluid behavior within devices.

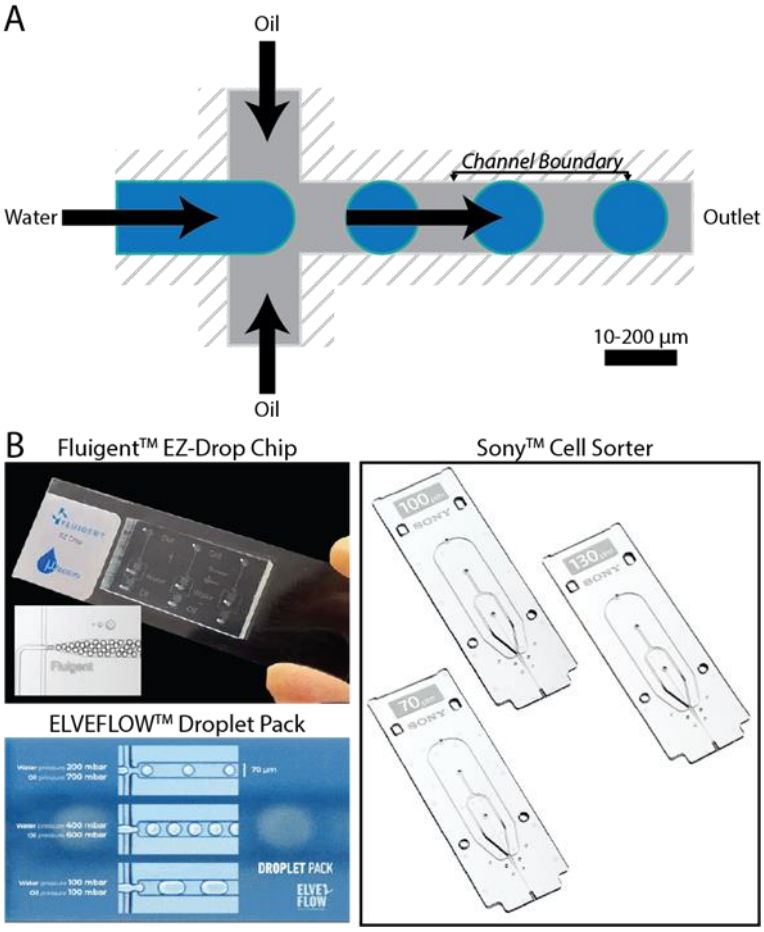

Figure 3: Description and commercial applications of flow-focusing junctions. A. The geometry of a flow-focusing junction resembles a 4-way intersection and uses fluid shear to produce drops, B. Commercial products use flow-focusing junctions, including (clockwise) Fluigent, Sony, and ELVEFLOW. Product images are collected from the respective company websites.

Microfluidic processes rely on controlled fluid flow through device channels. The flow is characteristically uniaxial and laminar [50, 51]. The first step of most drop-based microfluidic experiments is drop-generation. A dominant and commercialized method for producing drops (Figure 3B) used in this work is flow-driven droplet generation using a flow-focusing drop generation junction[1, 43, 52, 53]. This junction can be visualized as a microscale 4-way intersection (Figure 3A). To make water drops suspended in oil using a flow-focusing junction, a

single water channel and two oil channels flow into the intersection from the left and top/bottom, respectively, and converge as they flow out through the right side of the 4-way intersection (Figure 1). As the fluids converge, the water stream breaks into drops in a spontaneous process that evolves from Plateau-Rayleigh instabilities [54] (Figure 2A). Fluid flow regimes at the flow-focusing junction can be categorized as dripping or jetting, and designation in one or the other regime is predicted by the relationship between the fluid flow's Capillary (Ca) and Weber (We) numbers (Figure 2B):

$$\text{Capillary number: } Ca = \frac{\mu v}{\sigma}$$

$$\text{Weber number: } We = \frac{\rho v^2 l}{\sigma}$$

Where μ is viscosity, v is the fluid velocity, σ is surface tension, ρ is density, and l is length. Drops formed in the dripping regime are highly monodisperse, meaning 'of consistent size' for a certain population of drops [54] (Figure 2C). In practice, tuning the fluid flow rate and channel size controls drop size and production rate; microfluidic drops are generally 10-500 μm in diameter and produced at rates of hundreds to thousands per second.

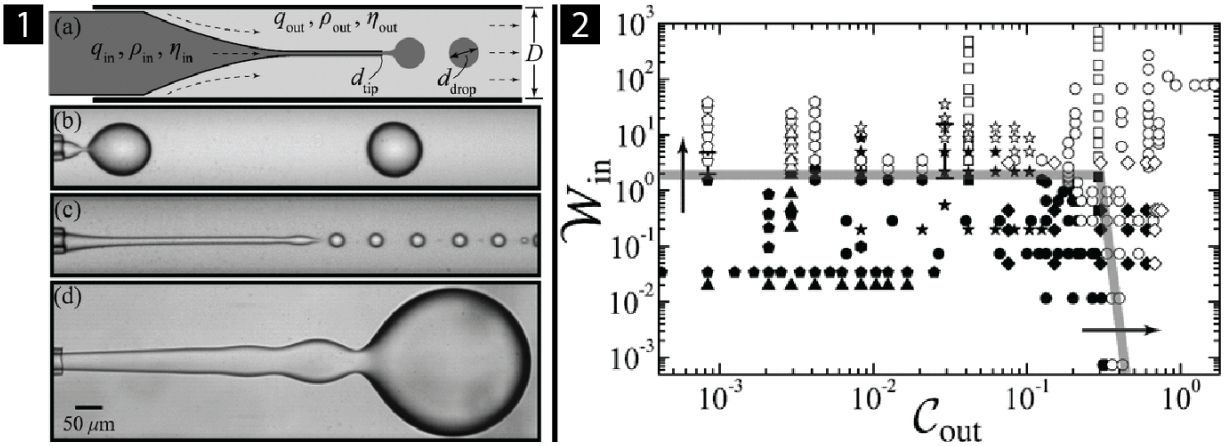

Figure 4: Dynamics of droplet breakup and distinction between the dripping and jetting drop-generation regimes, adapted from *Dripping to Jetting Transitions in Coflowing Liquid Streams* by Utada et al.[54] 1. Drop breakup occurs due to Plateau-Rayleigh instabilities, an energy-minimizing process related to surface tension and the ratio of surface area to volume. In a fluid stream, a Plateau-Rayleigh instability manifests as oscillations in the fluid stream's width that become increasingly extreme until the stream breaks into droplets. (1a) Here, droplet breakup in a glass capillary microfluidic device is represented. (1b) Under particular fluid flow dynamics, droplet breakup occurs at the nozzle orifice (glass capillary devices) or the droplet breakup junction (PDMS devices- not shown). This droplet breakup dynamic is described as the "dripping regime" and results in relatively more monodisperse droplets. (1c) Droplet breakup of a fluid stream away from the nozzle orifice or droplet breakup junction is described as the "jetting regime" and results in relatively less monodisperse droplets. (1d) Drop size and drop breakup regime can be modified and tuned by fluid flow, among other factors like device design and fluid characteristics. (2) The ratio between continuous phase Capillary (C_{out}) and disperse phase Weber (W_{in}) numbers can be used to predict whether droplet generation is in the dripping or jetting regimes. Experimental data corresponding to dripping and jetting regimes are shown in solid black and black-outlined/white-centered symbols, respectively.

In drop-based microfluidics, water-in-oil drops are referred to as a single emulsion, i.e., a single dispersed phase suspended in a continuous phase[55]. The same emulsion building blocks of water and oil can also be used to make higher-order emulsions, i.e., emulsions where each drop contains multiple phases[55]. Higher-order emulsions are made using similar, but slightly more complex, devices than planar flow-focusing junctions [56]. An adaptation of higher-order

liquid-in-liquid emulsion generation is used to make the hydrogel capsules discussed later in this background and at length in Chapter 4. Regardless of the drop-formation method or complexity of the drop particle, microfluidic drop emulsions are stabilized against coalescence by surfactants[57]. These molecules locate at the interface between two phases, which reduces the surface tension between the phases and stabilizes the water-oil interface.

A key result of microfluidic drop production is the high-throughput production of monodisperse, microscale "test tubes" and cultivation compartments. To grow bacteria in drops, cells and media-in-oil drops are produced using the above-described drop-generation method with biocompatible oils and surfactants; manipulating the concentration of cells in the aqueous phase controls the number of cells encapsulated in each drop to achieve single-cell isolation[42]. The drops are incubated in a bulk vessel, i.e., a microcentrifuge tube [43] or in microfluidic compartments and arrays[1, 43]. This basic process is used in Chapter 3 and many other microfluidic studies [40-42, 45, 58].

Hydrogel microparticles for single-cell studies and biological assays

The adaptation of microfluidic water-in-oil drop production into a method for growing cells in hydrogel microparticles was pioneered in mammalian cell biology research[59-61]. Previous work demonstrated that microscale hydrogels provide a useful alternative to water-in-oil drops. Hydrogel advantages are that hydrogels provide the structure necessary for anchorage-dependent cell lines and facilitate the aqueous transport of solutes, which, for instance, enables "passaging," a required step in many mammalian culture protocols where new, fresh media replaces spent media [61-63]. Chapter 4 adapts microfluidically-produced hydrogel capsules for

microbial cell culture for the same hydrogel-related advantages that enable passaging, i.e., the transport of aqueous solutes through hydrogels.

Hydrogels are produced by crosslinking or changing the conformation of aqueously dissolved polymers (hydrogel precursor) so that the polymers form a gel matrix. Examples of hydrogel-forming polymers include alginate and gelatin. Hydrogel precursor-in-oil drops are made instead of water-in-oil drops to make hydrogel particles [64]; these approaches can also be adapted to make higher-order hydrogel particles [61, 65-70]. Cells are included in the hydrogel precursor for cell encapsulation applications. After forming drops, a gelation agent is introduced or released in the system, and the hydrogel precursor solidifies. Gelation agents can include photoillumination[66], a temperature change[64], or the addition of a chemical crosslinker[69]. After the hydrogel has gelled, the hydrogel-in-oil emulsion is "broken" either by adding a chemical emulsion disruptor[71] or by diluting out surfactant[65]. The hydrogel particles and oil are then separated, and the hydrogel particles are resuspended in an aqueous solution; this solution is often media for hydrogel-based cell culture. Following the capsule production and washing process, hydrogel microparticles are ready for incorporation into biological assays.

Broadening drop-based approaches in microbial research

Chronic infections, and *P. aeruginosa* in particular, pose significant challenges to our healthcare today with the increased development of antibiotic resistance. A significant aspect of microbial physiology that makes infections more challenging to treat is cell-level phenotypic heterogeneity, a hallmark of biofilms. To study cell-level heterogeneity, the research community needs tools that can isolate single cells, and drop-based microfluidics is one of these tools. The remainder of this dissertation summarizes my efforts to improve and adapt drop-based

microfluidics approaches to answer questions about heterogeneity within *P. aeruginosa* populations. Broadly, these advancements enabled the long-term, monitored cultivation of bacterial cells in drops and multi-step cultivation of bacteria in hydrogel capsules, both of which resulted in the characterization of single-cell physiology in response to nutrient limitation (Chapter 3 [1, 43]) and antimicrobial treatment (Chapter 4).

CHAPTER THREE

DROPSOAC: STABILIZING MICROFLUIDIC DROPS FOR TIME-LAPSE QUANTIFICATION OF SINGLE-CELL BACTERIAL PHYSIOLOGY

Contribution of Authors and Co-Authors

Manuscript in Chapter 3

Author: Shawna L. Pratt

Contributions: Shawna Pratt designed all studies, conducted laboratory experiments, analyzed all data, and wrote the manuscript.

Co-Author: Geoffrey K. Zath

Contributions: Geoffrey Zath helped to analyze single-cell growth data.

Co-Author: Tatsuya Akiyama

Contributions: Tatsuya Akiyama assisted in bacterial study design and conducting experiments.

Co-Author: Kerry S. Williamson

Contributions: Kerry Williamson contributed to bacterial study design, conducting experiments, and manuscript editing.

Co-Author: Michael J. Franklin

Contributions: Michael Franklin contributed to the study design and manuscript writing.

Co-Author: Connie B. Chang

Contributions: Connie Chang contributed to the study design and manuscript writing and was the principal investigator or co-principal investigator on grants funding this work.

Manuscript Information

Shawna L. Pratt, Geoffrey K. Zath, Tatsuya Akiyama, Kerry S. Williamson, Michael J. Franklin, Connie B. Chang.

Frontiers in Microbiology

Status of Manuscript:

_____ Prepared for submission to a peer-reviewed journal

_____ Officially submitted to a peer-reviewed journal

_____ Accepted by a peer-reviewed journal

__X__ Published in a peer-reviewed journal

Frontiers in Microbiology

September 24, 2019

DOI 10.3389

frontiers in Microbiology

METHODS
published: 24 September 2019
doi: 10.3389/fmicb.2019.02112

DropSOAC: Stabilizing Microfluidic Drops for Time-Lapse Quantification of Single-Cell Bacterial Physiology

*Shawna L. Pratt[1,2], Geoffrey K. Zath[1,2], Tatsuya Akiyama[1,3], Kerry S. Williamson[1,3], Michael J. Franklin[1,3] and Connie B. Chang[1,2]**

[1] *Center for Biofilm Engineering, Montana State University, Bozeman, MT, United States,* [2] *Department of Chemical and Biological Engineering, Montana State University, Bozeman, MT, United States,* [3] *Department of Microbiology and Immunology, Montana State University, Bozeman, MT, United States*

The physiological heterogeneity of cells within a microbial population imparts resilience to stresses such as antimicrobial treatments and nutrient limitation. This resilience is partially due to a subpopulation of cells that can survive such stresses and regenerate the community. Microfluidic approaches now provide a means to study microbial physiology and bacterial heterogeneity at the single cell level, improving our ability to isolate and examine these subpopulations. Drop-based microfluidics provides a high-throughput approach to study individual cell physiology within bacterial populations. Using this approach, single cells are isolated from the population and encapsulated in growth medium dispersed in oil using a 15 μm diameter drop making microfluidic device. The drops are arranged as a packed monolayer inside a polydimethylsiloxane (PDMS) microfluidic device. Growth of thousands of individual cells in identical microenvironments can then be imaged using confocal laser scanning microscopy (CLSM). A challenge for this approach has been the maintenance of drop stability during extended time-lapse imaging. In particular, the drops do not maintain their volume over time during incubation in PDMS devices, due to fluid transport into the porous PDMS surroundings. Here, we present a strategy for PDMS device preparation that stabilizes drop position and volume within a drop array on a microfluidic chip for over 20 h. The stability of water-in-oil drops is maintained by soaking the device in a reservoir containing both water and oil in thermodynamic equilibrium. This ensures that phase equilibrium of the drop emulsion fluids within the porous PDMS material is maintained during drop incubation and imaging. We demonstrate the utility of this approach, which we label DropSOAC (Drop Stabilization On A Chip), for time-lapse studies of bacterial growth. We characterize growth of *Pseudomonas aeruginosa* and its Δ*hpf* mutant derivative during resuscitation and growth following starvation. We demonstrate that growth rate and lag time heterogeneity of hundreds of individual bacterial cells can be determined starting from single isolated cells. The results show that the DropSOAC capsule provides a high-throughput approach toward studies of microbial physiology at the single cell level, and can be used to characterize physiological differences of cells from within a larger population.

Keywords: drop-based microfluidics, single cell, growth rate, lag time, time-lapse imaging, biofilm, heterogeneity, emulsion stability

OPEN ACCESS

Edited by:
Alon Hochbaum, University of California, Irvine, United States

Reviewed by:
Wenbin Du, Institute of Microbiology (CAS), China
Matthew Cabeen, Oklahoma State University, United States

****Correspondence:***
Connie B. Chang
connie.chang@montana.edu

Specialty section:
This article was submitted to Systems Microbiology, a section of the journal Frontiers in Microbiology

Received: *16 March 2019*
Accepted: *27 August 2019*
Published: *24 September 2019*

Citation:
Pratt SL, Zath GK, Akiyama T, Williamson KS, Franklin MJ and Chang CB (2019) DropSOAC: Stabilizing Microfluidic Drops for Time-Lapse Quantification of Single-Cell Bacterial Physiology. Front. Microbiol. 10:2112. doi: 10.3389/fmicb.2019.02112

INTRODUCTION

Microbial populations contain cells in a variety of physiological states (Stewart and Franklin, 2008). Even in clonal populations under laboratory conditions, subpopulations of cells may be physiologically different from the rest of the population. This phenomenon is best exemplified by the presence of persister cells, where a minor subset of cells has enhanced resistance to killing by antibiotics, compared to the rest of the cells in the population (Lewis, 2007; Balaban et al., 2013). The persister antibiotic-resistant state is often induced by the activity of self-encoded toxin-antitoxin (TA) systems (Gerdes and Maisonneuve, 2012), where the toxin affects a small percentage of cells, and allows them to tolerate antibiotics that target the greater population. Another example of physiological heterogeneity is the subpopulations of cells that produce colony morphologies that differ from the majority of cells in the community, such as the rugose and mucoid colony morphology variants (Allegrucci and Sauer, 2007; Hansen et al., 2007; McEllistrem et al., 2007). The percentage of persister cells and colony variants increases when bacteria grow in biofilms, or surface-attached communities of bacteria and their extracellular matrices (Stoodley et al., 2002). Reaction and diffusion of nutrients, oxygen, and metabolic products also contribute to physiological heterogeneity of bacteria in biofilm communities (Stewart and Franklin, 2008). These chemicals form gradients within the biofilm and induce microscale variations in gene expression of individual cells. Bacterial physiological heterogeneity poses a significant challenge to the treatment of bacterial infections. In particular, colony variants, persister cells, or dormant cells within biofilms may resist antibiotic treatment or host defenses, and repopulate the communities when treatment is alleviated, resulting in chronic infections (Lyczak et al., 2002).

Technological advances, particularly with regard to miniaturization and single-cell resolution platforms, provide a means to characterize bacterial cell-level heterogeneity. Isolation of single cells for time-lapse observation has been approached through chamber (Leung et al., 2012), flow (Shi et al., 2008; Sun et al., 2011; Dewan et al., 2012), and drop-based microfluidic systems (Huebner et al., 2009; Shim et al., 2009; Khorshidi et al., 2014). Single-cell physiological studies allow direct observation of cell behavior that is otherwise masked by population-level studies (Brehm-Stecher and Johnson, 2004). Therefore, advances in characterizing single-cell physiology complement advances in DNA sequencing technologies that allow single-cell genomics studies. Microfluidic methods, characterized by microscale platforms, minimized reagent volumes, and high-throughput sample preparation, have a distinct advantage for single cell studies, and are suited for research on the physiology of biofilm cell heterogeneity (Weibel et al., 2007; Franklin et al., 2015; Akiyama et al., 2017).

Drop-based microfluidics provides an option that maximizes isolation of single cells and the high-throughput capabilities of microfluidic technology (Chang et al., 2015). Drop-based microfluidics can be used to produce water-in-oil drops with diameters between ten and several hundreds of microns. Single cells in growth medium can be encapsulated in these drops. Drops can be arrayed, held stationary, and imaged using time-lapse microscopy. Previous time-lapse studies involving the imaging of drops to monitor cell growth have used drops larger than 30 μm in diameter (Dewan et al., 2012; Leung et al., 2012; Khorshidi et al., 2014). Larger drops are advantageous in accommodating larger cells, such as algae (Pan et al., 2011) and mammalian cells (Khorshidi et al., 2014). However, smaller drops <20 μm in diameter are preferred to accommodate the growth of single bacterial cells while maximizing the number of drops per field of view. Polydimethylsiloxane (PDMS) is an inexpensive, optically clear polymer commonly used to manufacture microfluidic chips. Although ideal for imaging and rapid fabrication of microfluidic devices (Duffy et al., 1998), PDMS is a porous material that allows the diffusion of fluid from drop emulsions stored in microfluidic devices into the polymer matrix over time (Shim et al., 2007, 2009; Huebner et al., 2009; Schmitz et al., 2009; Pan et al., 2011; Dewan et al., 2012; Amselem et al., 2016). Thus, in time-lapse imaging studies of drops stored in PDMS, the drop volumes do not remain stable due to fluid transport through the porous PDMS matrix. Previous approaches have been developed to mitigate fluid transport through PDMS with varying levels of success. These methods include the incorporation of water reservoirs in PDMS devices (Shim et al., 2007, 2009; Dewan et al., 2012), submersion of devices in water prior to and during use (Pan et al., 2011; Khorshidi et al., 2014), and embedding a diffusion limiting glass layer within the devices above the drop storage areas (Schmitz et al., 2009). However, none of these methods have investigated the stability of a static array of small drops (<20 μm in diameter) for extended time-lapse imaging of single bacterial cells. Such an approach would maximize the number of individual cells that can be imaged and characterized to allow for high-throughput, physiological studies on bacteria.

Here, we present the DropSOAC (Drop Stabilization On A Chip) method for preparing PDMS devices that stabilize <20 μm diameter water-in-oil drops in a static array during time-lapse microscopy for over 20 h. Stability of the position, volume, and geometry of the packed drops relies upon the maintenance of phase equilibrium between the drops and a surrounding fluid reservoir. This phase equilibrium is maintained by soaking a PDMS device in water-saturated oil for at least 24 h before introducing drops into the device. The device is housed in a modified Petri dish with a tight-fitting lid, called a DropSOAC capsule, to prevent evaporation of fluid and maintain phase equilibrium. Filling the capsule with the soaking fluid allows the devices to remain submerged during time-lapse confocal laser scanning microscopy (CLSM) imaging. We demonstrate the utility of this approach for quantifying the heterogeneity of *Pseudomonas aeruginosa* and a *P. aeruginosa* Δ*hpf* mutant derivative with respect to their growth kinetics following resuscitation after starvation. Single cells of *P. aeruginosa* and the Δ*hpf* mutant were encapsulated in drops using a 15 μm drop making device, upon which the drops were introduced into the DropSOAC capsule and incubated at 37°C in a CLSM stage-top incubator. The growth of each fluorescently labeled cell within a drop was quantified and tracked over time using CLSM. Our results demonstrate that drop stability is maintained in the

PDMS devices using the DropSOAC approach. We demonstrate that growth rate and lag time heterogeneity can be determined starting from single bacterial cells as inocula, and that our DropSOAC method can capture heterogeneity at the single cell level that might otherwise be masked by bulk measurements of population growth.

MATERIALS AND METHODS

PDMS Microfluidic Device Fabrication

Polydimethylsiloxane (PDMS) microfluidic devices were fabricated using standard soft photolithography processes (Duffy et al., 1998). Photoresist (Microchem SU-8 2015) was patterned onto 76.2 mm silicon wafers (University Wafer) using photomasks (CAD/Art Inc., AutoCAD) to make negatives for PDMS molding. PDMS base and hardener (Dow SYLGARD 184) were mixed at a ratio of 10:1 by mass and poured onto the device molds. The uncured PDMS mix was degassed in a vacuum chamber and cured in a 65°C oven for 1 h. The cured PDMS slabs were removed from the master and ports were punched using a 0.75 mm biopsy punch (EMS Core Electron Microscopy Sciences). The slabs were bonded to 3 in × 2 in glass slides (VWR) for drop-making microfluidic devices and 25 mm × 25 mm type 0 coverslips (VWR) for drop incubation devices. The bonded PDMS and glass devices were baked at 65°C to increase strength of the plasma bonds. After baking, the device channels were filled with hydrophobic treatment (Pittsburgh Glass Works Aquapel), cured for 5 min, and flushed with air. The devices were again baked at 65°C for 1 h to evaporate the remaining hydrophobic treatment.

DropSOAC Capsule Preparation and Soaking

PDMS and glass drop incubation devices were inserted through 23.5 mm × 23.5 mm laser cut holes (Universal Laser Versa Laser VSL 3.5) in the bottom of 47 mm diameter petri dishes (Millipore Sigma Petri-Pad) and adhered with two-component epoxy (Devcon 5 Minute Epoxy). The resulting DropSOAC capsules were placed unlidded in an airtight container of approximately 400 mL of Novec HFE-7500 fluorocarbon oil (3M, St. Paul MN) and 400 mL of water, and submerged under the denser oil phase. The container was placed in an incubator at 37°C. Unlidded capsules were pre-soaked for a minimum of 24 h in the oil/water bath. After soaking, a DropSOAC capsule was briefly removed from the bath. Drops were injected into the PDMS devices embedded in the capsule from an inverted syringe. Inverting the syringe allows the less dense aqueous drops to float to the syringe outlet. The DropSOAC capsule was returned to the oil/water bath, submerged under the oil phase, and lidded, resulting in a water-saturated oil reservoir around the drop-filled PDMS device. The lidded capsule was removed from the bath, dried with a paper towel, and placed coverslip-side down in an environmental chamber (Pathology Devices Inc., LiveCell) set to 37°C and 85% RH on the stage of an inverted confocal microscope (Leica TSC SP5 II) for imaging. For the studies investigating water only and oil only soaking methods, the DropSOAC capsule was submerged either in 400 mL of oil without water or in 400 mL of water without oil, rather than water and oil in contact with one another. For the no treatment control studies, the DropSOAC capsules were not soaked in fluid prior to or during use and were kept in air.

Drop Production

Drops were prepared using a 15 μm PDMS flow-focusing microfluidic drop making device. Two different fluids, water as the disperse phase, and HFE7500 (3 M) fluorocarbon oil containing 1.5 wt% 008-FluorSurfactant (RAN Biotechnologies) as the continuous phase, were transported through 0.38 mm ID/1.09 mm OD polyethylene tubing (Scientific Commodities Inc.) from 1 mL syringes (BD Leur-Lok) and 27G × 1/2 needles (BD Precision Glide Needle) to the drop making device. The surfactant used, 008-FluorSurfactant, is composed of a biocompatible PFPE-PEG block copolymer (Holtze et al., 2008). Flow was achieved using a volume-displacement syringe pump (PHD 2000, Harvard Apparatus) at disperse and continuous flow rates of 200 and 600 μL/h, respectively. Drops exited the device through tubing and were collected into an inverted 1 mL syringe (BD Leur-Lok tip) for 15 min.

Behavior of Water-in-Oil Drops With Various Soaking Methods (No Bacteria)

Water-in-oil drop stability was tested in DropSOAC capsules prepared by soaking in an oil/water bath, soaking in an oil bath, soaking in a water bath, or left untreated, as described in section "DropSOAC Capsule Preparation and Soaking." Each soaking method was tested in triplicate by filling the prepared devices with water-in-oil drops and imaging over 4.5 h as described in section "Drop Imaging." During these tests, multiple images of drops held in the DropSOAC capsules (one capsule per trial) were collected every 30 min. For the oil/water soak and the oil only soak, diameter data were randomly sampled from each of the images and compiled across all trials. These images were analyzed using a custom Matlab code to identify drops and determine the drop diameters (data in **Supplementary Table S1**). The drop diameter data contains values from multiple capsules, devices within the capsules, and positions (fields of view) within the devices. Thus, a mixed effects model was fit to the data set with random effects for the trials (each in a separate capsule) and the positions imaged in each trial to account for the repeated measures from each trial and position, and fixed effects for time and soaking method. Three trials were also tested in the water only soaking method and the no treatment control, but drop diameters could not be quantified due to drop deformation. To quantify drop volumes in DropSOAC capsules prepared by soaking in water, the experiment was repeated in which 500 nM of the fluorescent dye, 5-carboxy-X-rhodamine (ROX), was added to the water drops for CLSM imaging and size quantification using Imaris software.

Preparation of Drop Phase for Cell Encapsulation

Cells were prepared similarly to the methods described in Akiyama et al. (2017). *P. aeruginosa* PAO1 and its Δ*hpf* derivative that constitutively expresses the green fluorescent protein (GFP) from plasmid (pMF230) (Nivens et al., 2001) were cultured overnight from freezer stock in tryptic soy broth (TSB) amended with 150 μg/mL carbenicillin. Aliquots (120 μL) of overnight cultures were inoculated into 4 ml of TSB without carbenicillin in culture tubes and incubated at 37°C on a roller until the optical density (OD_{600}) exceeded 7.0 (CE2041 Spectrophotometer, Cecil Instruments). This OD value corresponds to stationary phase of growth. Aliquots of cultures that resulted in a final concentration of 1.5×10^8 CFU/mL, based on the OD_{600} (approximately 1 mL) were centrifuged, washed twice with phosphate buffered saline (PBS), and resuspended in 25 mL of PBS buffer in a 125 mL baffled flask. Four aliquots of the cell suspension (two of PAO1 and two of Δ*hpf*) were prepared for 0-day starved cell growth studies, or "day zero" studies. Here, 100 μL of cells in PBS were removed from the 125 mL flasks, added to 900 μL of TSB media, and encapsulated into drops. Cells were promptly encapsulated (within 20 min) after reintroduction to media to begin acquiring growth data soon after encapsulation. Two aliquots of cells (one of PAO1 and one of Δ*hpf*) were prepared for 4-day starved cell growth studies, or "day four" studies, in which cells were incubated in PBS at 37°C with shaking at 200 rpm for 4 days. Following incubation, 100 μL of cells in PBS buffer were removed from the 125 mL flasks, added to 900 μL of TSB, and immediately encapsulated into drops. The prepared cell cultures were used as the disperse phase in the drop production method described above.

P. aeruginosa PAO1 and Δ*hpf* Single Cell Growth Studies

As a test case for evaluating drop stability during bacterial growth, and for quantifying bacterial growth curves, we evaluated *P. aeruginosa* PAO1 and Δ*hpf* growth in drops containing TSB growth medium. Diluted cell cultures resuspended in TSB, as described above, were used as the disperse phase in drop production, to achieve approximately one cell per 17 drops. Each DropSOAC capsule holds three arrays, and therefore can be used to evaluate up to three samples simultaneously. In these experiments, two arrays were used, one for PAO1 and one for Δ*hpf*, so that the two strains were assayed simultaneously. Both strains were analyzed prior to starvation, in two separate experiments, and then once after 4 days of starvation in PBS (Akiyama et al., 2017). Three image series were collected for each strain on each array. The change in drop diameters from all time-lapse studies (**Supplementary Table S2**), which consisted of two experiments of day zero PAO1 and Δ*hpf* and one experiment of day four PAO1 and Δ*hpf*, were analyzed using a mixed effects model, described in section "Behavior of Water-in-Oil Drops with Various Soaking Methods (No Bacteria)," to calculate the average drop size change after 21.5 h. Each field of view using the 20X objective of the CSLM can image approximately 1,150 drops. An additional study with three biological replicates of day four starved Δ*hpf* cell culture (prepared as described in section "Preparation of Drop Phase for Cell Encapsulation") was conducted to assess percent of cells that resuscitated in drops after 24 h. For these studies, cells were encapsulated in drops, incubated in DropSOAC capsules, and imaged after 24 h. To determine bulk growth rates, PAO1 (pMF230) and PAO1 Δ*hpf* (pMF230) overnight cultures were diluted to an OD_{600} of 0.1 in 200 μl TSB in 96 well plates. Plates were incubated with constant shaking at 37°C for up to 8 h in the SpectraMax190 (Molecular Devices), and OD_{600} was monitored every 10 min. The assay was performed on three biological replicates placed in three independent microtiter plates.

Drop Imaging

Filled DropSOAC capsules were placed in an environmental chamber (Pathology Devices Inc., LiveCell) at 37°C and 85% RH on an inverted confocal microscope (Leica TSC SP5 II). Drops were imaged with a 20× objective in a 60 μm *z*-stack with 2 μm increments. The middle of the *z*-stack was set to the center of the drops. Images were taken using brightfield and fluorescence imaging every 30 min for the duration of 21.5 or 4.5 h for the bacterial incubation studies and the drop stability studies, respectively. *Z*-stacks were used to capture the entire depth of the drop and to ensure that changes in focal plane from temperature fluctuations were captured. Multiple positions were captured for each study using the "Mark and Find" application within the Leica microscopy software (LAS AF). In the water soaking study with ROX dye, a 63X water immersion objective was used.

Image Processing and Analysis

The 4D image stacks, composed of three spatial dimensions and time, acquired from confocal imaging of *P. aeruginosa* in drops were processed with the Fiji (Schindelin et al., 2012) distribution of ImageJ (Rueden et al., 2017). A summed *z*-projection of the GFP channel was used to combine the pixel values of all focal planes, capturing fluorescence from bacteria at all locations within the drop. Drop size measurements for each device preparation method were collected with a custom MATLAB script using the brightfield channel. The Fiji plugin TrackMate (Tinevez et al., 2017) was used to identify fluorescent cells in drops and track the change in pixel intensity from the GFP channel, frame by frame, as the cells grew. Pixel intensity is linearly correlated with the concentration of cells within the drops over the range of the PMT output on the confocal microscope. The tracking data collected from TrackMate was then loaded into a custom MATLAB script to plot growth curves for each drop, calculate a maximum growth rate (μ_{max}), and calculate the lag phase length. Maximum growth rate was calculated from the slope of the linear portion of the growth curve when the natural log of the fluorescence was plotted against time. The lag phase length was determined from the time at the start of image acquisition until the fluorescence within a drop rose above background noise and was tracked by TrackMate. The frequency of cell resuscitation in drop growth assays was determined using TrackMate data. To quantify numbers of cells that resuscitated, the number of drops in which pixel intensity value was low, but non-zero

and constant for the duration of incubation was compared to the number of drops in which fluorescence value increased during incubation.

RESULTS

The DropSOAC (Drop Stabilization On A Chip) Capsule Design Allows High-Throughput Time-Lapse Imaging of <20 μm Diameter Water-in-Oil Drops

The DropSOAC capsule is designed to maximize the number of individual drops observed over time, and keep the PDMS device used to store these drops submerged in liquid. The DropSOAC capsule consists of a PDMS device plasma-bonded to a glass coverslip and interfaced with a modified Petri dish (**Figure 1**). The PDMS device inside the DropSOAC capsule contains three drop arrays. The channel design in these devices has been used in the past (Köster et al., 2009; Schmitz et al., 2009; Akiyama et al., 2017) and consists of an inlet for drop injection, a feeder channel that distributes the drops to a series of 31 parallel channels, and an outlet channel. Each of the parallel channels consists of a series of 31 circular wells 150 μm in diameter connected by 75 μm constrictions. The parallel channels are offset to maximize the number of channels possible in the device footprint (**Figure 1A**).

The DropSOAC capsule is a PDMS device/Petri dish hybrid in which a 23.5 mm × 23.5 mm square hole is laser cut into the bottom of a 47 mm × 47 mm Petri dish with a tight fitting lid. The PDMS device, bonded to a 25 mm × 25 mm cover glass, is inserted into the Petri dish through the laser cut hole and adhered with two-component epoxy (**Figure 1B**). The tight-fitting lid of the Petri dish allows a fluid reservoir to be maintained around the PDMS device after filling the DropSOAC capsule. The filled and lidded DropSOAC capsule prevents spills and the evaporation of reservoir fluid in a format that is compact and well-suited for microscope stage-top incubators (**Figures 1C,D**).

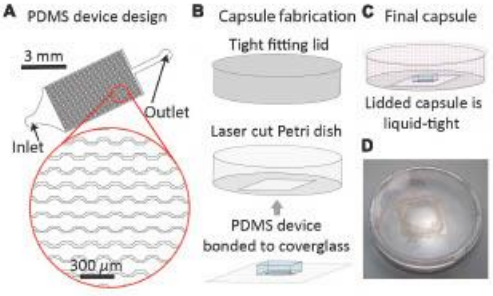

FIGURE 1 | DropSOAC capsule fabrication. **(A)** The drop array device design consists of 30 parallel channels. Design is based on prior work (Schmitz et al., 2009). Each channel connects thirty-one 150 μm diameter wells connected by 75 μm constrictions. Drops are distributed to the channels through a triangular inlet and exit through a shared outlet. **(B)** PDMS devices, plasma bonded to 25 mm × 25 mm type 0 cover glass, are inserted through the base of a 47 mm liquid tight Petri dish and bonded with two component epoxy. **(C)** Lidding the capsule forms a liquid tight seal that allows the PDMS to be submerged under fluid during CLSM while limiting evaporation of the soaking liquid. **(D)** Photograph of the DropSOAC capsule.

Soaking the PDMS Device in an Oil/Water Bath Allows for Drop Stability, Compared to Soaking the Device in No Fluids, Oil Only, or Water Only

The fluid used to soak PDMS devices in the DropSOAC capsule affects the behavior of drops in the PDMS array over extended periods of time. In this study, three soaking solutions were tested: water-saturated oil, oil, and water. An additional study with an unsoaked capsule was conducted to serve as a control for no treatment. The water-saturated oil soak is prepared by making a bath of water and fluorinated oil (HFE7500), approximately 400 mL each, in an air-tight container and allowing the phases to equilibrate until each phase approaches maximum solubility in the other. Since the density of the oil (1.614 g/mL) is higher than that of water, the oil phase sits at the bottom of the bath. Although the oil and water phases are considered immiscible, there is partial solubility of one phase within the other phase. The solubility of the oil phase in water is <4 ppb by weight; the solubility of water phase in oil is 45 ppm by weight (Novec 3M product information). The DropSOAC capsule is soaked in the prepared water-saturated oil for 24 h. During soaking, the water-saturated oil permeates the porous PDMS device. The stability of drops in the DropSOAC capsules was tested by filling the capsules with drops and imaging them over time using CLSM. The DropSOAC capsule soaked in water-saturated oil resulted in stable maintenance of drop size, geometry, and position over 4.5 h of imaging (**Figure 2A**).

By contrast, studies of drops held in DropSOAC capsules that were soaked in oil alone, soaked in water alone, or soaked in no liquid (no treatment control), showed distinct drop destabilization patterns. Drops incubated in an oil prepared DropSOAC capsule shrank over time (**Figure 2B**). Diameter comparison of drops indicated that oil prepared DropSOAC capsules shrink to 61% ± 16% of their original diameter after 4.5 h (270 min), while the drops stored in water-saturated oil prepared DropSOAC capsules shrink to only 97% ± 1.5% of their original diameter (**Figure 3A**). The apparent, top-down diameter of drops, D, in the device channels is larger than the expected drop diameter of 15 μm due to the buoyancy of the drops causing them to slightly flatten to yield an average initial diameter D_0 = 20.8 μm ± 0.6 μm in the oil/water case and D_0 = 21.0 μm ± 1.5 μm in the oil only case. The final diameters after 4.5 h are D = 20.2 μm ± 0.3 μm in the oil/water case and D = 12.9 μm ± 3.4 μm in the oil only case.

Drops incubated in a water prepared DropSOAC device showed changes in the shape, undergoing a transition from curved to planar drop interfaces (**Figure 2C**). The diameter comparison of the water prepared DropSOAC capsules was not possible due to the marked change in drop geometry. These drops transition from slightly flattened spheres at time t = 0 min, to drops that are faceted polyhedrons at t = 1 h. As the

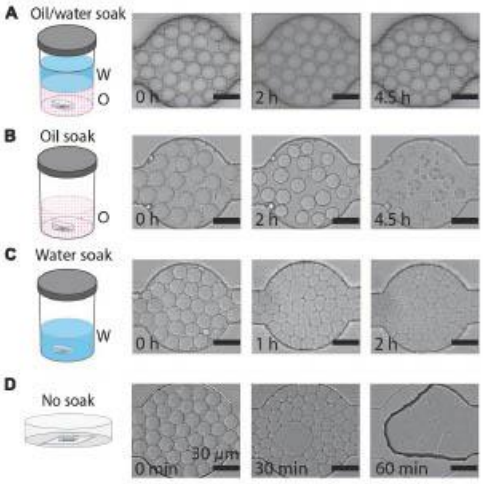

FIGURE 2 | Behavior of water-in-oil drops varies with soaking method. **(A–D)** Water-in-oil drops held in PDMS devices submerged in oil/water, oil, water, or with no soaking treatment. Scale bars are 30 μm. **(A)** Drops maintain diameter and geometry after 4.5 h when the PDMS device is soaked in an oil/water bath. **(B)** Drops shrink over 4.5 h when the PDMS device is soaked in an oil bath. **(C)** The geometry of drops undergoes a rapid transformation from round to faceted polyhedrons when the PDMS is soaked in a water bath. **(D)** Drops destabilize when held in untreated PDMS devices.

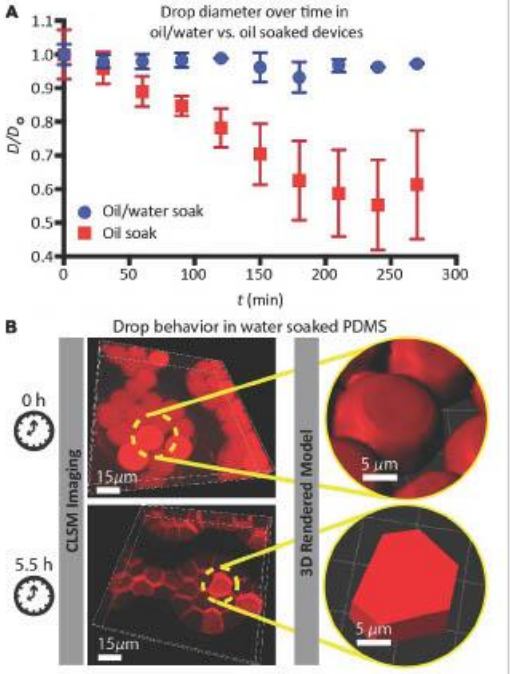

FIGURE 3 | (A) Comparison of the average normalized drop diameter D/D_0 of drops when the PDMS device is soaked in an oil/water bath (●, blue dots), versus drops when the PDMS device is soaked in an oil bath (■, red squares). **(B)** Geometry transformation and volume decrease of drops in the water-soaked PDMS device, imaged by CLSM. Water drops containing ROX fluorescent dye solution is imaged using CLSM and 3D images are used to render models that show shape of the drops at the initial and final time points. Scale bars are 15 μm in CLSM images. Scale bars are 5 μm in the 3D Rendered Model.

transition was difficult to observe using brightfield microscopy (**Figure 2C** at t = 1 h and t = 2 h), in a subsequent study we added an aqueous fluorescent dye (ROX) to the drops to characterize the structural changes of drops, distinguish drop interfaces, and to determine volume changes over time by CLSM. Three-dimensional projections of the fluorescence data show that soaking the DropSOAC capsule in water alone affects drop stability resulting in facetted polyhedrons. The polyhedrons have parallel upper and lower surfaces, and flat sides that are pressed against one another. Image analysis software (Imaris) was used to model the volumes of the drops. Interestingly, the drops in water-soaked PDMS decrease in volume after 5.5 h, to approximately 55% ± 29% (31 initial drops analyzed, 101 final drops analyzed in a single trial) of the original volume (**Figure 3B**). At the initial time point, CLSM imaging shows flattening of the tops of the drops in water soaked DropSOAC capsules (**Figure 3B**). Finally, a control study was performed in which drops were held in an untreated DropSOAC capsule. The drops evaporated through the ports and the PDMS, leaving empty channels within the PDMS device in under 1 h (**Figure 2D**).

The Water-Saturated Oil DropSOAC Method Allows for Drop Stability in Single-Cell Growth Studies

Since drops remained stable in the DropSOAC capsule soaked in water-saturated oil, we tested the applicability of the DropSOAC approach for studying single cell bacterial growth over time. DropSOAC capsules were soaked under the oil phase of an oil/water bath for 24 h, allowing the porous PDMS device to be filled with water-saturated oil (**Figure 4A**). After pre-soaking the DropSOAC capsule for 24 h, the capsules were filled with drops that contain single bacterial cells (**Figure 4B**). Cell loading is governed by Poisson statistics so that there is a low probability that one drop will be inoculated with more than one bacterial cell (Köster et al., 2008). A cell concentration corresponding to a drop loading ratio of one cell to every 17 drops was used in these experiments. After the DropSOAC capsule was filled with drops, it was returned to the oil/water bath and lidded under the oil phase, forming a water-saturated oil reservoir surrounding the PDMS device (**Figure 4C**). The lidded capsule was removed from the bath and the exterior of the capsule was dried. The lidded capsule was leak-proof and prevented the evaporation of the fluid reservoir around the PDMS. The DropSOAC capsule was then placed in a stage-top incubation chamber on the CLSM and

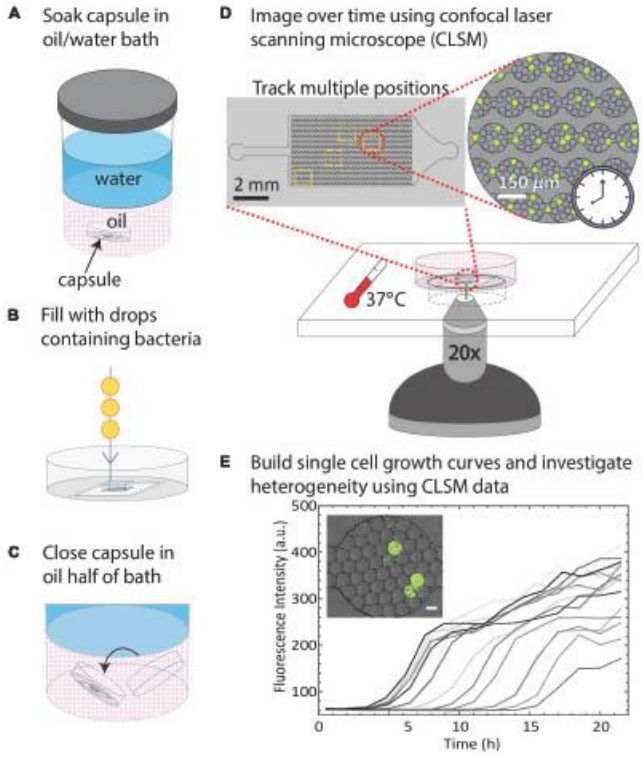

FIGURE 4 | Summary of DropSOAC method and application. **(A)** PDMS-based microfluidic devices embedded in the base of modified Petri dishes (DropSOAC capsules) are soaked in the oil phase of an oil/water bath for 24 h. **(B)** The DropSOAC capsule is removed, and the PDMS device within is filled with drops containing fluorescently labeled bacteria. **(C)** The DropSOAC capsule is lidded under the oil layer of the oil/water soaking bath resulting in a liquid tight capsule filled with water-saturated oil. **(D)** The bacteria-laden drops are imaged using CLSM from within the filled DropSOAC capsule for 21.5 h at 37°C. Multiple positions on the device are imaged, resulting in thousands of drops imaged per experiment. **(E)** Single cell growth curves are constructed from the time-lapse data. These growth curves reveal growth heterogeneity between individual cells.

incubated at 37°C. The "Mark and Find" multiple position tool in the confocal microscope software (Leica AF) was used to collect both brightfield and fluorescence images at multiple positions in the PDMS microfluidic array. Using time-lapse programing, each position was imaged every 30 min. The fluorescence signal within the drops was detected as the fluorescently labeled bacteria in the drops grew (**Figure 4D**). The change in fluorescence signal in each drop was quantified and used as an indicator of cell growth (**Figure 4E**). Because the growth curves are unique to individual cells within drops, they allow the heterogeneity between cells to be distinguished.

Growth Heterogeneity of *Pseudomonas aeruginosa* With Single Cells as Inocula

The drop stability of the water-saturated oil DropSOAC capsule allows the study of bacterial growth in drops starting from single cells. Drops containing single bacterial cells remain stable for over 21.5 h, and bacterial growth was observed through an increase in fluorescence over time. To demonstrate this, 0-day starved *P. aeruginosa* PAO1 (pMF230) cells that constitutively express green fluorescent protein (GFP) were washed twice with PBS, resuspended in TBS growth medium, and encapsulated in drops. The drops were injected into the water-saturated oil DropSOAC capsule and imaged every 30 min for 21.5 h by CLSM. Each field of view allowed imaging of approximately 1150 drops (**Figure 5A**). Increase in fluorescence starting from individual cells was observed over time within stable drops (**Figure 5B**).

To demonstrate the utility of the DropSOAC device for studying growth heterogeneity in *P. aeruginosa* populations, we compare the differences in regrowth of *P. aeruginosa* PAO1 and *P. aeruginosa* (Δ*hpf*), that is deleted for the hibernation promoting factor, following 4 days of starvation (Akiyama et al., 2017). The two strains of *P. aeruginosa* were washed in PBS,

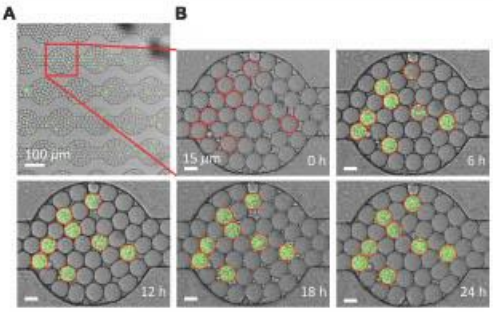

FIGURE 5 | Growth of *P. aeruginosa* PAO1 starved for 0 days in drops over time via CLSM. **(A)** Using a 20X objective lens, each field of view captures approximately 1150 drops. Scale bar is 100 μm. **(B)** *P. aeruginosa* labeled with green fluorescent protein grow from single cells in the drops over 24 h. Growth was quantified from the increase in fluorescent output from each drop. Drops circled in red contain cells. Drop position remains constant over time. Scale bar is 15 μm.

as described in the methods, and incubated in PBS for 4 days at 37°C. Day four starved cultures were then encapsulated in drops containing TSB regrowth medium, with approximately one cell in every 17 drops. The drops were injected into the DropSOAC capsule, and the capsule was incubated at 37°C in a stage-top incubator. Drops were imaged every 30 min for 21.5 h using CLSM (**Figure 6A**). The drops maintained consistent positions and geometry within the device during time-lapse imaging. At time zero, the average drop diameter was 19.6 μm $\pm$ 1.4 μm, and after 21.5 h, the average drop diameter was 19.9 μm $\pm$ 1.7 μm.

We quantified single-cell growth of bacteria cultured in microfluidic drops using the increase in fluorescence intensities over time for *P. aeruginosa* PAO1 and its Δ*hpf* mutant derivative (**Figure 6A**). The growth curves were used to calculate the distributions of maximum growth rates, and the length of time required for individual cells to recover from starvation (lag phase). Following 4 days of starvation, *P. aeruginosa* PAO1 regrew in TSB drops with most cells entering exponential phase at approximately 4 h. The drops inoculated with single cells were completely filled with bacteria by 8 h, as indicated by a homogenous, bright fluorescence signal in the entire drop. Regrowth of PAO1 (**Figure 6B**) had an average growth rate of 0.39 h^{-1} $\pm$ 0.11 h^{-1} (**Figure 6C**) and an average lag phase length of 3.10 h $\pm$ 0.62 h (**Figure 6D**). By contrast, the drops containing the day four starved Δ*hpf* cells had varying levels of fluorescence output at each time point (**Figure 6E**). Analysis of the Δ*hpf* growth curves yielded an average maximum growth rate of 0.36 h^{-1} $\pm$ 0.08 h^{-1} (**Figure 6F**). By comparison, the growth rate of PAO1 (pMF230) and Δ*hpf* (pMF230) is 0.784 h^{-1} $\pm$ 0.042 h^{-1} and 0.689 h^{-1} $\pm$ 0.067 h^{-1} when cultured in TSB media in bulk. For the Δ*hpf* cells that were capable of regrowth in drops, the growth rate was similar to that of PAO1. Despite consistent growth rates within the Δ*hpf* population, there was a wide distribution of lag times over the course of the 21.5 h incubation period. The lag times for the Δ*hpf* cells capable of resuscitation ranged from 3 h to 17.5 h (**Figure 6E**) with an average lag phase length of 7.71 h $\pm$ 3.98 h (**Figure 6G**). Most day four starved Δ*hpf* cells, approximately 86.6% $\pm$ 2.5%, did not resuscitate in drops following starvation. Cells that did not resuscitate from starvation were not included in the statistical analyses for growth rate and lag phase length. For each strain, three fields of view were monitored, resulting in approximately 3000 drops and over 200 cells imaged per strain.

DISCUSSION

Minimizing Drop Size Maximizes Efficiency of Drop-Based Microfluidic Cell Growth Assays

Previous time-lapse studies involving the imaging of cells in drops have used drops larger than 30 μm in diameter (Dewan et al., 2012; Leung et al., 2012; Khorshidi et al., 2014). Smaller drops, <20 μm in diameter, are preferred to accommodate the growth of single microbial cells since they maximize the number of drops per field of view within the array. In our study, we observe approximately 1150 drops per field of view using a 20X objective lens. We monitored three fields of view per sample in this study, however, up to 42 distinct fields of view in each array are available for imaging. This corresponds to approximately 48,300 drops that can be imaged in one array. Each DropSOAC capsule can hold up to three arrays, therefore, each capsule allows for the imaging a total of approximately 145,000 drops. Theoretically, cell concentrations that correspond to one cell per drop for 50 μm drop diameters and 15 μm drop diameters are 1.5×10^7 cells/mL and 5.7×10^8 cells/mL, respectively. Reducing the drop diameter from 50 μm to 15 μm allows an order of magnitude more cells to be studied in the same volume for single cell drop-based assays, which is important when investigating rare single cells in a population.

The device used in this work is a modification of a previously designed drop maker and array, which was designed to hold individual drops in wells connected by constrictions (Schmitz et al., 2009). Here, the drop maker is independent of the DropSOAC device. Separating the devices allows us to incubate 15 μm drops in 150 μm diameter wells with 75 μm width constrictions (**Figure 1**) and allows multiple bacterial strains to be studied simultaneously as one DropSOAC device contains three arrays. This system is intended to hold many drops in the wells and channels to increase the number of drops imaged per field of view. In addition, the resolution limitation of soft photolithography depends on the minimum mask resolution. Our mask printing source limits features to approximately 10 μm at their highest resolution, thus making it difficult to accommodate single drops with diameters <20 μm in features that allow for one drop per well. These same limitations make the fabrication of other drop arrays, such as floating arrays

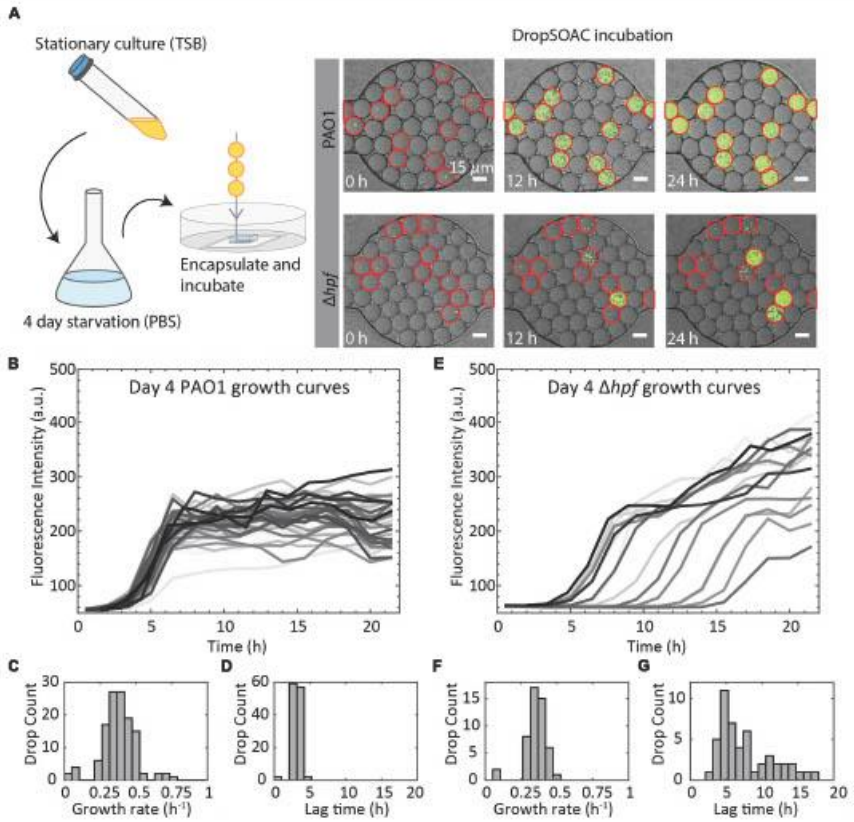

FIGURE 6 | Summary of *P. aeruginosa* PAO1 and Δ*hpf* growth resuscitation studies. **(A)** Cells were starved in PBS for 4 days. After starvation, cells were resuspended in TSB media and encapsulated in drops using a 15 μm drop maker. Drops are incubated in a DropSOAC capsule soaked in water-saturated oil and imaged using CLSM. Growth was monitored as increased fluorescence. Many of the Δ*hpf* cells show delayed growth or no growth following starvation, which can be seen from the image at 12 h. Drops circled in red contain cells. Scale bars are 15 μm. **(B)** Single cell growth curves of *P. aeruginosa* PAO1 following 4 d of starvation. Image shows 80 out of a total of 210 cells analyzed from one field of view, with non-growing cells omitted. **(C)** Histogram showing the distribution of maximum growth rates for *P. aeruginosa* PAO1 following starvation ($N = 210$). **(D)** Histogram showing the distribution of lag phase length of *P. aeruginosa* PAO1 ($N = 210$). **(E)** Single cell growth curves of *P. aeruginosa* Δ*hpf* following 4 d of starvation. Image shows 85 out of a total of 218 cells analyzed from one field of view, with non-growing cells omitted. **(F)** Histogram showing the distribution of maximum growth rates for *P. aeruginosa* Δ*hpf* following starvation ($N = 218$). **(G)** Histogram showing the distribution of lag phase length of *P. aeruginosa* Δ*hpf* ($N = 218$).

(Shim et al., 2009; Khorshidi et al., 2014; Håti et al., 2016), anchors (Abbyad et al., 2011), and hydrodynamic drop traps (Shi et al., 2008; Bai et al., 2010; Bithi and Vanapalli, 2010; Sun et al., 2011), unrealistic for small scale microfluidic drops.

PDMS Devices Require Oil/Water Soaking Treatment to Successfully Incubate Drops

The diffusion of water in stored emulsions within PDMS devices is a widely observed challenge for maintaining drop volumes (Shim et al., 2007, 2009; Huebner et al., 2009; Schmitz et al., 2009; Pan et al., 2011; Dewan et al., 2012; Amselem et al., 2016), which is also demonstrated in this work (**Figures 2B–D**). In prior work (Shim et al., 2007, 2009; Pan et al., 2011; Dewan et al., 2012; Khorshidi et al., 2014), water only reservoirs and soaking techniques have been used to maintain drop volumes. Similarly, we submerge the DropSOAC device both prior to and during imaging, but unlike prior work, water-saturated oil instead of water is used as the submersion liquid. The use of water-saturated fluorocarbon oil as the submersion liquid requires that the device also be designed to limit the evaporation of the highly volatile oil, which can be accomplished using a tight-lidded Petri dish in the DropSOAC capsule. Lidding the device

produces a liquid-tight, evaporation-reducing chamber that can be filled with fluid to maintain PDMS device submersion during imaging. The DropSOAC capsule provides a simple solution that allows for compatibility with CLSM and microscope stage-top incubation. The oil/water soak in the DropSOAC method resulted in no significant change in drop volume after 21.5 h of storage, which was demonstrated to be more effective than water only soaking methods used in previous studies of drops in a similar fluorinated oil continuous phase (3 M Fluorinert FC-40). These studies exhibited up to a 12% decrease in volume over 16 h (Amselem et al., 2016), and a 10% decrease in volume over 20 h (Shim et al., 2009). In addition, the DropSOAC method prevents the need for more complicated device fabrication, such as embedding a diffusion limiting glass layer above the drop storage areas (Schmitz et al., 2009), or a custom-made glass chamber (Boitard et al., 2012).

The DropSOAC Method for Soaking PDMS Results in Better Drop Stability Than in Oil or Water Alone

We observe varying drop stability depending on the fluid used to soak and fill the DropSOAC capsule. This is due to the partial miscibility of the water phase in the fluorocarbon oil phase and vice versa. The stability of the drop emulsion depends upon whether the drops are in contact with (i) water-saturated oil, (ii) oil only, or (iii) water only reservoirs in the surrounding PDMS matrix. (i) Drops incubated in PDMS soaked in a water-saturated oil bath maintain their drop volume, position, and geometry during 4.5 h of stage top incubation and CLSM imaging (**Figure 2A**). Furthermore, when applied to single cell studies of *P. aeruginosa* in drops, drops remained stable for 21.5 h. In the oil/water system, the PDMS is filled with water-saturated oil by placing the DropSOAC device in a large reservoir containing oil in contact with water (approximately 400 mL of each fluid) for at least 24 h at 37°C. This ensures phase equilibrium in which the concentration of each phase in the other phase approaches maximum solubility. Drops stored in a device that is soaked with oil/water solution maintain their volume because the thermodynamically driven, spontaneous transport of water from drops into the surrounding oil is minimized with an already water-saturated oil phase. (ii) By contrast, drops incubated in PDMS soaked in unsaturated oil shrink over 4.5 h while maintaining spherical geometry (**Figure 2B**). If given more time, the drops shrink until they are no longer observable. This is a result of water diffusion into the oil phase to achieve phase equilibrium in the system. Further experimentation is necessary to measure the solubility of the water in the fluorocarbon phase and to determine the kinetics of this transport. (iii) Finally, drops incubated in PDMS soaked in water also shrink and undergo geometric changes from flattened spheres to polyhedral volumes with facetted faces in which the drops are compressed against one another. This transition occurs rapidly, within the first 30 min after the drops are introduced into the device (**Figure 2C** shows $t = 1$ h, but the onset of this transition happens earlier). We hypothesize that drop shrinkage and compression are due to transport of both water and oil from the emulsion to the water reservoir in the PDMS. Drop shrinkage may occur due to coarsening of the small water drops into the larger water reservoir in the PDMS, while drop compression may occur due to surfactant depletion forces or drainage of the oil phase between neighboring drops, as observed in a similar system (Courtois et al., 2008). In the surfactant depletion mechanism, the oil phase of the drop emulsion solubilizes into the surrounding PDMS water reservoir, concentrating the surfactant in the oil phase. The increased surfactant concentration promotes the formation of reverse micelles. The presence of reverse micelles in the oil phase is expected, as our surfactant concentration is at 1.5 wt%, which is greater than the critical micelle concentration (CMC) of the surfactant (Wagner et al., 2016; Scanga et al., 2018). Thus, increased surfactant concentration should create additional micelles in solution. These micelles are capable of inducing depletion-attraction aggregation of drops due to the localized exclusion of micelles between drop interfaces. The micelles may also aid in transport of water from the drops to the surrounding PDMS water reservoir. Further experimentation is necessary to test the presence and effect of micelles; however, similar observations have been made in which drops aggregate due to absorption of the oil phase into the PDMS (Courtois et al., 2008).

The DropSOAC Method Allows for Analysis of Single Cell Growth Kinetics and Quantification of Heterogeneity in Microbial Populations

Using the DropSOAC device to stabilize drops, we were able to monitor growth heterogeneity within clonal populations of *P. aeruginosa* PAO1 and its Δ*hpf* mutant derivative. Our results show that PAO1 has a small standard deviation for the lag time, and that growth curves were tightly clustered. We are also able to track cells that did not grow. Though the average growth rate of both the wild-type and the Δ*hpf* mutant cells were similar under these conditions ($0.38\ h^{-1} \pm 0.12\ h^{-1}$ and $0.36\ h^{-1} \pm 0.08\ h^{-1}$), the lag time following 4 days of starvation differed. Consistent with our previous study (Akiyama et al., 2017), 86.6% ± 2.5% of the Δ*hpf* mutant cells were unable to recover from starvation and remained as single cells. The cells that recovered had extended and variable lag times, ranging from 3 h to 17.5 h. The Δ*hpf* strain lacks the hibernation promotion factor protein, a ribosomal accessory protein that helps maintain ribosome integrity during starvation. The heterogeneity in lag time in the Δ*hpf* mutant indicates that different cells have varied ability to perform *de novo* protein synthesis and grow following starvation (Akiyama et al., 2017).

The DropSOAC (Drop Stabilization on a Chip) Approach Is a Simple Method Used to Stabilize Thousands of 15 μm Diameter Drops on a Chip

The DropSOAC approach allows for real-time data acquisition of drops in a static array, circumventing the need to sample drops at various time points. We have demonstrated that DropSOAC allows observation of up to hundreds of single cells in <20 μm

diameter drops to quantify heterogeneity in recovery rate of starved bacterial cells. Approximately 145,000 drops of this size can be observed using one DropSOAC capsule. Larger designs can potentially accommodate up to millions of drops as the methods of soaking the PDMS in phase-equilibrated solutions are applicable to larger devices. The advantage of this method is in its simplicity. Compared to other microfluidic fabrication methods used to store drops on chip, such as glass fabrication (Boitard et al., 2012), pumps and valves to compartmentalize cells (Thorsen et al., 2002; Leung et al., 2012), multilayer PDMS devices with water reservoirs (Dewan et al., 2012; Leung et al., 2012), floating or sunken arrays (Shim et al., 2009; Khorshidi et al., 2014; Håti et al., 2016), or fabricating channels on a microfluidic device to trap single cells (Balaban et al., 2004; Rowat et al., 2009; Wang et al., 2010), the DropSOAC approach simply uses a tight-lidded Petri dish to maintain fluid phase equilibrium in the PDMS surrounding the drops. The enclosed, transportable, and compact DropSOAC capsule allows drops to remain stationary and maintain their size over long hours of time-lapse imaging. Greater than one order of magnitude more drops can be stored on chip using DropSOAC compared to prior work (Shi et al., 2008; Huebner et al., 2009; Schmitz et al., 2009; Shim et al., 2009; Bithi and Vanapalli, 2010; Sun et al., 2011; Dewan et al., 2012; Leung et al., 2012; Khorshidi et al., 2014) This is due to the smaller size of these drops and the ability to pack them together so that they are neighboring, while simultaneously stabilizing the drops against coalescence, coarsening, shrinking and aggregation. We have not tested the stability of the drops on chip for over 21.5 h, as this time span was long enough to capture the growth dynamics of the bacterial cells. However, we hypothesize that drops will remain stable as long as the DropSOAC capsule is completely sealed to evaporation and the contents of the drops do not affect drop stability. In the latter case, examples could include bacteria producing molecules that change the surface tension between drops, and osmotic pressure differences between drops containing bacteria and drops containing media leading to coarsening of the drops.

Drop stability during storage in PDMS devices is a challenge observed for water-in-oil emulsions, regardless of the oils used, such as other fluorinated oils (3 M Fluorinert) (Schmitz et al., 2009; Shim et al., 2009, 2011; Knowles et al., 2011; Dammann et al., 2012; Lagus and Edd, 2013; Khorshidi et al., 2014; Shemesh et al., 2014) or mineral oil (Courtois et al., 2008; Courtois et al., 2009; Huebner et al., 2009; Bai et al., 2010; Dewan et al., 2012). Applying the DropSOAC approach used here to other systems may provide improved emulsion stability. In addition, other emulsion formulations may provide even better drop stability than demonstrated in our system, such as emulsions formulated with a less volatile oil as the continuous phase, or oil and water phases in which the partial solubility of one phase in another is much lower. Certainly, other device materials such as glass (Boitard et al., 2012) and optical adhesive (Abbyad et al., 2011) can be used to prevent evaporation; however, these materials may have other disadvantages in their lack of optical transparency, resolution, ease of fabrication, and oxygen permeability. Further investigation is necessary to test the effects of laser exposure on the cells in drops when imaging under confocal microscopy, and to test the effects of oxygen and nutrient limitation in the DropSOAC capsule. Nonetheless, in this work, we have demonstrated the utility of DropSOAC in stabilizing tens of thousands of drops on chip for long-term, time-lapse imaging over 20 h. We used DropSOAC to obtain growth curves of hundreds of single cells, providing insight into the behavior of individual cells within a clonal population, which can easily be scaled up to thousands of cells. Other advantages of the DropSOAC approach include the ability to recover the drops from the device for downstream analysis or sequencing and the general applicability of the soaking method, which can be easily adapted to other types of geometries and drop sizes on chip.

CONCLUSION

The DropSOAC (Drop Stabilization On A Chip) method for preparing PDMS microfluidic devices stabilizes the position, volume, and geometry of <20 μm diameter water-in-oil drops in a static array for over 20 h. This is achieved by soaking the PDMS device in a water-saturated oil phase using a simple modified Petri dish with a tight-fitting lid. The DropSOAC method maintains phase equilibrium of the drop emulsion within the porous PDMS material structure throughout the course of drop storage and imaging. With this approach, the heterogeneity in growth rate and lag time of hundreds of cells within a clonal population of bacteria and its mutant derivative can be quantified using time-lapse confocal imaging. We expect that the DropSOAC approach can be widely applied toward the incubation and imaging of other microorganisms to observe individual cell growth kinetics of a population over time.

DATA AVAILABILITY

All datasets generated for this study are included in the manuscript/**Supplementary Files**.

AUTHOR CONTRIBUTIONS

SP, TA, KW, MF, and CC designed the study. SP, TA, and KW conducted the laboratory experiments. GZ and SP analyzed the data. SP, MF, and CC wrote the manuscript with contributions from all other authors.

FUNDING

This work was funded in part by the National Institutes of Health (National Institute of Allergy and Infectious Diseases) Grant AI140163 (MF and CC), National Science Foundation Grant 1736255 (CC), National Science Foundation CAREER Grant 1753352 (CC), and Thermal Biology Institute and the Vice President of Research and Economic Development at Montana State University (SP).

ACKNOWLEDGMENTS

We thank Neerja Zambare and Nada Naser for testing iterations of the DropSOAC capsule; Drs. Thomas Mason, James Wilking, Henry Fu, Howard Stone, Robin Gerlach, and Joe Seymour for helpful discussions; Dr. Emma Loveday for assistance with data plotting; Betsey Pitts, Dr. Heidi Smith, and the Center for Biofilm Engineering at Montana State University for microscopy assistance and facilities; Joe Eldring, Glen Foster, and the Montana State University Mechanical Engineering Machining Lab for assistance with the laser cutter; and Dr. Albert Parker for assistance with data analysis and statistics.

SUPPLEMENTARY MATERIAL

The Supplementary Material for this article can be found online at: https://www.frontiersin.org/articles/10.3389/fmicb.2019.02112/full#supplementary-material

REFERENCES

Abbyad, P., Dangla, R., Alexandrou, A., and Baroud, C. N. (2011). Rails and anchors: guiding and trapping droplet microreactors in two dimensions. *Lab. Chip* 11, 813–821. doi: 10.1039/c0lc00104j

Akiyama, T., Williamson, K. S., Schaefer, R., Pratt, S., Chang, C. B., and Franklin, M. J. (2017). Resuscitation of *Pseudomonas aeruginosa* from dormancy requires hibernation promoting factor (PA4463) for ribosome preservation. *Proc. Natl. Acad. Sci. U.S.A.* 114, 3204–3209. doi: 10.1073/pnas.1700695114

Allegrucci, M., and Sauer, K. (2007). Characterization of colony morphology variants isolated from *Streptococcus pneumoniae* biofilms. *J. Bacteriol.* 189, 2030–2038. doi: 10.1128/jb.01369-06

Amselem, G., Guermonprez, C., Drogue, B., Michelin, S., and Baroud, C. N. (2016). Universal microfluidic platform for bioassays in anchored droplets. *Lab Chip* 16, 4200–4211. doi: 10.1039/c6lc00968a

Bai, Y., He, X., Liu, D., Patil, S. N., Bratton, D., Huebner, A., et al. (2010). A double droplet trap system for studying mass transport across a droplet-droplet interface. *Lab Chip* 10, 1281–1285. doi: 10.1039/b925133b

Balaban, N. Q., Gerdes, K., Lewis, K., and McKinney, J. D. (2013). A problem of persistence: still more questions than answers? *Nat. Rev. Microbiol.* 11, 587–591. doi: 10.1038/nrmicro3076

Balaban, N. Q., Merrin, J., Chait, R., Kowalik, L., and Leibler, S. (2004). Bacterial persistence as a phenotypic switch. *Science* 305, 1622–1625. doi: 10.1126/science.1099390

Bithi, S. S., and Vanapalli, S. A. (2010). Behavior of a train of droplets in a fluidic network with hydrodynamic traps. *Biomicrofluidics* 4:044110. doi: 10.1063/1.3523053

Boitard, L., Cottinet, D., Kleinschmitt, C., Bremond, N., Baudry, J., Yvert, G., et al. (2012). Monitoring single-cell bioenergetics via the coarsening of emulsion droplets. *Proc. Natl. Acad. Sci. U.S.A.* 109, 7181–7186. doi: 10.1073/pnas.1200894109

Brehm-Stecher, B. F., and Johnson, E. A. (2004). Single-cell microbiology: tools, technologies, and applications. *Microbiol. Mol. Biol. Rev.* 68, 538–559. doi: 10.1128/mmbr.68.3.538-559.2004

Chang, C. B., Wilking, J. N., Kim, S. H., Shum, H. C., and Weitz, D. A. (2015). Monodisperse emulsion drop microenvironments for bacterial biofilm growth. *Small* 11, 3954–3961. doi: 10.1002/smll.201403125

Courtois, F., Olguin, L. F., Whyte, G., Bratton, D., Huck, W. T., Abell, C., et al. (2008). An integrated device for monitoring time-dependent in vitro expression from single genes in picolitre droplets. *Chembiochem* 9, 439–446. doi: 10.1002/cbic.200700536

Courtois, F., Olguin, L. F., Whyte, G., Theberge, A. B., Huck, W. T., Hollfelder, F., et al. (2009). Controlling the retention of small molecules in emulsion microdroplets for use in cell-based assays. *Anal. Chem.* 81, 3008–3016. doi: 10.1021/ac802658n

Dammann, C., Nöding, B., and Köster, S. (2012). Vimentin networks at tunable ion-concentration in microfluidic drops. *Biomicrofluidics* 6:022009. doi: 10.1063/1.4705103

Dewan, A., Kim, J., McLean, R. H., Vanapalli, S. A., and Karim, M. N. (2012). Growth kinetics of microalgae in microfluidic static droplet arrays. *Biotechnol. Bioeng.* 109, 2987–2996. doi: 10.1002/bit.24568

Duffy, D. C., McDonald, J. C., Schueller, O. J., and Whitesides, G. M. (1998). Rapid prototyping of microfluidic systems in poly (dimethylsiloxane). *Anal. Chem.* 70, 4974–4984. doi: 10.1021/ac980656z

Franklin, M. J., Chang, C. B., Akiyama, T., and Bothner, B. (2015). New technologies for studying biofilms. *Microbiol. Spectr.* 3, 1–23. doi: 10.1128/microbiolspec.MB-0016-2014

Gerdes, K., and Maisonneuve, E. (2012). Bacterial persistence and toxin-antitoxin loci. *Annu. Rev. Microbiol.* 66, 103–123. doi: 10.1146/annurev-micro-092611-150159

Hansen, S. K., Haagensen, J. A., Gjermansen, M., Jorgensen, T. M., Tolker-Nielsen, T., and Molin, S. (2007). Characterization of a *Pseudomonas putida* rough variant evolved in a mixed-species biofilm with Acinetobacter sp. *strain C6. J. Bacteriol.* 189, 4932–4943. doi: 10.1128/jb.00041-07

Hâti, A. G., Arnfinnsdottir, N. B., Østevold, C., Sletmoen, M., Etienne, G., Amstad, E., et al. (2016). Microarrays for the study of compartmentalized microorganisms in alginate microbeads and (W/O/W) double emulsions. *RSC Adv.* 6, 114830–114842. doi: 10.1039/c6ra23945e

Holtze, C., Rowat, A. C., Agresti, J. J., Hutchison, J. B., Angile, F. E., Schmitz, H. J., et al. (2008). Biocompatible surfactants for water-in-fluorocarbon emulsions. *Lab Chip* 8, 1632–1639. doi: 10.1039/b806706f

Huebner, A., Bratton, D., Whyte, G., Yang, M., Abell, C., and Hollfelder, F. (2009). Static microdroplet arrays: a microfluidic device for droplet trapping, incubation and release for enzymatic and cell-based assays. *Lab Chip* 9, 692–698. doi: 10.1039/b813709a

Khorshidi, M. A., Rajeswari, K. P., Wählby, C., Joensson, H. N., and Svahn, H. A. (2014). Automated analysis of dynamic behavior of single cells in picoliter droplets. *Lab Chip* 14, 931–937. doi: 10.1039/c3lc51136g

Knowles, T. P., White, D. A., Abate, A. R., Agresti, J. J., Cohen, S. I., Sperling, R. A., et al. (2011). Observation of spatial propagation of amyloid assembly from single nuclei. *Proc. Natl. Acad. Sci. U.S.A* 108, 14746–14751. doi: 10.1073/pnas.1105555108

Köster, S., Angile, F. E., Duan, H., Agresti, J. J., Wintner, A., Schmitz, C., et al. (2008). Drop-based microfluidic devices for encapsulation of single cells. *Lab Chip* 8, 1110–1115. doi: 10.1039/b802941e

Köster, S., Evilevitch, A., Jeembaeva, M., and Weitz, D. A. (2009). Influence of internal capsid pressure on viral infection by phage λ. *Biophys. J.* 97, 1525–1529. doi: 10.1016/j.bpj.2009.07.007

Lagus, T. P., and Edd, J. F. (2013). High-throughput co-encapsulation of self-ordered cell trains: cell pair interactions in microdroplets. *RSC Adv.* 3, 20512–20522.

Leung, K., Zahn, H., Leaver, T., Konwar, K. M., Hanson, N. W., Pagé, A. P., et al. (2012). A programmable droplet-based microfluidic device applied to multiparameter analysis of single microbes and microbial communities. *Proc. Natl. Acad. Sci. U.S.A.* 109, 7665–7670. doi: 10.1073/pnas.1106752109

Lewis, K. (2007). Persister cells, dormancy and infectious disease. *Nat. Rev. Microbiol.* 5, 48–56. doi: 10.1038/nrmicro1557

Lyczak, J. B., Cannon, C. L., and Pier, G. B. (2002). Lung infections associated with cystic fibrosis. *Clin. Microbiol. Rev.* 15, 194–222.

McEllistrem, M. C., Ransford, J. V., and Khan, S. A. (2007). Characterization of in vitro biofilm-associated pneumococcal phase variants of a clinically relevant serotype 3 clone. *J. Clin. Microbiol.* 45, 97–101. doi: 10.1128/jcm.01658-06

Nivens, D. E., Ohman, D. E., Williams, J., and Franklin, M. J. (2001). Role of alginate and its O acetylation in formation of *Pseudomonas aeruginosa* microcolonies and biofilms. *J. Bacteriol.* 183, 1047–1057. doi: 10.1128/jb.183.3.1047-1057.2001

Pan, J., Stephenson, A. L., Kazamia, E., Huck, W. T., Dennis, J. S., Smith, A. G., et al. (2011). Quantitative tracking of the growth of individual algal cells in microdroplet compartments. *Integr. Biol.* 3, 1043–1051. doi: 10.1039/c1ib00033k

Rowat, A. C., Bird, J. C., Agresti, J. J., Rando, O. J., and Weitz, D. A. (2009). Tracking lineages of single cells in lines using a microfluidic device. *Proc. Natl. Acad. Sci. U.S.A.* 106, 18149–18154. doi: 10.1073/pnas.0903163106

Rueden, C. T., Schindelin, J., Hiner, M. C., DeZonia, B. E., Walter, A. E., Arena, E. T., et al. (2017). ImageJ2: imageJ for the next generation of scientific image data. *BMC Bioinformatics* 18:529. doi: 10.1186/s12859-017-1934-z

Scanga, R., Chrastecka, L., Mohammad, R., Meadows, A., Quan, P.-L., and Brouzes, E. (2018). Click chemistry approaches to expand the repertoire of PEG-based fluorinated surfactants for droplet microfluidics. *RSC Adv.* 8, 12960–12974. doi: 10.1039/c8ra01254g

Schindelin, J., Arganda-Carreras, I., Frise, E., Kaynig, V., Longair, M., Pietzsch, T., et al. (2012). Fiji: an open-source platform for biological-image analysis. *Nat. Methods* 9, 676–682. doi: 10.1038/nmeth.2019

Schmitz, C. H., Rowat, A. C., Köster, S., and Weitz, D. A. (2009). Dropspots: a picoliter array in a microfluidic device. *Lab Chip* 9, 44–49. doi: 10.1039/b809670h

Shemesh, J., Arye, T. B., Avesar, J., Kang, J. H., Fine, A., Super, M., et al. (2014). Stationary nanoliter droplet array with a substrate of choice for single adherent/nonadherent cell incubation and analysis. *Proc. Natl. Acad. Sci. U.S.A.* 111, 11293–11298. doi: 10.1073/pnas.1404472111

Shi, W., Qin, J., Ye, N., and Lin, B. (2008). Droplet-based microfluidic system for individual Caenorhabditis elegans assay. *Lab Chip* 8, 1432–1435. doi: 10.1039/b808753a

Shim, J.-U., Cristobal, G., Link, D. R., Thorsen, T., Jia, Y., Piattelli, K., et al. (2007). Control and measurement of the phase behavior of aqueous solutions using microfluidics. *J. Am. Chem. Soc.* 129, 8825–8835. doi: 10.1021/ja071820f

Shim, J.-U., Olguin, L. F., Whyte, G., Scott, D., Babtie, A., Abell, C., et al. (2009). Simultaneous determination of gene expression and enzymatic activity in individual bacterial cells in microdroplet compartments. *J. Am. Chem. Soc.* 131, 15251–15256. doi: 10.1021/ja904823z

Shim, J.-U., Patil, S. N., Hodgkinson, J. T., Bowden, S. D., Spring, D. R., Welch, M., et al. (2011). Controlling the contents of microdroplets by exploiting the permeability of PDMS. *Lab Chip* 11, 1132–1137. doi: 10.1039/c0lc00615g

Stewart, P. S., and Franklin, M. J. (2008). Physiological heterogeneity in biofilms. *Nat. Rev. Microbiol.* 6, 199–210. doi: 10.1038/nrmicro1838

Stoodley, P., Sauer, K., Davies, D. G., and Costerton, J. W. (2002). Biofilms as complex differentiated communities. *Annu. Rev. Microbiol.* 56, 187–209. doi: 10.1146/annurev.micro.56.012302.160705

Sun, M., Bithi, S. S., and Vanapalli, S. A. (2011). Microfluidic static droplet arrays with tuneable gradients in material composition. *Lab Chip* 11, 3949–3952. doi: 10.1039/c1lc20709a

Thorsen, T., Maerkl, S. J., and Quake, S. R. (2002). Microfluidic large-scale integration. *Science* 298, 580–584. doi: 10.1126/science.1076996

Tinevez, J.-Y., Perry, N., Schindelin, J., Hoopes, G. M., Reynolds, G. D., Laplantine, E., et al. (2017). TrackMate: an open and extensible platform for single-particle tracking. *Methods* 115, 80–90. doi: 10.1016/j.ymeth.2016.09.016

Wagner, O., Thiele, J., Weinhart, M., Mazutis, L., Weitz, D. A., Huck, W. T., et al. (2016). Biocompatible fluorinated polyglycerols for droplet microfluidics as an alternative to PEG-based copolymer surfactants. *Lab Chip* 16, 65–69. doi: 10.1039/c5lc00823a

Wang, P., Robert, L., Pelletier, J., Dang, W. L., Taddei, F., Wright, A., et al. (2010). Robust growth of *Escherichia coli*. *Curr. Biol.* 20, 1099–1103.

Weibel, D. B., DiLuzio, W. R., and Whitesides, G. M. (2007). Microfabrication meets microbiology. *Nat. Rev. Microbiol.* 5, 209–218. doi: 10.1038/nrmicro1616

Conflict of Interest Statement: The authors declare that the research was conducted in the absence of any commercial or financial relationships that could be construed as a potential conflict of interest.

CHAPTER FOUR

SINGLE-CELL BACTERIAL CULTURING USING PERMEABLE HYDROGEL-SHELLED MICROCAPSULES

Contribution of Authors and Co-Authors

Manuscript in Chapter 4

Author: Shawna L. Pratt

Contributions: Shawna Pratt designed all studies in this paper, conducted the laboratory experiments, analyzed all data, and wrote the manuscript.

Co-Author: Kerry S. Williamson

Contributions: Kerry Williamson contributed to bacterial study design, conducting experiments, and manuscript editing.

Co-Author: Michael J. Franklin

Contributions: Michael Franklin contributed to study design and manuscript writing.

Co-Author: Connie B. Chang

Contributions: Connie Chang contributed to study design, and manuscript writing, and was the principal investigator or co-principal investigator on grants funding this work.

Manuscript Information

Shawna L. Pratt, Kerry S. Williamson, Michael J. Franklin, Connie B. Chang.

mBio

Status of Manuscript:

__X__ Prepared for submission to a peer-reviewed journal

_____ Officially submitted to a peer-reviewed journal

_____ Accepted by a peer-reviewed journal

_____Published in a peer-reviewed journal

American Society of Microbiology

Abstract

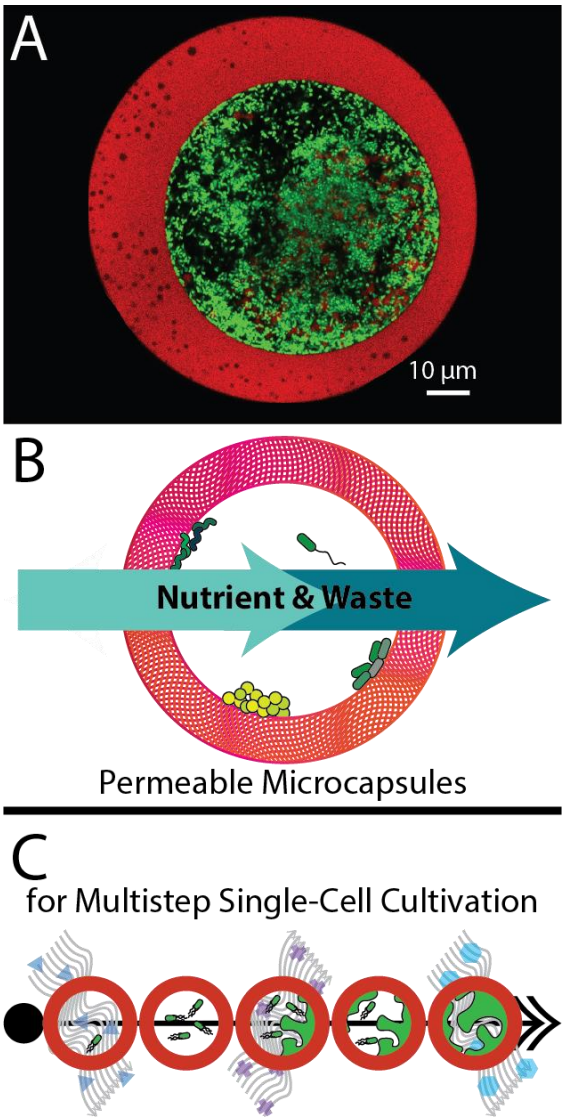

Figure 1: Graphical abstract of bacterial cultivation using microscale BioFlex capsules. A. *P. aeruginosa* PAO1 (pMF 230) expressing GFP grown in a BioFlex capsule. B. BioFlex capsules are permeable and allow for nutrient and waste transport between the capsule interior and exterior. C. Multiple chemical environment changes can be performed over time to observe the effect of varying antibiotic conditions upon single-cell growth.

Cell-to-cell heterogeneity in complex microbial communities such as biofilms can enable bacteria to survive antibiotic or bactericidal treatment due to small populations of cells that may have enhanced fitness under stressful conditions, which ultimately makes chronic infections such as cystic fibrosis lung infections challenging to treat. Single-cell methods can identify and isolate treatment-resistant microbial subpopulations to provide an evidence-based understanding of heterogeneity outcomes in these complex communities. Drop-based microfluidics, in which drops of water-in-oil can be used to encapsulate and culture individual cells, is a one such high-throughput method for investigating single cells. However, water-in-oil drop culture has several disadvantages, namely the possibility of emulsion destabilization during incubation [1], limited nutrient in nano- to picoliter drop volumes, and importantly, the inability to perform multiple chemical environment changes over time. The ability to transport nutrient and waste past the water and oil drop interfaces would enable observation of the effect of varying conditions upon single-cell growth. Here, we introduce a drop-based microfluidic method for generating hydrogel-shelled microcapsules, termed 'BioFlex' capsules, for observing single-cell cultivation and growth in contained microenvironments that are permeable to the surrounding media. The microscale hydrogel shells are biocompatible, tunable in size and composition, and allow for nutrient and waste exchange (Figure 1). We demonstrate the utility of the capsules by performing single-cell growth studies of *Pseudomonas aeruginosa* encapsulated within the capsules and subjected to varying antibiotic doses of ciprofloxacin over time. The BioFlex capsules provide a novel, high-throughput cultivation platform that can expand current single-cell methodologies for assaying cells in complex microbial communities and lend insight into the role of cellular heterogeneity in persistence infections.

Introduction

Single-cell studies can reveal the role of heterogeneity in the virulence and pathogenicity of chronic infections, including deadly cystic fibrosis lung infections and chronic wounds [72, 73]. Persistence, biofilm-associated heterogeneity, genetic divergence, and cooperative behaviors are all examples of cell-level traits that make microbial infections longer-lasting, more detrimental, and harder to treat [74]. The ability to assay many physiological parameters with single-cell resolution enhances research into the effects of single-cell-heterogeneity. However, the single-cell tool kit is not well-developed for conducting studies that require monitoring many single-cell inoculated populations over a long period of time, referred to as single-cell growth assays. Established single-cell resolved approaches include BONCAT [75, 76], FISH [77, 78], RAMAN or fluorescence-activated cell sorting (RACS and FACS, respectively) [79, 80], and single-cell sequencing [81]. Although powerful, these methods cannot track single-cells and single-cell lineages at multiple time points to evaluate physiology that evolves with time, such as growth. Approaches that do enable time-resolved data collection, such as microfluidic flow cell imaging [82, 83], compartmentalization [84], and microenvironment assays [85], provide single-cell resolved imaging data, but are low-throughput, with frequent sample sizes of 10's of cells or colonies. Utilizing this collection of methods requires selecting between high-throughput or time-resolved sampling, limiting the potential to monitor a large population of single cells over time.

In contrast to the above methods, drop-based microfluidic approaches [1, 58, 86] are uniquely valuable for high-throughput sample generation for single-cell resolved longitudinal studies. In drop-based microfluidic approaches, single cells and appropriate nutrients are isolated

inside water-in-oil drops. These drops can be collected and incubated in a microfluidic chamber for time-lapse imaging [1]. This methodology enables the study of microbial growth as an element of single-cell heterogeneity [86]. However, water-in-oil drop-based cultivation assays have two distinct drawbacks: (1) the drop storage environment must be carefully managed to maintain drop stability for time-lapse studies[1], and (2) water-in-oil drop interfaces have reduced permeability to nutrients and waste, meaning that microbial growth in drops is impacted by nutrient depletion and toxin accumulation [58]. Compounding these basic limitations, the ability to incorporate time-dependent chemical variables, such as antimicrobial dosing or transient nutrient environments, is technically challenging in drops; performing drop-based cultivation experiments with time-variation requires complex droplet processing such as picoinjection or droplet merging [87, 88].

Hydrogel-shelled capsules are particularly appealing as a solution for microbial single-cell cultivation due to (1) the permeability of hydrogels to aqueously soluble compounds, and (2) the hydrogel microsphere's liquid core, which can isolate single cells without imparting mechanical stress from embedment in a hydrogel network. Importantly, a permeable single-cell isolation method, like hydrogel capsules, would enable single-cell studies with easily varied chemical conditions. Only one prior study has demonstrated bacterial growth in hydrogel capsules [66] in a polyethylene glycol–diacrylate (PEG-DA) capsule, which requires photo-illumination and free-radical crosslinking chemistry. Polyethylene glycol (PEG) derivates are widely used in hydrogel formulations. However, PEG-maleimide is preferred over other PEG derivatives for cell and tissue cultivation due to the biocompatibility of the crosslinking process

[89], which proceeds at physiological pH, produces no by-products, and does not rely on free-radical based crosslinking cascades [90, 91].

Here, we present an optimized protocol to produce bacteria-encapsulating hydrogel microcapsules. The BioFlex capsule generation method produces permeable, biocompatible, hydrogel-shelled microcapsules developed specifically for single-cell microbial isolation and cultivation (Figure 1). In our approach, shell thickness and capsule size are easily varied during capsule production, without the need to modify device design or capsule precursor formulation. These advances are achieved by combining various microcapsule generation methods [44, 66, 69]; these methods were first developed for eukaryotic research. The resulting capsules enable longitudinal single-cell resolved microbial cultivation with multi-step processes or transient chemical conditions, broadening single-cell studies to systems requiring complex, time-varied parameters. Here, we demonstrate these capabilities, and the system's overall utility, by evaluating the growth of *Pseudomonas aeruginosa* PAO1 in capsules, before conducting a multi-step experiment where capsule-isolated single-cell lineages respond to varied antibiotic treatment schedules. Together, these studies demonstrate the power of the BioFlex method for producing highly tunable capsules, isolating and cultivating bacteria, and finally, employing these capsules to observe *P. aeruginosa* response to varied ciprofloxacin treatment schedules.

Materials and Methods

Core-Shell Templating Device Description and Fabrication

A novel microfluidic device was developed for generation of BioFlex microcapsules. The device's channel and junction architectures were modified from previously reported hydrogel-capsule generation devices [65, 69]. Compared with these devices, the channel architecture away from the channel junctions was modified to reduce backflow into the aqueous-phase channels by increasing the resistance in the aqueous channels compared to the outlet channel (Appendix C Figure 1). Computer aided design and fluid flow analysis were used to model and visualize this device (Appendix C Figure 1) (Autodesk Inventor, AutoCAD, and COMSOL).

The BioFlex capsule generation devices were fabricated in a manner consistent with previous PDMS-based non-planar flow-focusing device fabrication approaches [56]. The mold masters were made by patterning SU-8 3050 photoresist (Kayaku Advanced Materials) onto 4” silicon wafers (UniversityWafer, Inc.) using mylar patterning masks (ArtNetPro) and a photolithography contact aligner (ABM). Separate molds were generated for the top and bottom halves of the non-planar junction (Appendix C Figure 1). The top mold had two-layer thicknesses generated by a two-step SU-8 application and UV exposure process, resulting in a 45 µm layer and a 55 µm layer. The bottom mold had a single 10 µm thick layer of photoresist. The thicknesses of each layer and x-y feature fidelity in the mold masters were confirmed via optical profilometry (Filmetrics ProFilm 3D) (Appendix C Figure 1).

Together, the top and bottom mold set generated 14 microfluidic devices. After production, these molds were replicated in Sylgard 184 polydimethylsiloxane (DOW), referred to as PDMS. The bottom PDMS slab was 1-3 mm thick to ensure the microfluidic channels

could be visualized within the working distance of a 4x-20x microscope objective after bonding to a glass slide. After curing, the PDMS slabs were cut from the silicon wafer master molds. Ports were punched in the top slab using an EMS-Core Sampling Tool 0.75 mm biopsy punch (Electron Microscopy Sciences.)

The final devices were created via plasma bonding of the PDMS slabs and glass. To prepare for bonding, single devices were cut from the PDMS slabs corresponding to the top and bottom portions of the microfluidic device. Each slab had a smooth face and a featured face with depressions corresponding to the device channels. These single-device PDMS slabs and a 3 x 1in glass slide (VWR) were exposed to oxygen plasma (Harrick), taking care to ensure that plasma could reach both the top and bottom surface of the bottom PDMS slab. After plasma treatment, the smooth side of the bottom slab was bonded to the glass slide. A drop of 0.2 μm filtered distilled water was placed on the featured face of the bottom slab. The top slab was then placed on the bottom face, with a thin film of water between the featured faces. This thin film of water allowed the top slab to be translated across the bottom slab for alignment; without it, the bottom and top slabs immediately and irreversibly bonded upon contact. The features of both slabs were then visualized via brightfield microscopy and aligned by hand.

After alignment, the devices were cured at 65°C for a minimum of 12 h. The internal channel surfaces of the finished devices were made hydrophobic by filling the channels with a 0.2 μm-filtered solution of 10 μL/mL (tridecafluoro-1,1,2,2-tetrahydrooctyl) trichlorosilane (Gelest) in Novec HFE 7500 fluorinated oil (3M) and allowing this solution to deposit on the channel walls for 1 h at 65°C. For the inverted confocal flow characterization (Figure 2C) the

devices were bonded to a 25 x 40mm 1.5 coverglass (Electron Microscopy Sciences) in lieu of a 1x3 in slide.

Preparation of Microcapsule Components

All components were sterilized through a 0.2 µm PTFE (CELLTREAT Scientific Products) filter before use unless specified otherwise. The hydrogel precursor solution contained 200 mg/mL 10 kDa 4-arm polyethylene glycol – maleimide (4-arm PEG-mal) (Laysan Bio), 20 µL/mL 5.54 mg/mL Cy5.5- maleimide (Click Chemistry Tools) in DMSO (Sigma-Aldrich), and 1x phosphate buffered solution (PBS) (Becton, Dickinson and Company), pH 7.4. The core solution contained 260 mg/mL 10 kDa dextran (Chem-Impex, Intl.) suspended in 1x PBS. For capsule production, the dextran concentration was 260 mg/mL FITC-Dextran (10 kDa, 1 wt%) (Sigma Aldrich) was added to the dextran suspension for flow visualization via confocal microscopy (Figure 2 C). When incorporating bacterial cells in cores, filter-sterilized 300 mg/mL Dextran in PBS solution was added to the washed cell suspension and filter-sterilized PBS to achieve a final concentration of 260 mg/mL.

The oil solution contained 3 wt% Span™ 80 (TCI-chemical) dissolved in light mineral oil (Spectrum Chemical). The crosslinking nanoemulsion was a 1-part aqueous to 15-parts oil mixture of 0.2 µm filtered 50 mg/mL dithiothreitol (DTT) (Thermo Scientific) in 0.2 M / pH 8.0 triethanolamine (TEA) buffer solution (Thermo Scientific™) and 0.2 µm filtered 3 wt% Span80 in light mineral oil solution. This mixture of DTT and oil solutions was placed in a microcentrifuge tube and nano-emulsified using a wand sonicator. The microcentrifuge tube was kept in a -20 °C microcentrifuge tube cooler during sonication.

Microcapsule Generation

The flow of microcapsule components (core suspension, hydrogel precursor solution, oil solution, and crosslinking nanoemulsion) was driven from 1 or 3 mL leur lok syringes (BD) with 27 ga. leur lok needles (Excel Intl.) through microtubing (PE/2, Scientific Commodities) via syringe pumps (Harvard Apparatus) into the previously described microfluidic device through the device's four inlet ports. Flowrates used in the capsule size, shell thickness, and biological growth studies described in Figures 4-6 are listed in Appendix C tables 1-3. The resultant capsules flowed out of the microfluidic device and was collected into a 1.5 mL centrifuge tube (Eppendorf). Capsules were collected for 20 min for all biological studies in this paper. For abiotic studies, capsules were collected for 10-20 min. Time-resolved capsule generation (Figures 2 and 4) was visualized via brightfield microscopy on an inverted microscope (Eclipse Ti2 Series Inverted Microscope, Nikon) equipped with a high-speed camera (Phantom).

Post-collection, the capsules were washed to replace the mineral oil surrounding the capsules with aqueous media and facilitate diffusion of the dextran out of the capsule cores. Washing proceeded as follows: (1) The collection tube was centrifuged for 1 min at 500 x g, and the mineral oil supernatant was disposed. (2) Mineral oil (1 mL) was added to the collection tube and vortexed for 15 s or longer until capsule pellet was resuspended, before centrifugation for 1 min at 500 x g. The mineral oil supernatant was disposed after centrifugation. Step 2 was repeated twice. (3) Sterile PBS (1mL) was added to the collection tube and vortexed 15 s or longer to ensure capsule resuspension. The collection tube was centrifuged for 3 min at 500 x g. The aqueous supernatant and residual mineral oil were disposed after centrifugation. Step 3 is repeated 3 times. (4) PBS (50 µL) was added to the collection tube and vortexed for 30 s to break up any capsule clumps formed during centrifugation.

Capsule Shell Thickness and Diameter Analysis

Capsule shell thickness and diameter (Figure 4B, E) were determined from optically sectioned images of the capsules captured via inverted confocal laser scanning microscopy (iCLSM) (Stellaris DMI-8, Leica). The plane of the optical section analyzed corresponded with the mid-plane of the capsules' 3-D spherical structure. Images were thresholded by pixel intensity value to separate the core, shell, and background into 3 regions, and the areas of each region were quantified. To determine the percent capsule radius, the shell area was divided by the summed shell and core areas (Figure 4B). For each sample, 6-8 images were analyzed. Shell thickness was analyzed using base Fiji-ImageJ functionality. Capsule radius was determined by performing a Hough-transform on capsule images using the UCB vision sciences recommended workflow [92]. Images were intensity thresholded to separate shell and core from background prior to performing the Hough-transform processing. For each sample, the diameter of a minimum of 460 capsules was calculated. Statistical analysis and data representation was conducted in R-studio. Average and standard deviation values for shell thickness and capsule radius were calculated using a simple average and standard deviation.

ATPS Drop Production and Confocal Flow Visualization

Water-in-oil drops of the capsule precursor solutions were generated with simultaneous optically sectioned iCLSM imaging to determine the orientation of each phase during drop production (Figure 2C) and the equilibrium particle morphology of uncrosslinked mixtures of 4-arm PEG-mal and dextran in drops (Figure 3B.) Aqueous 10 kDa dextran and 10 kDa 4-arm PEG-mal solutions were prepared in a range of concentrations; the dextran concentrations were varied from 150-300 mg/mL and the 4-arm PEG-mal concentrations were varied from 50-240

mg/mL. The dextran and 4-arm PEG-mal solutions were labeled with 1 wt/wt% 10 kDa FITC-dextran (Sigma Aldrich) and 10 µL/mL 5.54 mg/mL Cy5.5 maleimide (Click Chemistry Tools) in dimethyl sulfoxide (Thermo Scientific), respectively.

For both the drop production imaging application and the equilibrium morphology study, drops of 4-arm PEG-mal and dextran were generated as described in the "Microcapsule Generation" methods section, with one significant protocol change: the drops were not crosslinked, and therefore DTT nanoemulsion was left out of the capsule generation process. To do this, the DTT nanoemulsion inlet on the microfluidic capsule generation device was plugged with a short section of tubing with a sealed end. During the drop imaging application, 200 mg/mL 4-arm PEG-mal solution and 200 mg/mL Dextran solutions were used, and during the equilibrium morphology study a combination of the various polymer concentrations was used. The flowrates used during droplet generation for phase separation analysis are described in Appendix C table 4. Phase orientation in the droplets was imaged using iCLSM.

Binodal Phase Separation Studies

Here, the binodal phase separation line was determined based on a human-eye visualized cloud-point titration [93] of dextran solution into 4-arm PEG-mal solution at laboratory room temperature (19-23°C.) No additional temperature control was included to manage temperature fluctuations during the titration and observation process. The titration was repeated for three technical replicates (Appendix C Figure 2). To conduct the titration, between 170 and 180 µL of 260 mg/mL 10 kDa dextran in water was dispensed into a spectrophotometric cuvette. 4-arm PEG-mal in water (350 mg/mL) was mixed in 5-10 µL increments with the cuvette contents via pipetting. After each 4-arm PEG-mal addition, the cuvette was backlit with diffuse white LED

light against a dark surface and observed by eye to evaluate turbidity. Once turbidity was achieved, water was added instead of 4-arm PEG-mal until the solution became clear. This sequence of adding 4-arm PEG-mal then water was repeated until the dextran in the cuvette was diluted to below 50 mg/mL. Throughout the titration process, the added volumes of dextran solution and water and the cloud and clarity transition points were recorded. Data processing and representation for the binodal diagram was conducted in Rstudio. An average curve and 95% confidence interval summarizing the results from the three phase separation trials were determined using Loess averaging (Figure 3).

Preparation of Bacteria for Encapsulation

Overnight cultures were prepared by incubating *Pseudomonas aeruginosa* PAO1 pMF230 [94] from frozen stocks in 125 mL baffled culture flasks containing 20 mL of tryptic soy broth (TSB) (Becton, Dickinson and Company) with 150 µg/mL carbenicillin (Fisher Scientific, Waltham, MA) for 12-15 h at 37 °C and 160 rpm shaking. Working cultures were prepared by incubating 100 µL overnight culture with 10 mL of TSB amended with 150 µg/mL carbenicillin in a 125 mL baffled culture flask for 4 h at 37 °C and 160 rpm shaking. One mL of the working culture was washed by centrifuging for 3min at 5000 × g, discarding the supernatant, and resuspending the pellet in 1 mL Phosphate Buffered Saline (PBS), pH 7.4 (Gibco, Thermo Fisher Scientific, Waltham, MA) by vortexing a minimum of 15 s. This process was repeated for a total of three centrifuge cycles. After the final washing cycle, the culture was incubated for 30 min at room temperature.

To prepare the core solution, the washed working culture was diluted 10-fold in PBS. Diluted culture was added to dextran-in-PBS solution at a ratio of 25 µL culture per 1 mL,

resulting in a final dextran concentration of 260 mg/mL in the core solution. The core solution was then used to generate capsules as described in the "Microcapsule generation" methods section.

Imaging and Quantification of Cell Growth

Time-lapse cultivation studies in the capsules were used to evaluate growth (Figures 5-7) and the effects of varying the timing of antibiotic introduction to cells growing in capsules (Figure 6-7). In the growth studies without antibiotic treatment (Figure 5), 10 µL of capsules and 200 µL of undiluted TSB were dispensed into wells on a chambered well slide (Cellvis). In the growth studies incorporating varied antibiotic introduction, 20 µL of capsules and 300 µL of 10^{-3} TSB in PBS with or without 0.1 µg/mL ciprofloxacin (Fluka) were dispensed. Additional 10^{-3} diluted TSB with or without ciprofloxacin was added after 4 h, 7 h, and 10 h of incubation. In these subsequent additions, the concentration of ciprofloxacin was adjusted to maintain a ciprofloxacin concentration of 1 µg/mL in the media around the capsules. For all time-lapse growth studies, the chambered cover glass was incubated at 37 °C in a microscope stage-top incubator (OKO Labs). Throughout incubation, z-stacks of the capsules were imaged at 30-40 min intervals using iCLSM (Leica).

The growth of bacteria in capsules (Figures 5, 7, Appendix C Figure 4) was calculated from XYZ-T imaging stacks collected via iCLSM during capsule incubation. Three biological replicates were conducted to analyze *P. aeruginosa* growth in TSB media in capsules (Figure 5). One biological replicate was conducted in the ciprofloxacin treatment assay (Figure 7). For each biological replicate in either assay, 3-4 imaging fields containing XYZ data were collected at 30-40 min intervals. Excitation and emission spectra collected during imaging corresponded to

Cy5.5 and green fluorescent protein. Gain and intensity values were consistent for all capsule cultivation experiments. The z-stack for each field of view at each time point was compressed into a single image using as a summed projection of pixel intensities. Each image was intensity thresholded to separate usable capsule data from discardable data. Usable data included cell-containing capsules where the entire capsule volume was captured in the z-stack, and fluorescent signal correlating to cell growth (GFP) from two different capsules did not overlap in the projected image. The ImageJ plugin "TrackMate" was used to quantify the fluorescence in each capsule at each time point. In the TSB growth assay, each field of view contained 5-54 cell-containing capsules that were analyzed for growth. In the ciprofloxacin treatment assay, each field of view contained 49-172 capsules that were analyzed for growth. The variation in this number reflects the variable concentration of capsules in the field of view. The resulting data was imported into Rstudio for data processing.

During processing, the average z-production summed fluorescence value in a sample of non-cell containing drops for each time point in each trial was calculated and the value was subtracted from the cell-containing capsule values to subtract fluorescence background. The background subtracted, summed intensity values for each capsule were plotted as summed fluorescence vs. time on a semi-log plot. To calculate the TSB-only capsule growth rates (Figure 5), natural log transformed fluorescence data for the period between 4.5 and 6 h, which corresponded to log-linear growth, was extracted. A linear regression was performed on the per-capsule fluorescence intensity values against time to determine the slope. The data sets for each trial were compiled and the mean growth rate value and standard deviation for capsule-based

growth on TSB was calculated using a mixed effects model with biological replicate and the field of view as random effects.

To calculate the onset of effect for the ciprofloxacin treatment assay, the dosage delivery time was subtracted from the time point corresponding to the onset of fluorescence decrease in an individual capsule-representing growth curve. A histogram of the effect timing incorporates each individual capsule observed for each treatment as an individual data point, and the averaged values reported in the text are simple averages. All reported time values for the time-varied growth studies inherently include a ± 40 min time, as response timing cannot be resolved below the 40 min imaging interval.

96 Well-Plate Growth Studies

Washed working cultures of *P. aeruginosa* PAO1, *P. aeruginosa* PAO1 pMF230, and *Escherichia coli* HB101 pMF230 [94] were prepared using the methods described in the "Preparation of bacteria for encapsulation" section. Following the 30 min incubation period, the optical density at 600 nm (OD_{600}) of the washed cultures was determined using an Ultrospec 2100 pro spectrophotometer (Amersham Biosciences). Cells were diluted to an OD_{600} of 1.0 in PBS (pH 7.4), and 10 µL volumes were used to inoculate the wells of sterile, black, clear bottom 96 well assay plates (Corning Incorporated) containing 190 µL media. Media conditions tested included PBS, TSB, and 1:10 V/V 4-arm PEG-mal microspheres (described below) in PBS, and 26 mg/mL dextran in PBS, to evaluate the potential of growth enhancement due to capsule components. All media conditions were amended with 150 µg/mL carbenicillin for use with the strains containing the pMF230 plasmid. For each type of media and strain, three wells were inoculated to serve as triplicate technical replicates. Positive growth control wells containing

TSB and negative sterile control wells containing media without cells were included in each assay. Microplates were lidded, sealed with parafilm, and incubated at 37°C with constant shaking in a Cytation 5 Microplate reader (Bio Tek Instruments). The OD_{600} and GFP fluorescence of each well were monitored every 15 minutes for 24 h. Five independent biological replicates were performed.

4-arm PEG-mal microspheres used to evaluate microbial ability to consume the capsule shell material were made using the same DTT nanoemulsion and 4-arm PEG-mal solution described in the "Microcapsule Components" methods section. The microspheres were generated as described in the "Microcapsule Generation" methods section, with one significant protocol change: the microspheres do not have a core, and therefore a dextran solution was left out of the capsule generation process. To do this, the core inlet on the microfluidic capsule generation device was plugged with a short section of tubing with a sealed end. The flowrates used during microsphere generation were 150 µL/h 4-arm PEG-mal solution, 800 µL/h span80/mineral oil solution, and 800 µL/h DTT nano emulsion.

The 96-well plate growth was calculated and analyzed using the same R analysis pipeline outlined for in-capsule growth analysis. In this method, each individual well was processed as analogous to an individual capsule, with exceptions made for the background subtraction approach and the timing of the log-linear growth period. The fluorescence measurements for non-GFP producing *P. aeruginosa* grown in wells was subtracted from the fluorescence measurements for GFP producing cells to subtract background fluorescence from the media from the fluorescence changes due to GFP production. The period assessed for growth in well plates was 2-3.75h.

Data Analysis and Representation

All imaging data was processed using Fiji/ImageJ [95]. Within ImageJ, the following plugins were used: the Hough circle transform [92] developed as part of the University of California, Berkeley Vision Sciences core grant NIH P30EY003176 and Track Mate7 [96]. Analysis and visualization of imaging data was performed in RStudio [97] using base R [98] with the following packages: tidyverse[99], ggplot2[100], dplyr[101], broom[102], modelr[103], scales[104], lme4[105], lmerTest[106], and a ridgeline plot coded in base R (https://github.com/R-CoderDotCom/ridgeline.)

For all boxplots, the boxplot elements represent: the median value of the data as a bar; the span of the 25th to 75th percentile, i.e. the 1st to 3rd quartile (Q1 and Q3, respectively) as a shaded box, i.e. the interquartile range (IQR); the minimum and maximum values, which are calculated as $Q1 - 1.5 \times IQR$ and $Q3 + 1.5 \times IQR$, represented as error bars; and outliers represented as points. The median and quartile ranges are calculated simply for all boxplots, and do not represent data from mixed effects models.

Results

Device Design, Hydrogel Selection, and Crosslinking Strategy to Optimize BioFlex Capsule Generation

The BioFlex method integrates microfluidic device design, hydrogel selection, and crosslinking strategy to generate hydrogel-shelled capsules for bacterial isolation and cultivation. Hundreds of capsules per second are produced in a non-planar microfluidic device by coflowing dextran and 4-arm PEG-maleimide solutions with mineral oil and a DTT nanoemulsion through microscale channels and channel junctions (Figure 2A-B, Appendix C Figure 1). During capsule

generation, the non-planar device design creates an annular flow of dextran-rich core solution in 4-arm PEG-mal shell precursor (Figure 2C). This flow intersects with mineral oil solution at a flow-focusing junction, forming drops of the aqueous phases in oil (Figure 2A-B). Upon droplet breakup, the annular flow profile created by the 3-D device construction translates to a radially heterogeneous droplet where 4-arm PEG-mal solution forms a shell-like layer at the drop's water-oil interface around a dextran-rich center.

The dextran–rich core and 4-arm PEG-mal shell precursor solutions are an aqueous two-phase system (ATPS), i.e., aqueous polymer solutions that phase separate when mixed at sufficiently high concentrations. The phase diagram of an ATPS describes the mixture compositions that result in either a homogenous solution or two-phase mixture. The separation between these states is the binodal curve, with a two-phase mixture above the curve and a single-phase solution below the curve (Figure 3A). Uncrosslinked drops of 4-arm PEG-mal and dextran demonstrate the ultimate state and geometric phase orientation of 4-arm PEG-mal and dextran mixtures above and below the phase-separation curve. Above the curve, drops form a Janus particle characterized by a geometrically eccentric dextran core surrounded by a layer of 4-arm PEG-mal [107], and below the curve, drops become a homogenous solution of both compounds (Figure 3B). Using an ATPS for the core and shell precursor solutions during capsule generation imparts a phase-separated interface between these solutions in the microfluidic device before drop breakup. This interface creates a distinct boundary between the core- and shell- regions in the capsules after shell crosslinking.

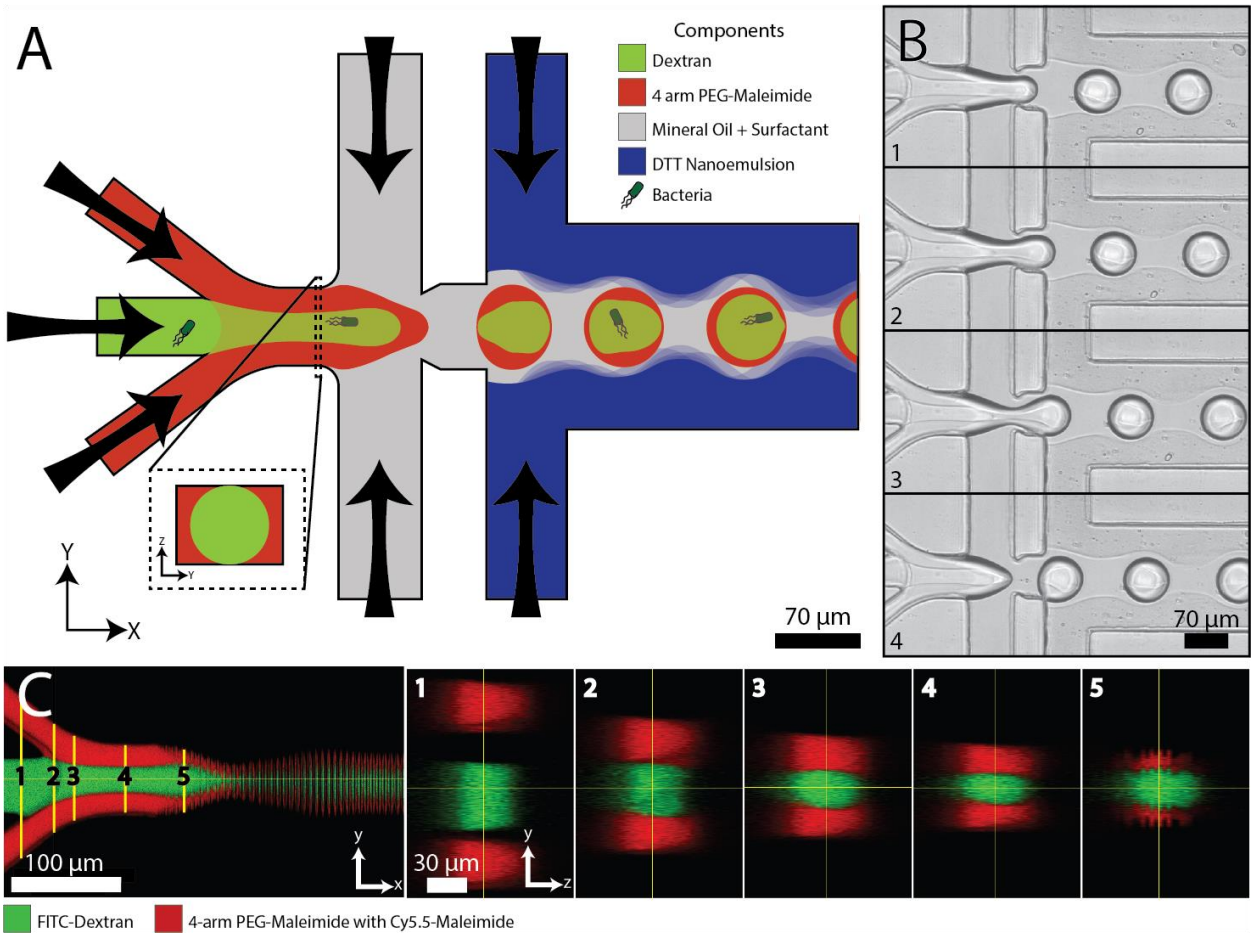

Figure 2: The BioFlex method utilizes drop-based microfluidics for high throughput generation of hydrogel-shelled, bacteria-encapsulating capsules. A. Capsules are generated in a co-axial, non-planar flow-focusing microfluidic device from four fluids: aqueous dextran (green), 4-arm PEG-mal (red), mineral oil/surfactant (gray) solution, and DTT nanoemulsion (blue). Bacteria are incorporated in the dextran solution for encapsulation. The device is designed to create a core-sheath upstream of droplet breakup (inset.) B. Capsule generation is high throughput. High-speed images (approx. 10^3 fps) show the sequence of droplet breakup. C. Orthogonal views of dextran (FITC labeled) and 4-arm PEG-mal (Cy5.5-maleimide labeled) flowing through a capsule generation device imaged via optical sectioning demonstrate the evolution of core-sheath flow profiles originating from the non-planar, coaxially aligned device design.

The merger of channels carrying DTT nanoemulsion with the stream of concentrically layered dextran in 4-arm PEG-mal drops downstream of the drop-breakup junction (Figure 2A-B) initiates crosslinking. DTT rapidly partitions into the aqueous drops[69, 108], and DTT's thiol

groups begin crosslinking the 4-arm PEG-mal, "freezing" the core-shell geometry as the 4-arm PEG-mal solidifies (Figure 3C). This strategy of introducing DTT downstream of the drop generation junction prevents gelation at the drop junction, which can cause device clogging[44].

After the final addition of DTT, the stream of crosslinking capsules, mineral oil, and DTT nanoemulsion exits the device and is collected in a microcentrifuge tube for further processing (Figure 2A). The dimensions and geometries of the capsule-generating device's channels are optimized so that the outlet channel segment has the least pressure drop of any channel on the device and the core channel has the greatest pressure drop (Appendix C Figure 1). This design feature aims to prevent the backflow of fluids within the device, especially into the aqueous channels, further easing device operation.

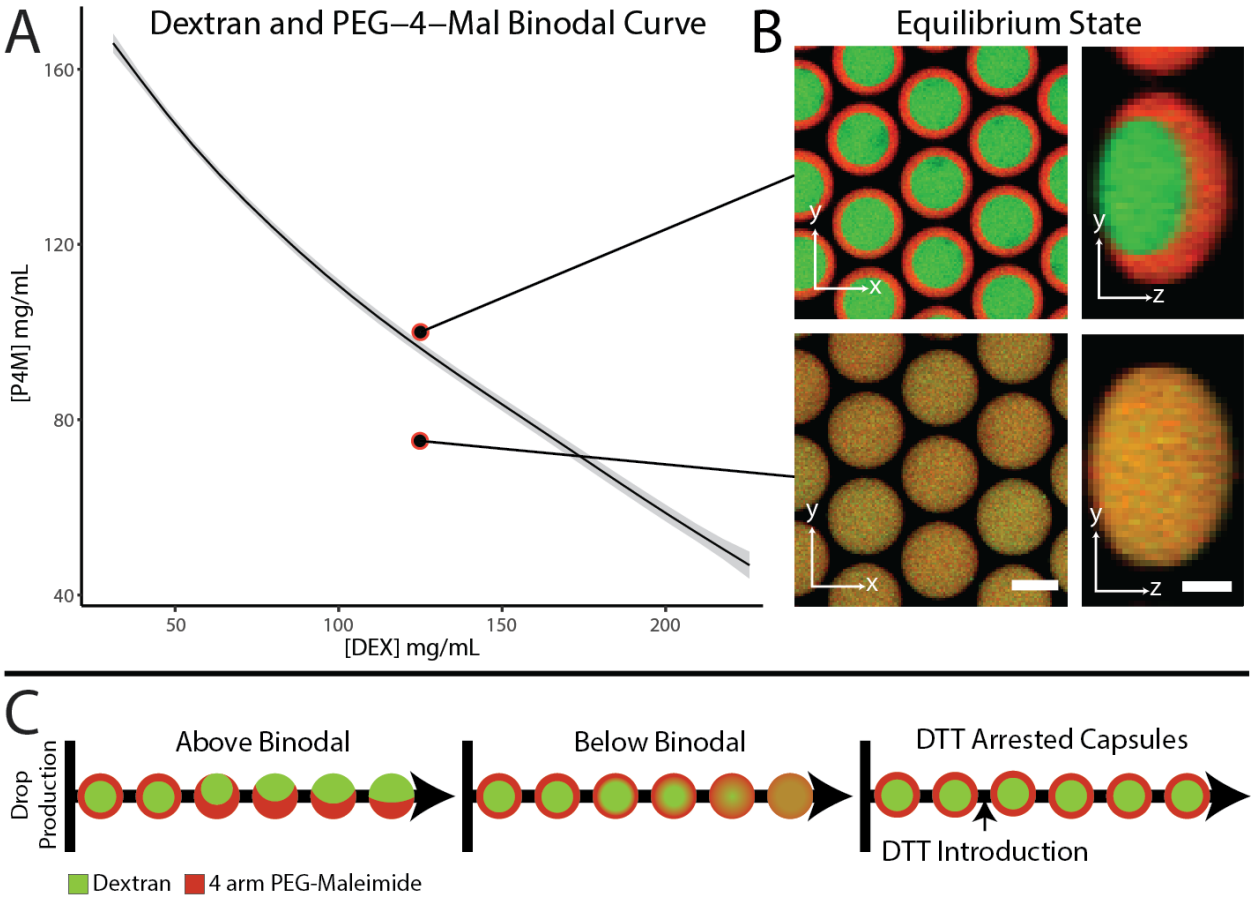

Figure 3: Location on the phase separation curve determines the equilibrium architecture of aqueous drops containing dextran and 4-arm PEG-mal. Introducing crosslinking agent 'freezes' drop architecture, preventing transition to equilibrium geometry. A. The binodal phase separation curve for 10kDa 4-arm PEG-mal and 10kDa dextran; concentrations below the curve (blue) are non-phase separating and concentrations above the curve (white) are phase separating. The binodal curve (black line) was determined via cloud point titration (three trials, loess fit). Gray regions indicate a 95% confidence interval of the loess fit average. B. Orthogonal optically sectioned microscopy of uncrosslinked dextran and 4-arm PEG-mal drops with phase separating (top) and miscible (bottom) concentrations of dextran and 4-arm PEG-mal: 125 mg/mL dextran / 100 mg/mL 4-arm PEG-mal and 125 mg/mL dextran / 75 mg/mL 4-arm PEG-mal, respectively.

Flowrate Controls Shell Thickness

The BioFlex method produces a wide range of capsule-shell thicknesses through flow-rate adjustments and without requiring adjustments to the capsule component formulation (Figure 4A-B). By decreasing the 4-arm PEG-mal volumetric flowrate from 80% to 30% of the

total aqueous flow, intact capsules were generated with shell thicknesses ranging from 28.1 ± 2.0% to 71.5 ± 0.9% of the total capsule radius. Core-shell capsules with defined core and shell regions were produced using 4-arm PEG-mal flowrates down to 10% of the total flow; however, capsules made with less than 30% 4-arm PEG-mal flow had poor structural integrity and consistency and, in many cases, did not form fully-enclosed, spherical capsules (Figure 4 A (5-6)). Specific flowrates used to generate each particle are listed in Appendix C table 1.

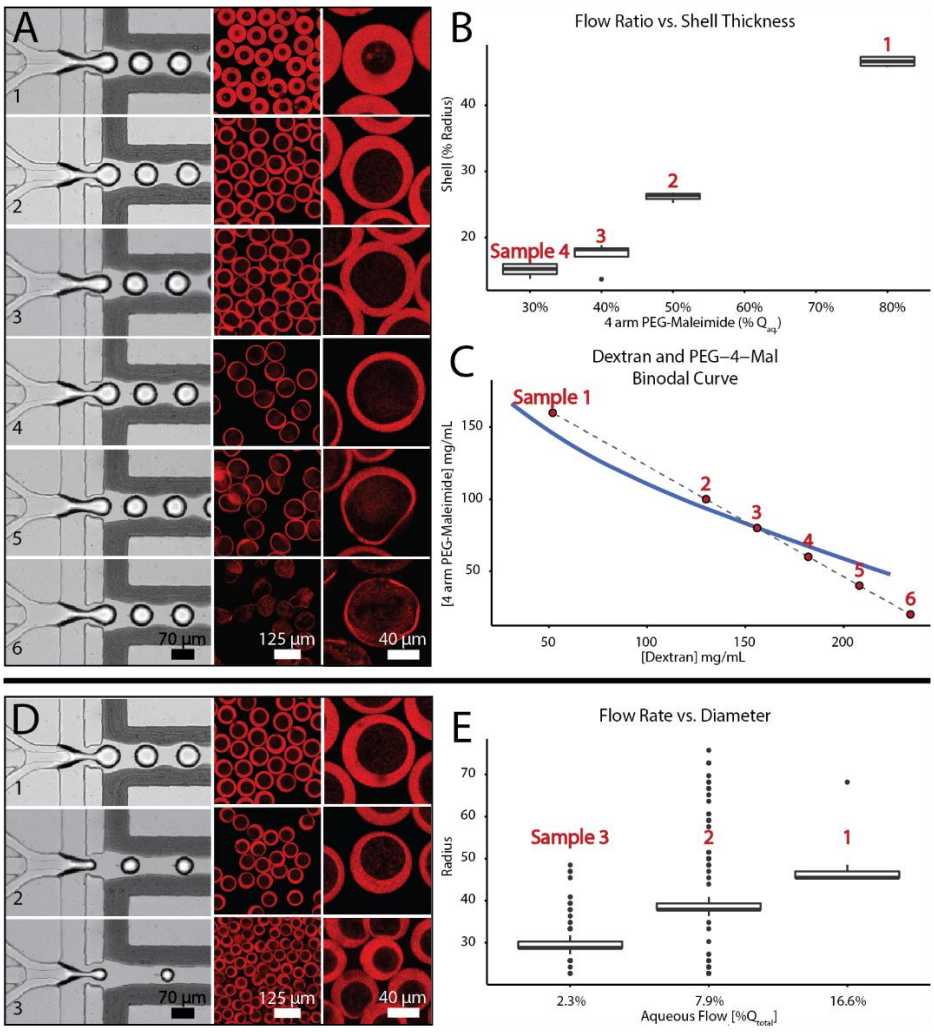

Figure 4: Flow rate controls shell thickness and capsule diameter. A-B. Adjusting the ratio of dextran to 4-arm PEG-mal volumetric flowrates (Q) alters capsule shell thickness. A. The left-side panels of each series are high-speed camera images of capsule generation. The right-side panels are CLSM images of capsules, taken at the capsules' mid plane. Cy5.5-maleimide (red) labels the 4-arm PEG-mal, and thus, the capsule shells. 4-arm PEG-mal solution comprised 80%, 50%, 40%, 30%, 20%, and 10% of the aqueous volumetric flow for images 1-6. Sample labeling in A, B, and C is consistent. B. Shell thickness vs. dextran to 4-arm PEG-mal flowrate ratios, calculated as a percent radius vs. percentage of the volumetric aqueous flowrate. C. Comparison of each capsule composition to the binodal phase separation curve, calculated based on the total capsule volume. D. Adjusting the ratio of total aqueous flow (the sum of dextran and 4-arm PEG-mal flowrates) to oil flow alters the capsule size. The left-side panels of each series are high-speed camera images of capsule generation. The right-side panels are CLSM images of capsules (not z-projected.) 4-arm PEG-mal capsule shells are labeled with Cy5.5-maleimide (red). The aqueous flow comprised 16.6%, 7.9%, and 2.9% of the total volumetric flow for samples 1-3. Sample labeling is consistent with E. E. Quantification of capsule radius compared to the percentage of aqueous flow vs. total flow.

Capsules are Generated Below Phase-Separating Concentrations of 4-arm PEG-mal and Dextran

To determine the BioFlex method's capability to produce capsules from 4-arm PEG-mal and dextran concentrations below the ATPS binodal curve, the composition of BioFlex generated core-shell capsules were compared to the 4-arm PEG-mal and dextran phase separation diagram (Figure 4C). Varying the ratio of 4-arm PEG-mal solution to dextran solution during capsule generation resulted in a range of total capsule concentrations in the phase diagram's non-phase separating and phase-separating regions. With the BioFlex method, phase separation and shell gelation was achieved for all flowrate combinations tested, including conditions where the 4-arm PEG-mal flowrate was less than 50% of the total flowrate, resulting in total-capsule concentrations of 4-arm PEG-mal and dextran that lay in the non-phase-separating region of the phase separation diagram (Figure 4: A, C).

Flowrate Controls Particle Size

Like shell thickness, the overall capsule diameter can be tuned by modifying flowrates during capsule generation (Figure 4: D-E). Decreasing the combined aqueous flow from 20% to 3% of the overall flow produced capsules with diameters from 91.8 ± 2.5 μm to 58.9 ± 4.5 μm. Refer to Appendix C Table 2 for specific flowrates used during device operation.

Capsule-Based Growth is Biocompatible and Single-Cell Resolved

Bacterial growth in capsules was compared to growth in a 96-well plate to evaluate if capsule cultivation negatively impacts bacterial growth. Capsules containing single *P. aeruginosa* PAO1 (pMF230) cells that constitutively express green fluorescent protein (GFP) via a plasmid were suspended in nutrient media (TSB) in the wells of a chambered coverglass and

incubated for 12 h at 37 °C. The capsules were imaged via iCLSM during incubation at 30 min intervals. The images show increasing cell-associated fluorescence signals, indicating the growth of *P. aeruginosa* inside the capsules (Figure 5A). Fluorescence changes in the time-lapse capsule incubation images were analyzed to quantify the per-capsule growth and build growth curves starting from single-cells. The similar shape and timing of the growth curves (Figure 5B and Appendix C Figure 3) suggest a homogenous growth response of *P. aeruginosa* in capsules containing nutrient rich medium. The growth rate of *P. aeruginosa* on a per-capsule basis was determined to be $1.08 \pm 0.031\ h^{-1}$.

Separately, *P. aeruginosa* PAO1 pMF230 was incubated in TSB in a 96-well plate, and growth was monitored as fluorescence and optical density using a plate reader. The growth rate of cells grown in a 96-well plate was determined to be $1.16 \pm 0.025\ h^{-1}$ based on fluorescence and $1.36 \pm 0.021\ h^{-1}$ based on optical density (OD_{600}) (Appendix C Figure 5). Analysis of variance (ANOVA) was used to determine that fluorescence-based growth rates were reduced compared to optical-density based rates ($p = 2.20 \times 10^{-16}$). This comparison and comparisons of the growth rates determined from independent biological replicates (Appendix C Figure 3) indicate that, while fluorescence is a measure of growth, fluorescence-based growth likely underestimates the true growth rate in the system. Likely causes for this underestimation may be some degree of plasmid loss during growth or a light-blocking effect as cells accumulate. Acknowledging the limitations of fluorescence-based growth, it is important to note that fluorescence-based growth in capsules and 96-well plates was not significantly different, (p=0.127). Together, these results indicate that while there is a scaling issue for fluorescence-

based growth vs. optical density-based growth, the fluorescence-based growth in capsules vs. bulk wells was nonetheless the same.

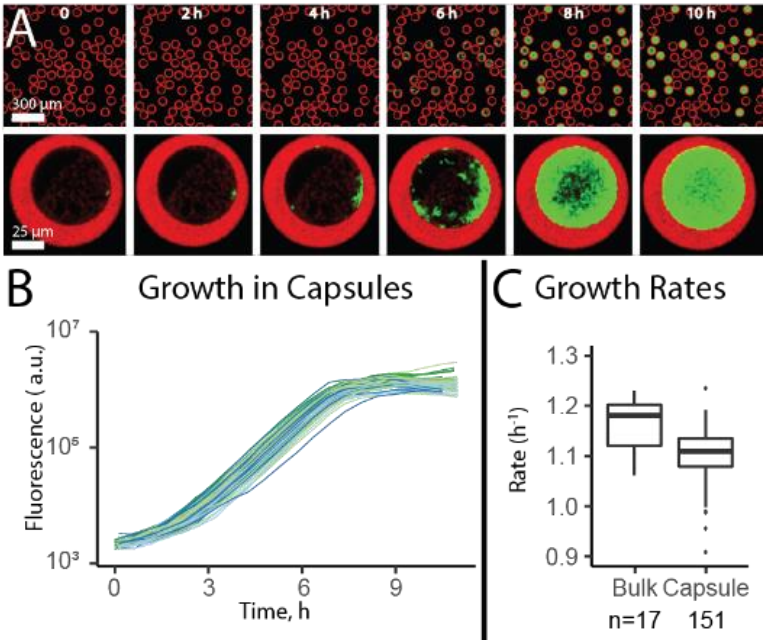

Figure 5: *P. aeruginosa* PAO1 growth in capsules is comparable to growth in 96-well (bulk) formats. A. The growth of bacteria in capsules was visualized over a 10 h incubation period using CLSM. Capsule shells are labelled with Cy5.5-maleimide (red) and *P. aeruginosa* express GFP, shown in green. The bottom image panel visualizes a cell containing capsule selected at random for the same 10 h incubation. B. Growth curves were produced for bacteria in individual capsules based on an increase in fluorescence signal. Fluorescence measurements reflect CLSM collected fluorescence summed across multiple slices of a z-stack. Plot represents growth curves from a single trial. C. Growth rates of *P. aeruginosa* in 96 well plate (bulk) and capsule formats, calculated via analysis of growth curves. Sample sizes (18 for bulk and 151 for capsules) indicate the number of wells analyzed across five biological trials for bulk and the number of capsules analyzed across three biological trials for capsules.

Bacteria are Unable to Utilize Capsule Components for Growth

Bacteria were incubated with crosslinked 4-arm PEG-mal or dextran to address concerns that these compounds may affect growth in capsules (Appendix C Figure 4). *Pseudomonas*

aeruginosa (*P. aeruginosa*) PAO1 (pMF230) and *Escherchia coli* (*E. coli*)HB101 (pMF230) were selected as test strains due to their divergent carbon utilization strategies; *P. aeruginosa* prefers complex carbon sources, and *E. coli* prefers simple carbon sources [109]. Each strain was incubated in a 96 well plate in PBS or TSB with or without added dextran or crosslinked P4M microspheres. Growth, monitored as optical density using a plate reader, did not occur in PBS over 22 h (Appendix C Figure 4). There was no difference in OD between PBS containing 0 or 26 mg/ml dextran for either strain (*P. aeruginosa* $p = 0.891$, *E. coli* $p = 0.818$). The inclusion of concentrated P4M microspheres in PBS also did not result in an increase in OD or fluorescence for either strain (*P. aeruginosa* $p = 0.82$, *E.coli* $p = 0.849$), demonstrating that capsule components do not result in a detectably level of growth in bulk assays.

Capsules Enable Multi-Step Incubation Assays

To demonstrate the utility of capsule-based microbial cultivation for time-varied or dosed chemical assays, we introduced ciprofloxacin (cipro) to *P. aeruginosa* growing in capsules at various time points over a 20 h incubation period. Capsules containing single *P. aeruginosa* cells were dispensed into a chambered well-slide and suspended in 10^{-3} TSB. Additional 10^{-3} TSB with was added at 4, 7, and 10 h from the initial nutrient introduction (Figure 6A). Four antibiotic treatment schedules were used, in addition to an untreated control: In the 0 h treated well, i.e. continuously treated, cipro was added in the 0, 4, 7, and 10 h nutrient additions. For the remaining wells, the name of the treatment schedule, i.e. 4 h, 7 h, or 10 h treated, refers to the first time cipro was added to that well. At each addition point, the concentration of the added cipro in media was adjusted to achieve an in-well cipro concentration of 1 µg/mL.

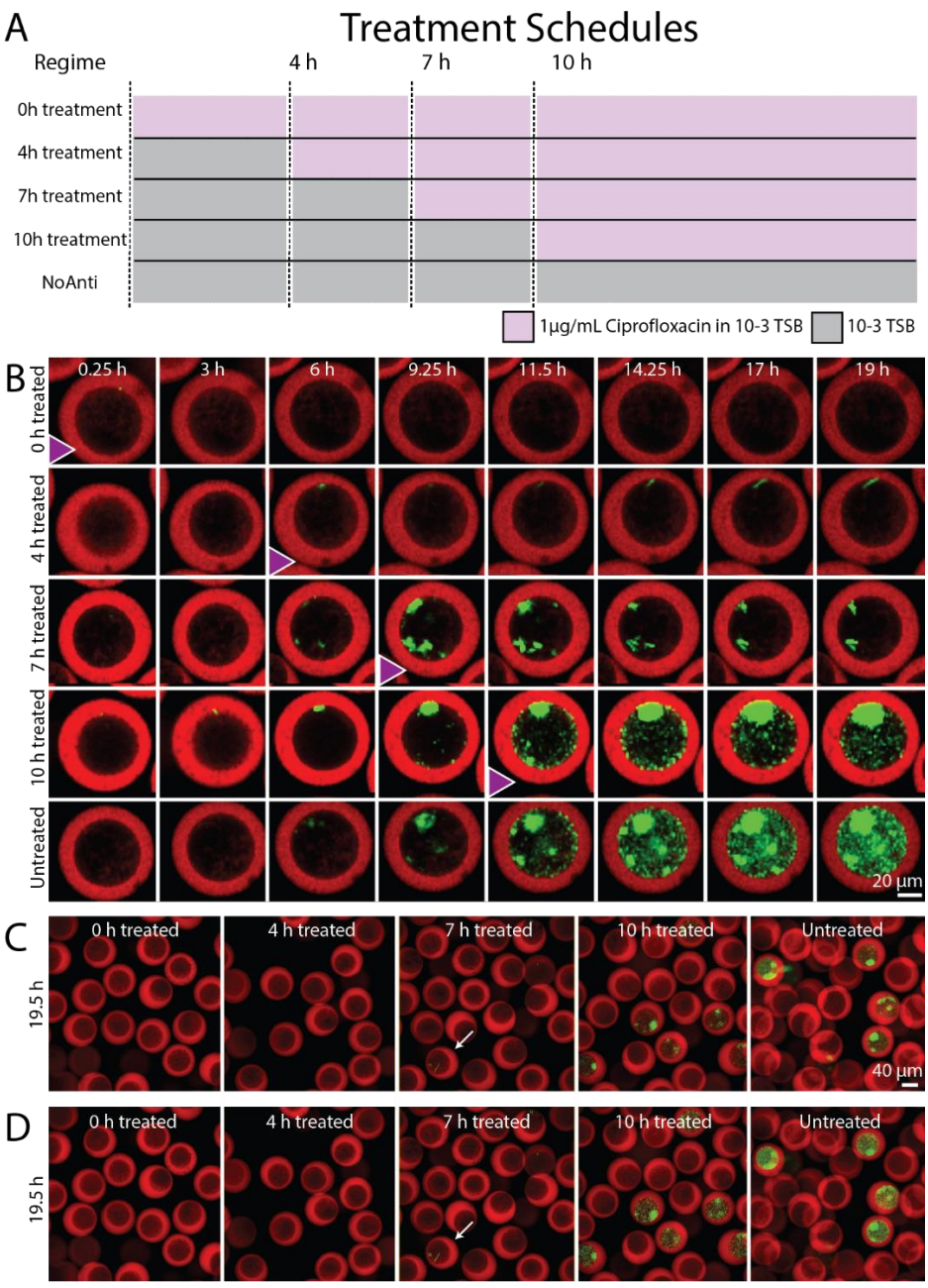

Figure 6: Experimental format for time-varied antibiotic treatment trial and microscopy results. A. Capsules containing P. aeruginosa PAO1 were placed in the wells of a chambered coverglass, and media, either with or without ciprofloxacin, was added to each well. Additional media was added throughout incubation at 4, 7, and 10 h. Antibiotic was added to wells at these timepoints along with the nutrient addition according to the dosing schedule presented in the lower portion of panel A. B. Bacterial growth in capsules is imaged via CLSM for the five dosage regimes presented in panel A. The initial antibiotic addition to each well is represented by a purple triangle. Capsule shells are labelled with Cy5.5-maleimide (red) and *P. aeruginosa* expresses GFP, shown in green.

Images were taken using iCLSM at 40 min intervals throughout 19.5 h of incubation (Figure 6B, Appendix C Figure5). The time-lapse cycle was paused around each solution addition, resulting in a varied imaging interval at these time points. The resulting time lapse image series reveal different morphology and growth outcomes depending on the phase of growth and the number of cells contained in each capsule at the time of antibiotic addition (Figure 6B, Appendix C Figure 5). These images were analyzed to determine the fluorescence-based biomass at each timepoint to create growth curves originating from single cells for each capsule (Figure 7, Appendix C Figure 9).

The time-lapse images (Figure 6B and Appendix C Figure 7) show an observable increase in fluorescent signal per capsule for all samples prior to onset of an antibiotic effect, aside from the sample initially dosed with Cipro at 0 h. The growth per capsule is visually similar for each sample aside from the 0 h dosed sample prior to an effect from antibiotics. When antibiotics were added following 4 and 7 h of growth, there was a decrease in fluorescence that was observable to the eye during the 20 h experiment. When antibiotics were added following 10 h of growth, a decrease in fluorescence was not obvious. Aggregates appeared as dense, contained regions of fluorescence that stayed in one location between frames, while planktonic cells appeared as disperse punctate fluorescent signals. Aggregates appeared to be located at internal shell-core interfaces, while planktonic cells moved throughout the capsule core. Some cell elongation, a characteristic of ciprofloxacin treatment [110], was observed (Appendix C Figure 5).

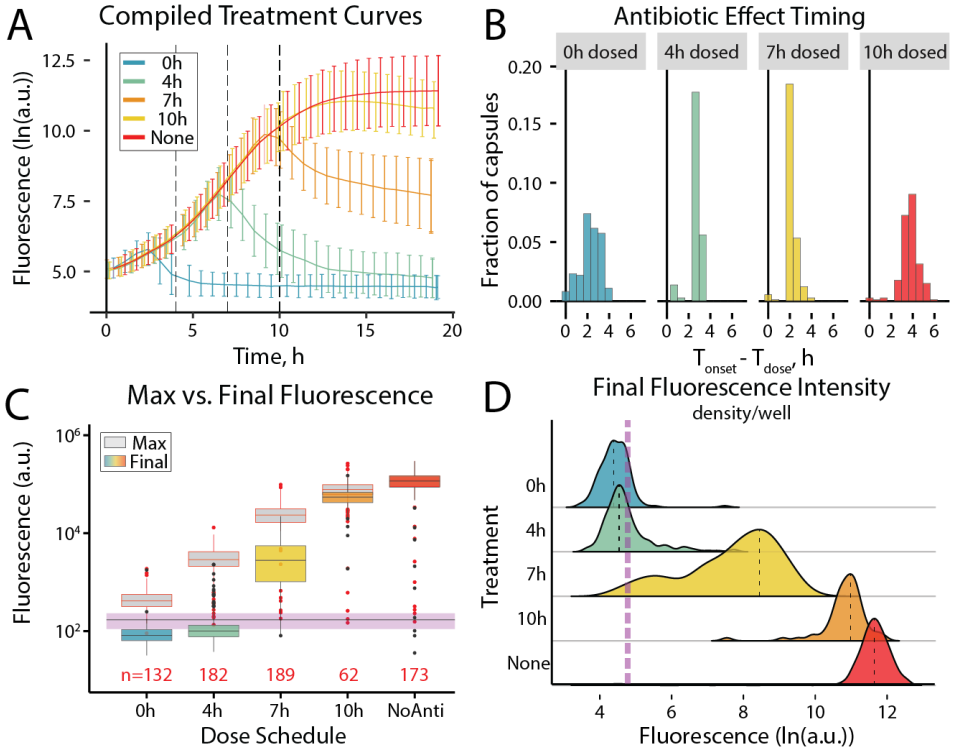

Figure 7: Diverse data captured from single-cell seeded, time-resolved assay of ciprofloxacin treatment in *P. aeruginosa* PAO1 grown in a capsule format. Data represents one biological replicate, with multiple capsules within that biological replicate, for each treatment regime, as indicated in panel C. Treatment regimes shown correspond with the treatments described in Figure 6A, treatment color representation if consistent throughout Figure 7. A. Averaged growth curves calculated based on summed fluorescence intensities obtained from CLSM z-stacks. The solid lines pass through the mean of the population at a time-point, and the error bars represent standard error. B. Histograms of the time span between the ciprofloxacin treatment and the observable effect. Effect was defined as a the first timepoint with a decrease in fluorescence between frames. No decrease in fluorescence was observed for any capsule in the undosed sample. C. Comparison of the initial, maximum, and ultimate fluorescence totals in capsules for each treatment. The horizontal, dashed black line and surrounding purple bar represents the average fluorescence measurement and standard deviation for the study's initial time point. The gray boxes indicate the maximum fluorescence values for capsules in that sample. The colored boxes indicate the final fluorescence for that sample. The difference between the maximum and final fluorescence values indicates the effect of the antibiotic on constitutively-expressed fluorescence. Boxes positioned below the purple line indicate the final fluorescence was below the fluorescence output of a single cell. D. Staggered density plots of total fluorescence intensity at the final time-point for capsules exposed to each treatment regime. The vertical purple dashed line indicates the average of the compiled populations at the initial time point, and the black dashed lines within each density distribution indicate the mean of that distribution.

The averaged growth curves for each sample show that treating cells growing in capsules with antibiotic at varied incubation time-points resulted in distinct population effects (Figure 7A). Additionally, these results demonstrate the ability of external, aqueously dissolved treatments to permeate the capsules, and the potential of data-analysis on a per-capsule basis. Times reported in the following are approximate, reflecting a 40 min imaging window. All decreases and increases in total fluorescence intensity reported are significant at a 95% confidence level ($\alpha = 0.05$) (Appendix C Table 4). Fluorescence values reported reflect the average per-capsule total intensity for each population and are in relation to the per-capsule total fluorescence value at t = 0 h.

Continuously treating the capsules with antibiotic resulted in a very different growth outcome than the antibiotic-free capsules. The population of cells in untreated capsules grew, showing a log-linear increase in fluorescence from 2 to 12 h before transitioning to stationary phase after 12 h. At the conclusion of the study (19.5 h) the fluorescence in each capsule increased to $1.08 \times 10^5 \pm 2.47 \times 10^3$ arbitrary units (a.u.). Fluorescence did not decrease throughout the incubation period for any of the analyzed untreated capsules. In contrast, the fluorescence signals from capsules in the well continuously treated with antibiotic increased, measuring 97.5 ± 18.4 a.u. at 2.5 h, before decreasing in fluorescence four orders of magnitude to a final fluorescence value of -65.5 ± 14.3 a.u.

The remaining capsules, with antibiotic introduced at 4, 7, and 10 h, resulted in growth outcomes between the untreated and continuously treated extremes. On average, the 4 h dosed sample increased in fluorescence until 6.5 h, corresponding to $1.62 \times 10^3 \pm 46.8$ a.u., before decreasing four orders of magnitude to -7.36 ± 1.8 a.u. at the final time point. The 7 h dosed

sample increased in fluorescence until 9 h, corresponding to $1.78x10^4 \pm 1.29x10^2$ a.u., before decreasing one order of magnitude to a final fluorescence value of $2.77x10^3 \pm 90$ a.u. The 10h dosed sample showed the least antibiotic effect compared to other samples (Figure 7C), increasing in fluorescence until 14 h, corresponding to $7.33x10^4 \pm 1.02x10^2$ a.u., before decreasing less than an order of magnitude to a final fluorescence value of $5.51x10^4 \pm 1.66 \times 10^2$ a.u.

Plotting the individual growth curves of each capsule illustrates largely homogenous patterns of fluorescence increase in capsules for each trial (Appendix C Figure 9). However, the growth curves for 4h dosed and 7h dosed capsules begin to diverge from one another after treatment, suggesting more heterogeneity in the magnitude of antibiotic effect the capsule level after exposure, while the 0 h dosed and 10 h dosed capsules remained largely homogenous in their antibiotic response. The per-treatment distributions of fluorescence at the final time-point show the broadest range of values for the 7 h treated capsules. (Figure 7D.)

The effect onset curves (Appendix C Figure 9), overlaid over the individual growth curves, indicate regions of each growth curve with a negative slope between adjacent time points. No negative slopes (0%) were determined for any of the analyzed untreated capsules. Thus, our analysis of antibiotic effect uses a decrease in fluorescence to indicate the onset of an antimicrobial effect (Figure 7B.) The time lapse interval of 40 min prevents us from resolving the effect onset timing beyond a ±40 min approximation, however, the trends are still useful to determine the timing of antibiotic effect. An antibiotic effect was detected at 2.5, 6.5, 9, and 14 h for the majority of capsules in the 0, 4, 7, and 10h dosed samples. These times correspond to an onset time of 2-2.5 h for the 0,4, and7 h dosed samples, and an onset time of 4 h for the 10 h

dosed sample. Thus, the time to effect onset increased approximately 2-fold for the 10h dosed capsule compared to samples dosed earlier.

Discussion

A Combinatorial Approach of Hydrogel Capsule Technologies Optimizes the Capsule Generation Process

The use of ATPS capsule components in the BioFlex method reduces the necessity for rapid crosslinking and improves the definition of capsule geometry compared to non-ATPS approaches. For this discussion, a comparison to capsule generation methods that produce a liquid core by disintegrating a solid-core template within a shell, was not considered [111, 112], as the benefits of all-liquid capsule production have largely replaced these earlier methods. In non-ATPS systems, forming core-shell capsule geometry requires crosslinking the shell precursor before mixing dissipates the radial concentration gradient between the core and shell solutions. In these systems, the challenge of core-shell mixing imparts sensitivity to crosslinking timing [69, 113]. Additionally, because the core and shell solutions of a non-ATPS system start mixing upon contact, the boundary between the core-shell regions of these capsules is inevitably less distinct than similarly produced ATPS-based capsules[69, 113]. In comparison, using an ATPS decreases the need for rapid crosslinking kinetics and ensures distinct core-shell morphology through phase separation.

When generating ATPS-based capsules in planar (not 3D) microfluidic devices, the desired core-shell geometry of the capsule develops after drop generation [44, 66, 70] as the phases separate and reorient to achieve their most energetically favorable arrangement. In these systems, capsule production is only possible using ATPS concentrations above the phase

separation line, and delaying crosslinker introduction or slowing the kinetics of crosslinking is required to allow for an optimal amount of phase separation[44, 66, 70]. If crosslinking happens too quickly, the phases do not have time to reorient in concentric core-shell geometry; if crosslinking occurs too slowly, the orientation of the two phases progresses undesirably far towards a geometrically eccentric Janus particle [107]. Comparatively, the BioFlex method's 3-D, non-planar device geometry, which is similar to those used for non-ATPS capsule production [65, 69], templates the phase separation and geometric orientation of the two phases before droplet breakup, resulting in precise, flow-controlled templating of the ultimate core-shell geometry. Using nanoemulsion-delivered DTT crosslinking in conjunction with the 3-D device "freezes" the particle geometry rapidly after drop generation, solidifying the templated geometry. Additionally, this method allows for the generation of capsules with 4-arm PEG-maleimide and dextran concentrations below the binodal curve, as the local concentrations at the interface during drop-making impart phase separation long enough to produce the core-shell geometry in the rapidly crosslinked capsules.

The Bioflex Capsule Generation Method Tolerates Widely Varied Operating Dynamics

The shell thickness and capsule diameter results indicate that the BioFlex method is compatible with a wide range of flowrates and dextran or 4-arm PEG-mal concentrations. This flexibility, along with the clog-preventing device design, makes the BioFlex method easy to use and enable the production of varied particle geometries without requiring precursor reformulation. The ability to vary shell thickness and capsule size could be leveraged to study spatial dependencies of cell-to-cell signaling[84] and polymicrobial interaction[23], as well as for fine-tuning the dynamics of multi-capsule neighborhoods. Additionally, these results and

advancements suggest that researchers can likely adapt the core and shell compositions to meet their experimental needs without disrupting capsule generation.

Acknowledging these advancements, the capsule method could be further improved by reducing instances of eccentric (asymmetric) core position inside the capsules. The capsule images show some occurrences of eccentric capsules where the shell thickness varies on opposite sides of the capsule. One solution to this problem may be density-matching the core and shell solutions to eliminate differential buoyancy between the phases, as demonstrated elsewhere [66], and by modifying the core and shell channel junction to improve the symmetry of the annular flow upstream of the drop-breakup junction.

Suitability of 4-arm PEG-mal Capsules for Growth Assays

P4M has been used in various eukaryotic cell culture formats, suggesting biocompatibility [44, 65, 69, 114]. We demonstrated that *P. aeruginosa* growth in P4M capsules was comparable to bulk culture formats by comparing in-capsule fluorescence-based growth rates to those obtained from an analogous 96 well-plate format. Separately, *P. aeruginosa* and *E. coli* growth was also assayed in the well plates in the presence and absence of capsule components with and without nutrient media. This study confirmed that the capsules may be considered inert for simple cultivation schemes, as the components alone did not result in growth (measured as an increase in optical density.) For different experiment designs, such as extended in-capsule cultivations, mutant screenings, or starvation studies, it may be necessary to reassess the ability of bacteria to consume or otherwise degrade the capsule components.

Another consideration for soft-material microculture approaches is the ability of the microculture platform to maintain cell containment. In this work, intact capsule shells proved an

effective barrier to cell escape, indicated by a lack of cells outside capsules during extended cultivation times. Previous studies utilizing microspheres instead of capsules require processes such as particle coating or surface sterilization to prevent contamination of the bulk media by escaping bacteria [115, 116]. However, there is one caveat to in-capsule growth: while working with capsules, we discovered that robust bacterial growth in the capsules can rupture capsules and release single cells into the surrounding media. This phenomena has also been reported elsewhere [44]. Even in the absence of capsule rupture, bacterial growth resulting in densely filled capsules can limit the ability to image capsules using light microscopy and subsequently conduct quantitative fluorescence analysis. With these observations in mind, we found it was simple to prevent capsule overgrowth and rupture by reducing the nutrient available for in-capsule cultivation by simply diluting the nutrient media. We used 10-3 diluted TSB in the time-varied antibiotic exposure study and observed no capsule rupture or image quality issues.

In the future, increasing the uniformity of capsule shell thickness, as discussed earlier, or tuning the capsule shell composition may improve capsule resilience to rupture. Other 4-arm PEG-maleimide capsule research indicates the ability of P4M capsules to swell[44]. In work related to this study, we likewise observed increased capsule size for capsules full of cells in some instances. Tuning the composition of the cross-linkable hydrogel used in hydrogel capsule production to improve mechanical properties, i.e., improving the capsule elasticity, durability, and structural symmetry, may all be worthwhile in further enhancing the utility of capsules for microbial cultivation.

Capsules Represent a High Throughput Single-Cell Assay Necessary for Screening Rare Phenotypes

One advantage of the BioFlex method is enabling high throughput single-cell assays. Kilohertz rate capsule generation and the ability to image hundreds of microscale capsules simultaneously make this technique orders of magnitude higher-throughput than microfluidic chamber or well-plate cultivation microbial growth assays. Compared to water-in-oil cultivation assays [1, 43], this method also allows testing of many different aqueous cultivation conditions without requiring the production of multiple drop samples, as a single batch of capsules can be split after generation to test various conditions. Large single-cell resolved sample sizes are critical to the study of microbial heterogeneity, as rare phenotypes are frequently responsible for high-impact community traits, for example, the role of persister cells in infection recalcitrance[35]. This method of single-cell cultivation, assay, and associated analysis allows for not only the identification of subpopulations but also for characterization of those subpopulations regarding time-dependent traits such as growth.

Bioflex Capsules Enable Multistep, Single-Cell Assays, and Rich Data Output

Integrating multistep protocols with a single-cell compartmentalizing format as described here allows for single-cell resolved studies of medically relevant topics such as the impact of antimicrobial dosing schedules effects[117, 118], intermittent nutrient limitation[119], and changes in the chemical environment[120], all of which can be factors in the treatment or ecology of a chronic infection. Here, diffusing ciprofloxacin antibiotic into capsules containing growing *P. aeruginosa* PAO1 demonstrated the adaptability of capsules for multistep assays. The observable effects of this treatment demonstrate the ability of water-soluble compounds to penetrate capsules and deliver a molecular payload.

Data output from this experiment encompassed many factors reflecting the response to antibiotics: the morphology of growing bacterial colonies, the growth characteristics of bacteria in individual capsules, the heterogeneity of treatment outcomes, and the period between antimicrobial treatment and a measurable treatment effect. In addition to the time-dependent introduction of antibiotic demonstrated here, other studies show that 4-arm PEG-mal microspheres and capsules are amenable to introducing dyes and other compounds useful in microbial analysis [66], further demonstrating the use of permeable, hydrogel-shelled capsules for multistep assays. The data shown in this paper demonstrates that individual capsules were tracked successfully over the course of multiple media additions. These multi-step workflow capabilities would be improved by demonstrating the ability to fully replace the media around capsules while maintaining individual capsule tracking.

Capsules may Provide a Model for Microscale Microcosms:

Bacteria growing in capsules exhibited phenotypic and morphologic complexity, where dense, capsule interface-associated aggregates coexisted with planktonic, non-community-associated organisms, all arising from a single-cell inoculum. These results indicate richness in phenotypes possible in capsules not observed in other microculture approaches such as microspheres, microwells, and water-in-oil drops. Previously, bacterial cells have been grown in 3-D printed hydrogels and solid hydrogel microspheres [115, 116, 121]. However, in these systems, the hydrogel structure impacts the microbial growth physiology and renders observing a freely motile, "planktonic" phenotype impossible. Important physiological transitions, i.e., the transition from a planktonic to aggregate or biofilm phenotype, are also masked in these systems. Previously, our research group grew the same *P. aeruginosa* PAO1 pMF230 strain utilized here

in water-in-oil drops [1, 43]. In contrast to a microsphere format, even for full-strength nutrient conditions (TSB media), bacterial growth was disperse and planktonic. The complex, aggregate-like colony morphology and dense, capsule-filling growth observed in a capsule-based format were not observed in water-in-oil drops.

Capsules are Amenable to Down-Stream Processing

Capsule-based single-cell cultivation demonstrates a clear advantage in identifying phenotypically diverse population subsets with high sample numbers. This work does not include processing or analysis after the cultivation studies of *P. aeruginosa* with or without antibiotic treatment. However, separate studies demonstrate the ability to use stains on cells grown in capsules[66] and the sorting and recultivation of organisms grown in capsules using fluorescence-activated cell sorting (FACS)[44]. These studies demonstrate the range of assays compatible with the hydrogel-based format.

Conclusion

The BioFlex capsule generation method produces permeable, biocompatible, and structurally tunable hydrogel-shelled microcapsules developed specifically for single-cell microbial isolation and cultivation. The BioFlex method optimizes capsule production for microbial growth assays by integrating three capsule production technologies: ATPS, non-planar device design, and nanoemulsion-delivered crosslinking agent. The resulting capsules enable longitudinal single-cell resolved microbial cultivation with transient chemical conditions, broadening single-cell studies to systems requiring complex, time-varied parameters. The results of this work demonstrate the utility of capsule-based cultivation for a time-varied study of

antibiotic treatment, and the data collected in this study allowed for time and cell-resolved characterization of colony morphology, cell growth, treatment effect, and treatment effect timing. The multi-faceted, descriptive single-cell study demonstrated here using BioFlex-generated capsules provides a foundation for complex single-cell resolved studies necessary to understand the role of cell-level heterogeneity in microbial infection and pathogenicity.

CHAPTER FIVE

CONCLUSION OF "BACTERIAL CULTIVATION IN MICROSCALE DROPS AND CAPSULES TO RESOLVE SINGLE-CELL GROWTH PHYSIOLOGY"

Introduction

In this dissertation conclusion, the research aim addressed by the presented body of work is reintroduced and compared to the outcomes. Next, the broader contributions are presented, categorized as tools, techniques, and the advancement of fundamental knowledge in microfluidics. A discussion of the limitations of the work and suggestions for addressing these limitations follows the contribution section. Before concluding this dissertation, I present a broader challenge for the continued development of single-cell microfluidic assays, and discuss potential approaches for addressing this challenge. Finally, I conclude the dissertation by highlighting the overarching achievements of this work.

Research Aim

This research aims to establish methods for studying growth dynamics as an aspect of microbial cell-level heterogeneity, considered in the broader context of understanding the role of heterogeneity in chronic infection pathogenicity. This aim was achieved by developing the DropSOAC and BioFlex methods described in Chapters 3 and 4. DropSOAC (Drop Stabilization on a Chip) is a method for stabilizing microfluidic water-in-oil drops for long-term, microscope-monitored microbial cultivation. The BioFlex method is a novel method for generating hydrogel-shelled microcapsules for bacterial isolation and multi-step cultivation. The DropSOAC and

BioFlex methods each enable single-cell isolation for single-cell resolved data, high-throughput sample generation for identifying rare phenotypes, and time-lapse microscopy monitoring for characterizing the time dynamics of growth and morphology.

The specific challenge addressed by the DropSOAC method is the destabilization of water-in-oil drops during storage in microfluidic devices, which can include drop swelling, shrinking, and the deterioration of interface stability between the water and oil phases. These challenges hinder the ability to monitor drop arrays via time-lapse microscopy and, thus, the ability to monitor single cells growing in drops. DropSOAC prevents destabilization by pre-treating the microfluidic drop-array device to promote long-term phase equilibrium in the stored drop emulsion. With the DropSOAC method, single-cell growth curves of *Pseudomonas aeruginosa* were generated to help understand bulk-level population phenomena observed in dormancy and resuscitation assays. The results of these studies highlighted the utility of DropSOAC in revealing the dynamics of single-cell heterogeneity.

The goal of developing the BioFlex method was to add aqueous permeability to microbial single-cell cultivation by isolating and cultivating cells in hydrogel-shelled microcapsules. The BioFlex method represents an all-aqueous analog to the DropSOAC approach by maintaining DropSOAC's high-throughput sample generation, single-cell isolation, and time-lapse, single-cell resolved growth monitoring. However, because aqueous molecules, including waste, nutrients, and various treatments, can diffuse in and out of the BioFlex capsules, the chemical conditions inside the capsule can be controlled and changed throughout cultivation. After developing this method, the suitability of BioFlex capsules for bacterial growth and multi-step assays was demonstrated in a time-lapse study where encapsulated *P. aeruginosa* cells were

grown in nutrient media for varied lengths of time before being treated with antibiotics. Defined differences in the cultivation outcomes depending on the timing of antibiotic introduction indicated that antibiotics had diffused into the capsules from the surrounding media, resulting in a biological effect. The results of these studies show the potential of BioFlex capsules to conduct multi-step assays that incorporate time-dynamic chemical environment changes into the study of single-cell heterogeneity. Cumulatively, this body of work indicates that drop-based microfluidics is a powerful tool for conducting single-cell studies. Furthermore, these presented results show that drop- and microcapsule-based cultivation can be used to evaluate heterogeneity in time-dependent aspects of physiology and phenotype.

Contributions

Tools and Techniques

This work generated two novel microfluidic tools: DropSOAC, and the BioFlex method for hydrogel-shelled capsule generation. DropSOAC encompasses a protocol for drop generation, polydimethylsiloxane (PDMS) microfluidic device pretreatment, and an incubation chamber that stabilizes water-in-oil microfluidic drops. DropSOAC incubation chambers were constructed from plastic cell culture dishes at the time of publication. After publication, aluminum versions of the DropSOAC chamber were developed (Appendix B), further enhancing the quality and value of this approach. Between publication in 2019 and today, the DropSOAC method has been included as a reference point for conducting single-cell studies in multiple reviews [122-126] and has been implemented as a research method in two published studies outside the Chang lab [127, 128].

The BioFlex method is an intended-for-publication approach for generating hydrogel-shelled microcapsules that strategically incorporates the elements of disparate hydrogel-microcapsule approaches to optimize hydrogel-shelled capsules for microbial assays. The development of this approach provides microbiologists with a resource for conducting single-cell resolved assays that are compatible with multi-step processing. Beyond its microbiology applications, the theory and analysis incorporated in the documentation of the BioFlex method contribute to the advancement of hydrogel-capsule approaches, which are only gaining in popularity throughout biology and materials research.

In addition to novel microfluidic tools, this dissertation outlines techniques for analyzing microscale cultivation studies, applying single-cell studies to understand population-level observations, and conducting multi-step biological workflows in microcapsules. Microbial heterogeneity, which can contribute to population-level fitness, is an essential research topic as we face increasing health threats due to continuously rising levels of antimicrobial resistance [17, 25]. As the interest in single-cell resolved microbial assays increases[41, 42, 77, 81, 86, 123, 124, 129], demonstrating the analysis and interpretation of data from microscale cultivation studies may contribute to the increased use of these techniques. This dissertation repeatedly generates fluorescence-based growth curves from cells isolated in microscale drops and capsules and uses those curves to quantify heterogeneity in growth dynamics and outcomes. This data is frequently plotted as histograms or density plots. These data representation styles illuminate the heterogeneity across the population by refraining from collapsing the data into a single point. The use of high-end confocal microscopy to conduct these studies further increases the value of

these datasets by enabling a linkage between specific, quantified outcomes and the morphology of cells generating those outcomes.

This work provides a roadmap for applying single-cell studies to targeted microbiology questions and quantifying microbial growth dynamics as an aspect of intrapopulation heterogeneity. The DropSOAC method was motivated by a hard-to-explain bulk observation in a *P. aeruginosa* dormancy and resuscitation assay. Developing and applying the DropSOAC method to this system provided insight into the bulk observation [1, 43] (Appendix A) and generated new hypotheses and research targets. Investing in single-cell resolved tools, including the drop-based microfluidics approaches used in this dissertation, requires financial and training commitments. The application of DropSOAC to study *P. aeruginosa* dormancy [43] demonstrates the types of observations that may be interesting to investigate using single-cell resolved approaches like DropSOAC or BioFlex. Adding multi-step capabilities to these assays, as demonstrated in the BioFlex method, only increases the range of questions assayable with these techniques. The BioFlex and DropSOAC methods add microbiology-focused demonstrations to an increasing body of interdisciplinary biology and drop-based microfluidics research. In the future, this contribution may help motivate increased cross-disciplinary research between microbiologists and microfluidicists.

Fundamental properties of microfluidic systems

Microfluidic drop-stabilization during storage in PDMS devices is a widely observed challenge [130-136] impacting the application of microfluidic assays. The DropSOAC study investigated the mechanism of water-in-oil drop destabilization in PDMS devices and created a better understanding of the disequilibrium agents that contribute to drop emulsion deterioration.

As a resource, the DropSOAC method and application can help inform microfluidic device material selection and drop-storage approaches for assays involving long-term drop storage. And, although enabling monitored in-drop cultivation is the goal of DropSOAC method, the concepts discussed within the explanation of this method can inform the design of other demanding in-drop incubation workflows, such as chip-based in-drop gene amplification that requires elevated temperatures and temperature cycling [137].

The development of DropSOAC and the BioFlex method both involved investigating the suitability of drops and hydrogels for bacterial culture. The compatibility of microfluidic drops and microcapsules for in-drop cultivation was investigated first by comparing growth in drop or hydrogel microcapsule constructs to bulk growth. However, while producing the BioFlex method, the investigation of the suitability of microfluidic constructs for cultivation continued beyond the inhibition of growth by the microscale format. While building BioFlex, we evaluated the ability of bacteria to utilize the BioFlex capsule components as a growth substrate, which has not been investigated in other microculture formats. This demonstration was informed by designing BioFlex with guidance from a team of both microfluidicists and microbiologists. The logic of developing the BioFlex method argues that the diverse metabolism of bacteria is worth considering while developing microfluidic microbial cultivation approaches.

Aqueous two-phase systems (ATPSs) are a tool of interest for generating complex materials in microfluidic systems, especially for the formation of microcapsules. The 3-D visualization of ATPS phases flowing through microfluidic channels performed while developing BioFlex supports a different path towards the core-shell geometry of ATPS microcapsules than previously reported [44, 66]. As we continue to leverage the dynamics of

complex soft materials to generate novel material constructs, including hydrogel microcapsules, we must clearly understand these systems' fundamental processes. The BioFlex study adds a new hypothesis to the routes of ATPS phase separation in microfluidic channels, which can inform future investigations and approaches.

The production and application of hydrogel microcapsules is a rapidly expanding research area (Figure 1). The development of the BioFlex method required a survey and comparison of hydrogel advancements, approaches, and techniques. Ultimately, approaches and techniques were integrated from disparate hydrogel production methods to build BioFlex. As the focus on hydrogel capsule engineering grows, extracting tools from the advancing science and combining and modifying those tools to create improved capsule generation methods, as was done in BioFlex, meaningfully expands the quality of these hydrogel capsule approaches.

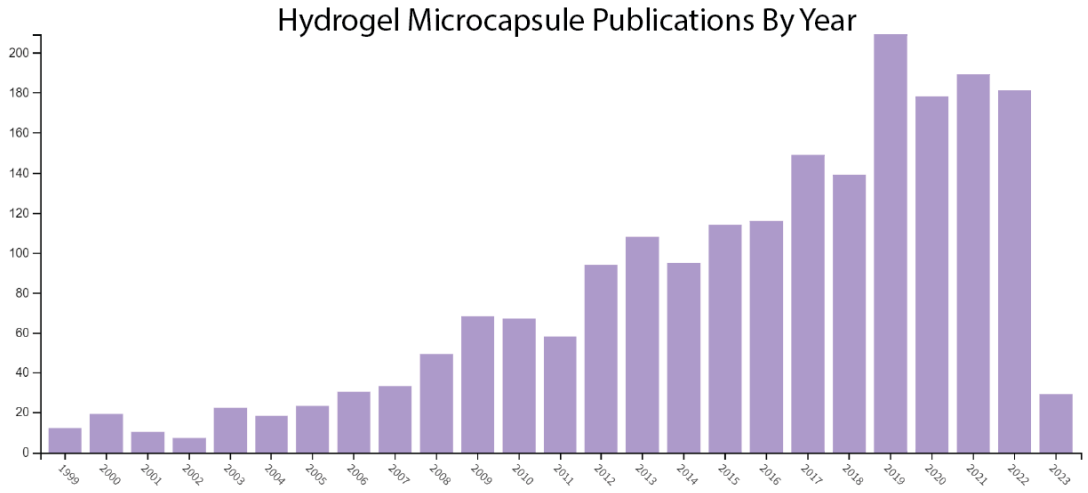

Figure 1: Publications on the topic “Hydrogel Microcapsule” as a function of year, spanning from 1999 to 2023. Generated using Web of Science.

Limitations and Future Work

Microfluidic processing time exceeds the timescale of bacterial lifecycles

Microfluidic encapsulation is a high throughput process owing to rapid drop and microcapsule production rates. However, the high throughput characteristics of drop generation do not correlate to faster sample preparation times than compared to bulk. For the drop and capsule-based studies presented in this dissertation, the biological assay workflows required all of the steps necessary for preparing a bulk study, plus additional steps specific to microfluidic encapsulation. Microfluidic-associated processing times are further increased by troubleshooting drop formation start-up dynamics, which is a necessary process at the beginning of each drop-making session. Adding set-up time for multiple position time-lapse microscopy further exacerbates these issues. Even after taking steps to minimize processing time, the experimental logistics of time-lapse monitored microfluidic cultivation meant that cells underwent processing for one to three hours in each experiment, which is a considerable period for many bacteria with 15 min to 1.5 h doubling times. In the case of water-in-oil drop cultivation, this resulted in cell exposure to nutrients and the potential for growth before the start of microscope-observed incubation. In the case of hydrogel capsules, this meant that cells were nutrient limited and suspended in a-typical culture environments prior to studying the effects of other treatments using the capsule format. Improvements that may reduce processing time include better small-volume-liquid-handling methods so that researchers could work with a smaller bulk volume of drops or capsules and thus require less generation time, and improvement in microfluidic device design and fabrication to reduce the time associated with troubleshooting drop-production during start-up.

Logistics of time-lapse microscopy on 3-d microcapsules somewhat diminish the high-throughput potential of microfluidics

The studies in this work used inverted confocal laser scanning microscopy (iCLSM) to conduct time-lapse growth studies. In these studies, multiple fields of view capturing tens to hundreds of drops or capsules were imaged to produce multidimensional (X, Y. Z, and time) imaging sequences. Acquiring these sequences and moving between fields of view accumulates imaging time; this effect increases when observing larger drops or capsules requiring broader z-stacks to capture the total drop volume. These aspects of time-lapse confocal microscopy ultimately decrease the number of drops or capsules that can reasonably be observed during an experiment to a fraction of the total drop or capsule population. Future work could address this limitation by reducing the magnification used during microscopy to image a larger sample size in each field of view, using non-optically sectioned microscopy to remove the time associated with Z-stack acquisition, or using ultra-high-speed imaging tools such as digital light sheet microscopy.

Approaches for retrieving and tracking drops and capsules for multi-step processing are unaddressed

A question that often followed presentations of this work regarded the possibility of retrieving drops [or capsules] after observation via time-lapse microscopy. This capability was never demonstrated or tested in this body of work. The lack of investigation into post-microscopy drop or capsule retrieval stemmed from a lack of readily accessible methods for maintaining drop or capsule identification during retrieval. For example, it was unclear how to identify a drop of interest using microscopy and select it for additional sampling. Without this capability, there are no advantages to post-time lapse retrieval compared to generating a large

sample of drops at the outset and aliquoting the sample for time-lapse microscopy and other applications. In future work, this capability may be achieved through barcoding approaches [46] that label drops with unique fluorescent identifiers.

The ability to track individual drops and capsules likewise manifested as a limitation in multistep cultivation using BioFlex. Washing cells describes removing and replacing the aqueous portion of a cell suspension. Processes where washing is important include intermittent stress experiments, for instance, intermittent osmotic stress [138, 139], and cell fixation and staining, including sophisticated labeling approaches like bio-orthogonal, non-canonical amino-acid tagging (BONCAT)[75] and fluorescent in-situ hybridization (FISH)[77, 78]. These processes have either been demonstrated [66], or are likely feasible in the hydrogel format, owing to the aqueous permeability of hydrogels. Developing the ability to maintain capsule identification during processes that require washing would represent a considerable advancement in using hydrogel microcapsules as a platform for conducting microbial research. This ability was explored while developing the BioFlex method through microfluidic array design. However, that work did not generate implementable solutions in the time frame of this research.

Reliability of Microfluidic Processes

In my and my peers' research, microfluidic processes (i.e., the active flow of fluids through microfluidic devices) would frequently and unexpectedly fail. Commonly observed issues associated with microfluidic processes included: the inability to maintain a consistent drop-making flow regime, undesirable wetting dynamics of channel surfaces, device clogging, polydisperse drop production, device leaking, and drop coalescence upon collection or drop reinjection. Steps mitigating these failure modes are introduced during device fabrication and

operation; However, these steps do not completely resolve these challenges. In this work, microfluidic processing issues slowed research progress and questioned the repeatability of proto-methods. More broadly, these issues, and the expertise necessary to troubleshoot microfluidic processes, represent a roadblock to implementing many microfluidic methods outside non-microfluidic-specific research groups. While the commercialization of drop-based microfluidics by companies like Fluigent™ and Elveflow™ has made strides in microfluidic accessibility, any work to improve the reliability and ease of use for microfluidic processes would significantly aid the implementation of microfluidics to ask biological questions.

Oversimplification of transport in and out of microfluidic microcompartments

In general, researchers consider water-in-oil drops as chemically isolated microcompartments. This simplification ignores transport phenomena (Ostwalt ripening, micellular transport, and limited solubility dynamics) and experimental outcomes [128] that suggest drops are not chemically isolated microenvironments. Although the oil-water drop interface certainly impacts the transport of aqueous molecules, the degree of chemical isolation in drops used for microbial cultivation is unclear. To fully characterize drop permeability related to microbial culture, one would have to characterize the molecular make-up of microbial culture supernatant and create a methodology to quantify the transport of each supernatant component within a specific surfactant stabilized oil-in-water drop emulsion. The methods for the later transport analysis are not immediately clear, though this work is worthwhile.

Transport through hydrogels is overly simplified at the opposite end of the molecular transport spectrum. Generally, the capacity for a molecule to diffuse through hydrogels is estimated by its molecular weight [44, 140, 141]. This generalization ignores many properties

that are understood to impact transport through a matrix, including the bulky or slender structure of the molecule and chemical interactions between a given molecule and a hydrogel structure[141, 142]. Some molecules can be easily fluorescently tagged, making the transport of the molecule through the hydrogel easier to observe. However, even this processes modify the molecular structure of the molecule in question and could result in changes in transport dynamics.

In practice, these transport unknowns are insufficient to invalidate simple studies of bacteria cultivated in drops or hydrogels. In the DropSOAC work, we rely on the conventional understanding of drop isolation. In the BioFlex method, we show that, at a minimum, growth-sustaining concentrations of nutrient and effect-inducing antibiotic concentrations can diffuse through hydrogels. However, if drops or hydrogel capsules are applied to cell-to-cell interaction or metabolic questions, generating a clearer understanding of specific transport dynamics in these systems will grow in importance.

Definition of Single-Cell Research and Comparison to Bulk Growth Paradigms

The studies in this dissertation generate so-called single-cell growth curves. However, in the case of growth studies, a single cell does not remain “single” for very long. So far, the convention in microfluidics is to refer to approaches where single cells are seeded into drops as single-cell studies, despite the slightly misleading nature of that description. In water-in-oil drops, where a single cell is encapsulated in a more-or-less isolated environment with no additional material introduction, the description of single-cell is more applicable. However, the ‘single-cell’ label is confusing for multi-step assays like those enabled by the BioFlex method. Single cells were isolated in hydrogel capsules to demonstrate the BioFlex method; These cells

divided, forming multi-cellular populations in each capsule. After varying periods of growth, resulting in varied population sizes, an antibiotic was introduced to the nutrient media. Because the single cells in each capsule had become cell populations and because the size of the population likely plays a role in the treatment outcome, describing these studies as single-cell studies can be misleading in meaningful ways. Research in this field would be improved by establishing clear terms to describe these microscale cultivation studies that begin with single-cell encapsulation.

Contextualizing single-cell data in fields largely informed by bulk data also introduces challenges to understanding in-drop growth outcomes. To validate that drops and microcapsules were viable cultivation tools, the growth rate of bacteria in these platforms was compared to growth rates in bulk. In-drop and in-capsule growth rates were reduced compared to standard optical density-measured growth rates from bulk culture. It is difficult to interpret the meaning of reduced growth rates because there is no well-established understanding of growth from single-cells in microscale formats. Comparing microscale and bulk growth generates several questions: Is growth in microscale formats reduced due to biocompatibility issues, is the growth quantification method used accurate or valuable only for comparison, and should researchers expect bulk growth rates in microscale cultivation platforms?

A Broad Recommendation for Advancing Single-Cell Growth Studies

Single-cell seeded drop and microcapsule assays challenge the accepted standards of biological research design. Specifically, defining biological vs. technical replicates in drop- or microcapsule-based studies is unclear. For example, van Zee et al. [44], Fattahi et al. [65], and Fredrikson et al. [71] count individual microfluidic compartments as sample replicates without

additional factor levels for biological or technical replicates. Separately, Akiyama et al. [43] and Pratt et al. [1], discussed in this dissertation, consider individual drops as data within a technical replicate within a biological replicate, with multiple levels of replication in each of these sample types. Clarifying these answers is important on a practical basis to ensure the validity of comparisons between studies. These issues also exemplify a more complex problem integral to understanding the results of single-cell studies: how should researchers conceptualize individual-cell resolved data, and how should we expect those data to compare to bulk results?

Considering the increasing popularity of single-cell cultivation methods, it is pertinent to develop and standardize valid methods for measuring and analyzing single-cell data through modeling and an understanding of statistical theory. The current methods for analyzing single-cell data are adapted mainly from bulk microbiology experiments; separately, there are standard methods for analyzing data initially developed for human population research. An example is the Gini coefficient, an economic inequality measure[143] recently utilized in microfluidic single-cell biology [129]. A first step to address the challenge of inconsistent analysis in microfluidic studies could be to critically assess how to classify data from microscale culture formats, especially when those microscale cultures initiate from single cells. Once the data type is well understood, the validity of existing and novel statistical methods can be explored to analyze these data, and standard experimental design principles can be established.

Closing Summary

Drop-based microfluidics and hydrogel microcapsule offshoot technologies have demonstrated potential as a tool in the study of single-cell heterogeneity in microbial populations. Here, I presented two methods that develop microfluidics as a platform for

conducting time-lapse single-cell growth assays: DropSOAC and BioFlex hydrogel-shelled capsule generation. These methods were used to understand the heterogeneity of microbial populations, and to subject those populations to single cell resolved multi-step biological assays. These findings, and the discoveries made while developing these methods, advance the field of drop-based microfluidics by enhancing its applicability to microbial research.

APPENDICES

APPENDIX A

PUBLICATION: RESUSCITATION OF PSEUDOMONAS AERUGINOSA FROM DORMANCY REQUIRES HIBERNATION PROMOTING FACTOR (PA4463) FOR RIBOSOME PRESERVATION

Resuscitation of *Pseudomonas aeruginosa* from dormancy requires hibernation promoting factor (PA4463) for ribosome preservation

Tatsuya Akiyama[a,b], Kerry S. Williamson[a,b], Robert Schaefer[b,c], Shawna Pratt[b,c], Connie B. Chang[b,c], and Michael J. Franklin[a,b,1]

[a]Department of Microbiology and Immunology, Montana State University, Bozeman, MT 59717; [b]Center for Biofilm Engineering, Montana State University, Bozeman, MT 59717; and [c]Department of Chemical and Biological Engineering, Montana State University, Bozeman, MT 59717

Edited by William R. Jacobs Jr., Albert Einstein College of Medicine; Howard Hughes Medical Institute, Bronx, NY, and approved February 6, 2017 (received for review January 21, 2017)

Pseudomonas aeruginosa **biofilm infections are difficult to treat with antibiotic therapy in part because the biofilms contain subpopulations of dormant antibiotic-tolerant cells. The dormant cells can repopulate the biofilms following alleviation of antibiotic treatments. While dormant, the bacteria must maintain cellular integrity, including ribosome abundance, to reinitiate the de novo protein synthesis required for resuscitation. Here, we demonstrate that the *P. aeruginosa* gene PA4463 [hibernation promoting factor (HPF)], but not the ribosome modulation factor (PA3049), is required for ribosomal RNA preservation during prolonged nutrient starvation conditions. Single-cell–level studies using fluorescence in situ hybridization (FISH) and growth in microfluidic drops demonstrate that, in the absence of *hpf*, the rRNA abundances of starved cells decrease to levels that cause them to lose their ability to resuscitate from starvation, leaving intact nondividing cells. *P. aeruginosa* defective in the stringent response also had reduced ability to resuscitate from dormancy. However, FISH analysis of the starved stringent response mutant showed a bimodal response where the individual cells contained either abundant or low ribosome content, compared with the wild-type strain. The results indicate that ribosome maintenance is key for maintaining the ability of *P. aeruginosa* to resuscitate from starvation-induced dormancy and that HPF is the major factor associated with *P. aeruginosa* ribosome preservation.**

dormancy | resuscitation | hibernation promoting factor | ribosome | rRNA

Biofilms are communities of microorganisms that are attached to surfaces through their secreted extracellular polymeric substance material (1, 2). Biofilms are found in most aqueous environments but become problematic when associated with infectious diseases (3). In particular, bacteria growing in biofilms on host tissue or artificial implant devices are difficult to eradicate with antibiotic treatments and often result in chronic infections (4). For example, *Pseudomonas aeruginosa* growing in biofilms on pulmonary tissue is associated with chronic infections of cystic fibrosis (CF) patients (5). Even though the population of *P. aeruginosa* associated with biofilm infections can be reduced with antibiotic treatments, it is rarely eliminated. Results of longitudinal genomics studies of *P. aeruginosa* strains infecting CF pulmonary tissue show that strains within a patient are usually clonal over time (6, 7), suggesting that even though antibiotics reduce the bacterial loads of pulmonary biofilms, clones of the original infecting strains are able to re-emerge and establish new biofilm infections. One mechanism for enhanced tolerance of biofilm-associated bacteria to antibiotics is that biofilms contain heterogeneous populations of cells, including subpopulations of cells that are tolerant of the treatments (8, 9).

Bacterial heterogeneity in biofilms may arise by several mechanisms (10) including adaptation to local environmental conditions. Cells within regions of the biofilm with low nutrients or oxygen may enter a slow-growth or dormant state. Because antibiotics generally target active metabolic functions, dormant bacteria are tolerant of most antibiotic treatments. The dormant bacteria may then resuscitate and repopulate the biofilms following alleviation of antibiotics. Supporting this mechanism for biofilm-associated antibiotic tolerance, in prior research, we differentially labeled *P. aeruginosa* cells with the green fluorescent protein (GFP) and sorted them based on their metabolic activity (9). In those studies, the slow-growing *P. aeruginosa* cells in biofilms were tolerant to ciprofloxacin or tobramycin at concentrations 10-fold greater than their minimum inhibitory concentrations, whereas the active bacteria were killed by those antibiotics. We also used transcriptomics in combination with laser capture microdissection to identify mRNA transcripts that were abundant in the different biofilm subpopulations (9). As expected, most mRNA transcripts were in low abundance in the dormant subpopulation. However, the slow-growing antibiotic-tolerant subpopulation had a high abundance of mRNA transcripts for several genes, including PA4463 [a homolog to the *Escherichia coli* hibernation promoting factor (HPF)]. In *E. coli*, HPF along with ribosome modulation factor (RMF) inactivates ribosomes during stationary phase (11).

RMF and HPF have been well characterized in *E. coli* as ribosome-interacting proteins (12–15). RMF binds to the ribosome near the mRNA exit tunnel on the 30S ribosomal subunit,

Significance

The dormant subpopulations of *Pseudomonas aeruginosa* biofilms are linked to chronic infections because dormant cells tolerate antibiotic treatment and then repopulate the infections when conditions become favorable. Dormant cells must maintain cellular integrity, including preformed ribosomes, to resuscitate. The small-ribosome–binding proteins, ribosome modulation factor, and hibernation promoting factor (HPF) have evolved to maintain ribosomes in an inactive state. Using both population and single-cell–level studies, we show that HPF provides the primary mechanism used by *P. aeruginosa* to maintain ribosome integrity during dormancy, and that HPF is required for optimal *P. aeruginosa* resuscitation from dormancy. Preventing regrowth of the dormant subpopulation by targeting HPF may provide an effective means for eliminating the dormant subpopulations of *P. aeruginosa* infections.

Author contributions: T.A., K.S.W., R.S., S.P., C.B.C., and M.J.F. designed research; T.A., K.S.W., R.S., and S.P. performed research; C.B.C. contributed new reagents/analytic tools; T.A., K.S.W., R.S., S.P., C.B.C., and M.J.F. analyzed data; and T.A., K.S.W., C.B.C., and M.J.F. wrote the paper.

The authors declare no conflict of interest.

This article is a PNAS Direct Submission.

[1]To whom correspondence should be addressed. Email: franklin@montana.edu.

This article contains supporting information online at www.pnas.org/lookup/suppl/doi:10.1073/pnas.1700695114/-/DCSupplemental.

and HPF binds at the channel of the 30S ribosomal subunit where tRNA and mRNA bind, thereby inhibiting translation (12, 16, 17). RMF and HPF also cause conformational changes to the ribosome, which results in dimerization of two ribosomes to form an inactive 100S form (18). Ueta et al. (11) developed a model for ribosome inactivation during stationary phase of *E. coli*. They concluded that RMF binds the ribosome, forming an inactive 90S dimer, and that HPF stabilizes the ribosome in an inactive 100S form. *E. coli* also encodes an HPF paralog, YfiA, that inactivates the 70S ribosome, but inhibits the formation of the 100S dimer (11).

Homologs to RMF and HPF are found in many bacterial taxa, but vary depending on the organism. *E. coli* and most other gamma Proteobacteria have genes for *rmf*, *hpf*, and *yfiA*, whereas bacteria other than the gamma Proteobacteria lack the gene for *rmf*. *Staphylococcus aureus* does not encode *rmf*, but has an *hpf* with an extended C-terminal tail, termed long HPF (19). Long HPF results in 100S ribosome formation in stationary-phase *S. aureus* cells, even in the absence of an RMF homolog (19). *P. aeruginosa* PAO1 contains genes for *rmf* (PA3049) and *hpf* (PA4463), but does not encode the *hpf* paralog, *yfiA* (20). The involvement of HPF and RMF on maintenance of cell viability also varies among bacterial species. In *E. coli*, RMF, but not the HPF homologs, is required to maintain cell viability during stationary phase (11, 14). *Vibrio cholerae*, which has an *rmf* and two *hpf* homologs, requires at least one copy of *hpf* to maintain cell viability during stationary phase (21). *Mycobacterium* spp. and *Listeria monocytogenes*, which encode long HPF, require HPF for cell viability maintenance during prolonged incubation and during hypoxic conditions (22, 23).

In our prior study (9), biofilms of *P. aeruginosa* PAO1 with deletions of *rmf* or *hpf* had increased uptake of the membrane-impermeable stain, propidium iodide, compared with wild-type cells, suggesting that the nutrient- or oxygen-starved *P. aeruginosa* cells may lose viability in the absence of these ribosome-interacting factors. Here, we investigated the roles of *hpf* and *rmf* in the maintenance of viability of *P. aeruginosa* undergoing nutrient-deprived conditions. Under starvation conditions, wild-type *P. aeruginosa* PAO1 maintained the ability to resuscitate for weeks with little loss of viability. Surprisingly, the Δ*rmf* mutant also had little loss of viability during extended starvation. However, the Δ*hpf* mutant was impaired in its ability to resuscitate from starvation. To investigate the molecular mechanism for impaired resuscitation of the mutant strain, we analyzed the rRNAs of the starved cells both at the population level and at the single-cell level. Unlike the wild-type cells and the Δ*rmf* mutant cells, the Δ*hpf* mutant strain lost most of its rRNA by day 4 of starvation. In addition, by using drop-based microfluidic approach, we show that most of the Δ*hpf* mutant cells were unable to divide and remained as single nonreplicating cells following extended starvation. Overall, the results demonstrate that, in *P. aeruginosa*, HPF is required to protect cells from ribosome loss during extended nutrient-deprived conditions and that ribosome protection by HPF is necessary for *P. aeruginosa* to resuscitate from dormancy.

Results

HPF, but Not RMF, Is Required for Maintenance of *P. aeruginosa* Viability Under Starvation Conditions. To characterize the physiological roles of HPF and RMF in *P. aeruginosa*, we tested the ability of *P. aeruginosa* PAO1 with Δ*hpf*, Δ*rmf*, and Δ*hpf*/Δ*rmf* mutations to resuscitate following prolonged nutrient deprivation. Wild-type and mutant cells were cultured to early stationary phase, washed in PBS, and then incubated in PBS with shaking at 37 °C. Aliquots of the cultures were sampled daily for their ability to form colonies on Tryptic Soy Agar (TSA) plates. The wild-type *P. aeruginosa* PAO1 was able to survive the starvation conditions with no apparent loss of viability ($P = 0.96$) (Fig. 1*A*). Based on results from *E. coli* (11, 14), RMF is predicted to play a role in ribosome inactivation. However, no observable phenotype with respect to recovery from starvation conditions ($P = 0.37$) was observed for *P. aeruginosa* Δ*rmf* (Fig. 1*A*). In addition, and in contrast to published results for RMF in *E. coli* (24–27), the *P. aeruginosa* Δ*rmf* mutant did not show an observable survival phenotype compared with the wild-type strain when exposed to osmotic shock, heat shock, acid stress, or sensitivity to gentamicin. In contrast, a deletion of PA4463 (Δ*hpf*) resulted in a decrease in cell recovery following starvation ($P < 0.0001$). The Δ*hpf* mutant strain initially produced 1.9×10^8 cfu × mL^{-1} after 30 min of starvation and reduced to 2.5×10^7 cfu × mL^{-1} by 5 d of starvation (Fig. 1*A*). When Δ*hpf* was complemented *in trans* (Δ*hpf* + *hpf*), survival under nutrient-limited conditions was restored to wild-type levels ($P = 0.25$), but not for the vector control strain (Δ*hpf* + VC) ($P < 0.0001$). The Δ*hpf*/Δ*rmf* double mutant also showed loss of recovery following starvation compared with the wild-type strain ($P = 0.0002$) (*SI Appendix*, Fig. S1). The Δ*hpf*/Δ*rmf* double mutant could be restored to wild-type levels of resuscitation with a plasmid containing *hpf* alone, but not with a plasmid containing *rmf* alone (*SI Appendix*, Fig. S1).

The stringent response plays a role in the ability of *P. aeruginosa* to survive in stationary phase (28). In the stringent response, guanidine penta- and tetra-phosphate [(p)ppGpp], produced by the activities of RelA and SpoT when RelA interacts with stalled ribosomes (29), acts as a signaling molecule that induces expression of genes required for survival during stationary phase (30). We tested a Δ*relA*/Δ*spoT* mutant under the same starvation conditions as the Δ*rmf* and Δ*hpf* mutant strains. The Δ*relA*/Δ*spoT* mutant showed a similar response to starvation as the Δ*hpf* mutant, where cell recovery was impaired compared with the wild-type strain ($P = 0.03$) (Fig. 1*A*). The results indicate that HPF and the stringent response, but not RMF, is necessary for prolonged *P. aeruginosa* survival under nutrient-limited conditions.

HPF Is Required for Optimal Recovery of *P. aeruginosa* from Nutrient Starvation. During the starvation experiments, we noted that, in addition to the reduced number of cfu's for the Δ*hpf* mutant strain, the colonies that arose were heterogeneous in morphology (Fig. 1*B* and *SI Appendix*, Fig. S2). The starved wild-type strain produced large, uniform colonies. Although some colonies of the Δ*hpf* strain were similar to those of the wild type, many were small and required extended incubation time to become visible. The Δ*hpf* + *hpf* complemented strain had smaller colonies than the wild type, but the colonies were uniform (Fig. 1*B* and *SI Appendix*, Fig. S2). The Δ*relA*/Δ*spoT* strain had colony morphologies with heterogeneity in size, but did not require extended incubation time to become visible. When the small Δ*hpf* colonies were restreaked onto new TSA plates, the wild-type colony morphology was restored, indicating that heterogeneity in recovered colony size was not heritable. To determine if the reduced cfu counts following starvation of the Δ*relA*/Δ*spoT* mutant strain were due to the role of the stringent response in regulation of *hpf* expression, we introduced a plasmid copy of *hpf* under control of the isopropyl β-D-1-thiogalactopyranoside-inducible P_{tac} promoter into the Δ*relA*/Δ*spoT* strain. The Δ*relA*/Δ*spoT* + *hpf* strain had a similar survival phenotype as the Δ*relA*/Δ*spoT* strain (*SI Appendix*, Fig. S3), indicating that loss of cell viability in the Δ*relA*/Δ*spoT* mutant is not associated with loss of *hpf* expression.

HPF Is Required for Preservation of 23S rRNA During Nutrient Starvation. HPF and RMF are ribosome-associated proteins that in *E. coli* cause formation of inactive 100S ribosome dimers during stationary phase (11). To characterize the roles of RMF and HPF on ribosomes under starvation conditions of *P. aeruginosa*,

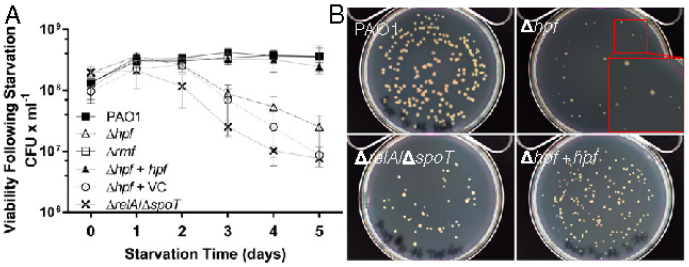

Fig. 1. Recovery of *P. aeruginosa* following extended incubation under nutrient-deprived conditions. (*A*) The cfu's on TSA agar following incubation in aerated PBS. (*B*) Colony morphology of *P. aeruginosa* on TSA, following 4 d of incubation in PBS for wild-type *P. aeruginosa* PAO1, PAO1 Δ*hpf*, PAO1 Δ*relA*/Δ*spoT*, and PAO1 Δ*hpf* + *hpf*. Colony morphologies of each strain and at each time point are shown in *SI Appendix*, Fig. S2.

we extracted total RNA from nutrient-deprived cultures and assayed the relative abundance of the 23S and 16S rRNAs using the Agilent Bioanalyzer. *P. aeruginosa* PAO1 cells cultured to stationary phase showed a 23S/16S rRNA ratio of ~1.6 (Fig. 2 *A* and *B*). Remarkably, this ratio was maintained in *P. aeruginosa* PAO1 throughout the starvation period (Fig. 2*B* and *SI Appendix*, Fig. S4), indicating little loss of ribosome quality during prolonged nutrient deprivation. Similarly, the Δ*rmf* mutant maintained a 23S/16S rRNA ratio of ~1.5 throughout starvation (Fig. 2*B* and *SI Appendix*, Fig. S4). In contrast, the Δ*hpf* strain had 23S/16S rRNA ratios of 1.4 before starvation, which rapidly decreased to 0.1 by day 4 of starvation (Fig. 2 *A* and *B* and *SI Appendix*, Fig. S4). The differences between the Δ*hpf* mutant and the wild-type strain were significant throughout starvation, except on day 0 ($P < 0.000001$). When the Δ*hpf* mutant strain was complemented with *hpf*, the ratio of 23S and 16S rRNA was restored to levels that were not significantly different from the wild type ($P = 0.83$), whereas the vector control (Δ*hpf* + VC) did not restore the rRNA ratios ($P < 0.0001$) (Fig. 2 *A* and *B* and *SI Appendix*, Fig. S4). We also determined the 23S/16S rRNA ratios of the Δ*hpf*/Δ*rmf* double mutant. As with the Δ*hpf* mutant, the Δ*hpf*/Δ*rmf* double mutant had loss of the 23S rRNA during nutrient starvation (*SI Appendix*, Fig. S5). The 23S/16S rRNA ratio for the double mutant was complemented by a plasmid copy of *hpf* without *rmf*, but not with *rmf* alone (*SI Appendix*, Fig. S5). The results indicate that HPF, but not RMF, is required for maintenance of the 23S rRNA under starvation conditions. Interestingly, although the Δ*relA*/Δ*spoT* mutant had reduced viability during starvation compared with wild type, the strain did not show selective loss of the 23S rRNA compared with wild type ($P = 0.30$) (Fig. 2*B* and *SI Appendix*, Fig. S4). The results indicate that the molecular mechanism for reduced viability in the starved Δ*relA*/Δ*spoT* mutant likely differs from that of the Δ*hpf* mutant.

During nutrient starvation of *E. coli*, ribosome degradation is initiated by site-specific endoribonuclease cleavages of the 16S and 23S rRNAs, leading to reduced 70S ribosome abundances and proteolysis of ribosomal proteins (31–33). To determine the fate of the rRNA during nutrient starvation of the *P. aeruginosa* Δ*hpf* strain, we performed time-course Bioanalyzer studies over the first day of starvation. The Δ*hpf* mutant showed reduction of the 23S peak and a concomitant increase in peak-associated small-molecular-weight RNAs (~100 nt in length), characteristic of degraded rRNA fragments (*SI Appendix*, Fig. S6*A*). In contrast to the wild-type cells and the Δ*hpf* + *hpf* cells, the small-molecular-weight RNA comprised most of the cellular RNA of the Δ*hpf* mutant strain by day 4 of starvation (*SI Appendix*, Fig. S6*B*). The total RNA content of the Δ*hpf* culture also decreased, compared with the wild-type control, after 4 d of starvation ($P = 0.01$) (*SI Appendix*, Fig. S6*D*). We next analyzed the relative amounts of 16S and 23S rRNA of the Δ*hpf* mutant strain compared with wild-type strain following 0 d and 4 d of starvation by reverse transcription-quantitative PCR (RT-qPCR). The results showed a reduction of both rRNA subunits in the Δ*hpf* mutant cells on day 4 ($P = 0.03$), but with greater reduction of the 23S rRNA subunit than the 16S subunit (*SI Appendix*, Fig. S6*E*).

Heterogeneity of HPF-Based rRNA Protection Determined at the Single-Cell Level. Although cell viability was reduced in the Δ*hpf* mutant, viability was not completely eliminated during nutrient deprivation (Fig. 1). In addition, loss of the rRNA was characterized for the entire population of cells, which may have masked the amount of rRNA present in individual cells within the population. Therefore, we used FISH analysis to determine the 16S rRNA levels of individual nutrient-deprived cells. To analyze the FISH results quantitatively, we determined the average fluorescence intensity per pixel within the area of single cells using ImageJ (https://imagej.nih.gov/ij/index.html). The fluorescence intensity for each cell was background-subtracted and then normalized by the spike-in control cells, consisting of exponentially growing *P. aeruginosa* PAO1 (pMF230). The spike-in cells were differentiated from the starved test cells because they were larger, had higher abundances of rRNAs, and had GFP fluorescence

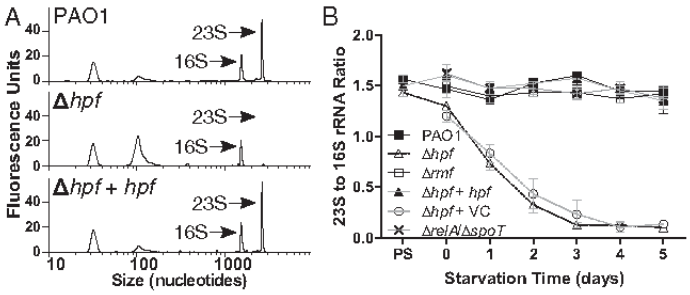

Fig. 2. *P. aeruginosa* 23S-to-16S rRNA ratios following extended incubation under nutrient-deprived conditions with shaking at 37 °C. (*A*) Bioanalyzer traces of 23S and 16S rRNA following 4 d of starvation for wild-type strain PAO1, the Δ*hpf* mutant, and the Δ*hpf* mutant complemented with *hpf* (Δ*hpf* + *hpf*). (*B*) *P. aeruginosa* 23S-to-16S rRNA ratios following extended starvation conditions. Representative bioanalyzer traces showing 23S and 16S rRNAs for all strains at each time point are shown in *SI Appendix*, Figs. S4 and S5.

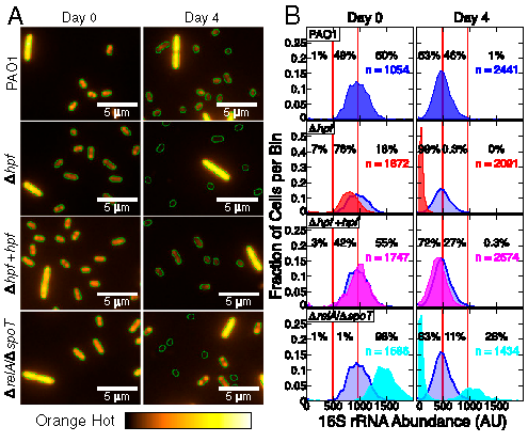

Fig. 3. (*A*) FISH analysis of 16S rRNAs for *P. aeruginosa* PAO1 and mutant derivatives, starved for 4 d in PBS at 37 °C. The16S probe labeled with Cy3 is false-colored orange. Each field contains a spike-in control cell of exponential phase PAO1 (pMF230) (the large cell with high rRNA abundance). The edges of cells were determined by using bright-field microscopy and are outlined in green. (*B*) The mean fluorescence intensity for 16S-Cy3 probe was quantified, normalized to the spike-in controls, and binned based on the fluorescence intensity of individual cells. The dashed vertical lines represent the average FISH fluorescence intensity for the wild-type strain before starvation and after 4 d of starvation. Data for the wild-type strain are shown on each plot in blue. Data shown are from three independent biological replicates per strain at each time point with the total number of cells quantified indicated. Histograms showing the FISH fluorescence intensities for each day of starvation are shown in *SI Appendix*, Fig. S7. Box-whisker plots showing the average and range of these data are shown in *SI Appendix*, Fig. S8.

(Fig. 3*A*). The results from the wild-type cells showed a gradual reduction in the average FISH fluorescence intensity per cell over time ($P = 0.008$) (Fig. 3 and *SI Appendix*, Fig. S7). However, the FISH fluorescence of the wild-type cells was maintained at high levels throughout the starvation conditions, indicating that most cells maintained abundant ribosome content during starvation (Fig. 3 and *SI Appendix*, Fig. S7). The FISH-fluorescence intensities for the Δ*hpf* mutant strain were at similar levels to the wild-type cells before nutrient starvation ($P = 0.17$) (Fig. 3). However, the average FISH-fluorescence intensity of Δ*hpf* decreased following 1 d of starvation ($P < 0.001$) and continued to decrease compared with wild-type cells with continued starvation incubation (Fig. 3*B* and *SI Appendix*, Fig. S7 and Table S1). The complemented Δ*hpf* + *hpf* strain had restored FISH fluorescence, comparable to the wild type (Fig. 3 and *SI Appendix*, Fig. S7 and Table S2).

The FISH results for the Δ*relA*/Δ*spoT* mutant showed a strikingly different response to starvation than either the wild-type strain or the Δ*hpf* mutant strain. During the first 2 d of starvation, the Δ*relA*/Δ*spoT* cells had higher abundances of 16S rRNA than the wild-type cells (*SI Appendix*, Fig. S7). Continued incubation in nutrient-free medium resulted in Δ*relA*/Δ*spoT* mutant cells segregating into two populations with bimodal distribution. One subpopulation of Δ*relA*/Δ*spoT* cells continued to have higher 16S rRNA content than the wild-type cells, whereas the other subpopulation of cells had little detectable rRNA (Fig. 3 and *SI Appendix*, Fig. S7). By day 4 of starvation, most (~63%) Δ*relA*/Δ*spoT* cells had little signal for the 16S rRNA, whereas 26% had signals greater than the average of the wild-type cells.

The presence of outliers with high and low FISH fluorescence intensities were observed for all strains. The box and whisker plots (*SI Appendix*, Fig. S8) show a greater average decrease of 16S rRNA for the Δ*hpf* cells than for the wild-type cells. However, all strains had outliers where either high or low abundances of rRNAs were observed, including a small fraction of Δ*hpf* mutant cells that had fluorescence intensity as high as the average intensity of 4-d-starved wild-type cells. The observation of outliers at the single-cell level suggests that HPF may not be the sole mechanism for maintenance of ribosome integrity of *P. aeruginosa*.

Role of HPF in the Resuscitation of Individual Dormant Cells. The colony size and variable rRNA levels of the starved Δ*hpf* mutant cells suggested that there was heterogeneity in the resuscitating population. Therefore, we used a drop-based microfluidic approach (34) to quantify the heterogeneity in this population. These drop-based experiments allowed us to differentiate and quantify individual cells undergoing resuscitation from the nondividing cells within many drop-based bioreactors. We compared resuscitation of the wild-type cells and the Δ*hpf* mutant cells, both expressing GFP, so that they could be visualized by confocal scanning laser microscopy (CSLM) (Fig. 4 *A* and *B*). Cultures were starved using the conditions described above, and then individual cells were encapsulated in 15-μm-diameter, water-in-oil drops containing TSB medium as the dispersed phase in oil. The ratio of drops containing one cell to empty drops was set at ~1:5–1:10. The cells were then incubated in the TSB contained in each drop for 24–48 h to allow resuscitation of individual cells from the starvation-induced dormancy. Drops were then analyzed by CSLM and quantified by image analysis for cell growth (drops that were completely or partially filled with bacteria versus drops that contained only one cell) (Fig. 4). Similar to the cfu counts, there was an increase in total number of cells from day 0 to day 1 of starvation for both the wild-type ($P = 0.037$) and Δ*hpf* mutant cells ($P = 0.003$) (Fig. 1 and *SI Appendix*, Fig. S9), suggesting that the cells had divided in the PBS-starvation medium. To determine if cells were capable of division during the first day of starvation, we encapsulated and incubated cells in drops containing PBS. Under these conditions, most drops contained multiple cells after 24 h (*SI Appendix*, Fig. S10), indicating that the cells had undergone at least one round of cell division during the first day of incubation in PBS.

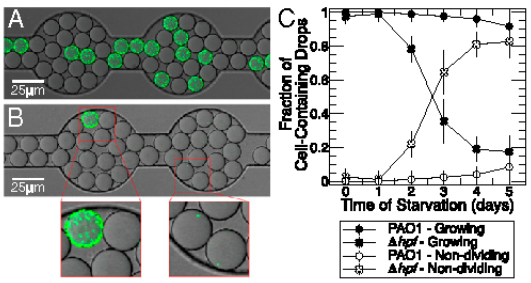

Fig. 4. Examples of cell resuscitation of individual *P. aeruginosa* (pMF230) cells within 15-μm-diameter oil drops with visualization by CSLM. Cells were incubated in PBS for 4 d, and encapsulated in drops containing TSB medium. (*A*) *P. aeruginosa* PAO1 following 4 d of starvation and then regrowth for 24 h in TSB. (*B*) *P. aeruginosa* PAO1 Δ*hpf* after 4 d of starvation and then regrowth for 24 h in TSB. (*Insets*) Cell regrowth and single nondividing cells in drops. (*C*) Percentage of cells that replicated inside of TSB-containing drops versus cells that remained as single intact nondividing cells following starvation in PBS. Cell counts of replicating and nonreplicating cells are shown in *SI Appendix*, Fig. S9. Regrowth of PAO1 and the Δ*hpf* mutant cells in drops over 24 h is shown in Movies S1 and S2.

Following the initial cell division in PBS from day 0 to day 1 of starvation, the total number of cells captured in drops remained essentially constant throughout the starvation period for both the Δ*hpf* mutant ($P = 0.41$) and wild-type cells ($P = 0.88$) (*SI Appendix*, Fig. S9), indicating little cell lysis during starvation. However, the percentage of cells that remained as single nonreplicating cells versus cells that grew within the drops differed over time for PAO1 ($P = 0.03$) and the Δ*hpf* mutant strains ($P = 0.01$) (Fig. 4*C* and *SI Appendix*, Fig. S9). Initially, ~100% of the wild-type cells were capable of resuscitation inside of drops. The number of PAO1 cells capable of resuscitation decreased to 96% by 4 d of starvation (Fig. 4*C* and *SI Appendix*, Fig. S9). In contrast, the number of Δ*hpf* mutant cells capable of resuscitation inside of the drops decreased over time of starvation, with most cells (81%) remaining as single nondividing cells by day 4 of starvation (Fig. 4*C* and *SI Appendix*, Fig. S9). Additional incubation to 48 h inside drops did not result in a significant increase in the number of cells that could resuscitate ($P = 0.81$). The results indicate that the number of nondividing *P. aeruginosa* cells increases during starvation in the absence of a functional HPF.

The resuscitating Δ*hpf* mutant cells had heterogeneous colony morphology (Fig. 1), suggesting that some of the recovering Δ*hpf* cells either had an increased lag time or a reduced growth rate. To distinguish these two possibilities, we performed time-course imaging of single cells in microfluidic drops following 4 d of starvation. Most wild-type cells (98.7%) recovered from starvation and had a relatively uniform growth rate averaging 0.56 h^{-1} (Movie S1 and *SI Appendix*, Fig. S11), whereas most of the Δ*hpf* mutant cells (84.4%) did not recover following 4 d of starvation. The Δ*hpf* cells that recovered had a slightly lower average growth rate (0.44 h^{-1}) than the wild-type cells. However, the Δ*hpf* cells had highly variable lag times (Movie S2 and *SI Appendix*, Fig. S11). The results indicate that the small-colony variants of the Δ*hpf* cells as seen in Fig. 1 are likely caused by an increased lag time required for these cells to recover from starvation.

Discussion

Heterotrophic bacteria living in aqueous environments often experience conditions where nutrients are scarce, including the nutrient-depleted zones of biofilms (10). Rapidly growing bacteria contain sufficient ribosome concentrations for maximum protein biosynthesis during exponential phase (35, 36). When the cells switch to slow-growth conditions, the number of ribosomes per cell diminishes through degradation or by partitioning to daughter cells. However, slowly growing and dormant cells must have mechanisms to maintain sufficient quantities of premade macromolecules, including ribosomes, to allow de novo protein synthesis and cell regrowth when conditions become favorable (37). Mechanisms have evolved to avoid complete loss of these essential macromolecules when cells are dormant. Here, we demonstrate that the small-ribosome–interacting protein, HPF, is required for ribosome preservation during dormancy of *P. aeruginosa*. Surprisingly, although important for *E. coli* ribosome inactivation (13) and abundant in most *P. aeruginosa* biofilm transcriptomic experiments (38), RMF does not appear to play a significant role in ribosome preservation in *P. aeruginosa* under the conditions tested here. Mechanisms for starvation responses may be specific for a certain nutrient. In *P. aeruginosa*, *hpf* is located downstream of the nitrogen-stress–associated sigma factor, *rpoN*, and is expressed, in part, from the *rpoN* promoter. However, *hpf* also has its own promoter(s), allowing high expression under certain conditions.

In a previous study, we measured the ribosome abundance of cells at different vertical strata within *P. aeruginosa* biofilms by microdissecting the biofilms and then assaying 16S rRNA amounts from the different microzones using RT-qPCR (39). Because rRNA is rapidly degraded when not associated with ribosomes (40), quantification of rRNA provides an estimate of the ribosome copy number per cell. From that study, we showed that exponentially growing *P. aeruginosa* had ~70,000 ribosomes per cell, whereas cells in the slowly growing subpopulation of biofilms had ~20,000 ribosomes per cell (39). This relatively high concentration of ribosomes in the slow-growing cells was maintained even for cells with little transcriptional activity, suggesting that ribosomes are preserved in the cells in the interior of the biofilms. Identification of transcripts for the ribosomal accessory protein, *hpf*, as abundant in the interior of the biofilms indicated that the product of this gene may be important for ribosome preservation in the dormant subpopulation of cells (9). Here, we show that, in the absence of *hpf*, starved cells have reduced capacity to resuscitate following nutrient deprivation and have reduced rRNA levels. The population-level experiments of the Δ*hpf* strain showed greater loss of the 23S rRNA than of the 16S rRNA (Fig. 2), but with a significant loss of both rRNA species (*SI Appendix*, Fig. S6), compared with only a modest decrease of 16S and 23S rRNA levels for starved wild-type cells. The FISH single-cell results also showed loss of the 16S rRNA in the Δ*hpf* mutant, whereas the wild-type strain maintained relatively high levels of 16S rRNA during starvation (Fig. 3).

Ribosome degradation during nutrient starvation in *E. coli* is initiated by site-specific endoribonuclease cleavages of 16S and 23S rRNAs, leading to the loss of detectable free subunits as well as reduced 70S ribosome abundance (31, 33). Ribosomal proteins dissociated from rRNAs are susceptible to proteolysis and likely recycled as nutrients (32). We observed an additional peak in the Δ*hpf* mutant in the Bioanalyzer studies, which may indicate the product of 23S rRNA cleavage (Fig. 2 and *SI Appendix*, Fig. S6). Cleavage of 23S rRNA may initiate rRNA degradation to small fragments as observed here in the Bioanalyzer studies. The crystal structures of ribosomes with HPF and its paralog revealed that the HPF-binding site overlaps with the binding sites of translation initiation factors on the 30S subunit (12, 41). In vitro studies also indicate that the HPF paralog YfiA competes for 30S binding with IF-3 in the presence of polyamines (41). Binding of IF-3 to the 30S subunit prevents the association of the 50S subunit until IF-2 promotes subunit joining to form the 70S initiation complex (42). Because the interaction of ribosomal subunits with HPF induces subunit joining (12, 16, 41), HPF may protect unused ribosomes from endoribonucleases through 70S-HPF complex formation, whereas IF-3 binding to the 30S subunit in the absence of HPF would leave free 50S subunits available for endonuclease cleavage.

The heterogeneity observed in microfluidic studies of resuscitating cells indicates that HPF may not provide the sole mechanism for ribosome preservation. A percentage of the Δ*hpf* cells was capable of regrowth in microfluidic drops (Fig. 4). In addition, some Δ*hpf* cells maintained their ribosomal content even after extended starvation (*SI Appendix*, Fig. S8). Therefore, an alternative strategy to ensure ribosome preservation may exist in *P. aeruginosa*. The microfluidic studies of wild-type cells also showed that a percentage of cells (4% by day 4 of starvation) were unable to regrow following starvation. Whether these cells still had metabolic activity and were unable to grow (e.g., viable but nonculturable cells), or whether the cells were not viable, is not known yet. In either case, the results demonstrate that, even in a clonal population of cells, heterogeneity in ribosome content and cellular capacity for regrowth exists.

The stringent response mutant had a similar loss of recovery from starvation as the Δ*hpf* mutant. However, the mechanism for impaired recovery of the stringent response mutant differs from the Δ*hpf* mutant strain. Our preliminary data using a transcriptional reporter of *hpf* indicate that the stringent response has a small modulatory effect on *hpf* expression, but that *hpf* expression is not abolished in the Δ*relA*/Δ*spoT* mutant. A plasmid copy of *hpf* did not have any effect on the survival phenotype of the Δ*relA*/Δ*spoT* strain (*SI Appendix*, Fig. S3). Therefore, we conclude that expression of *hpf* is not solely regulated through the product of the stringent response alarmone, (p)ppGpp. Overall, the

results demonstrate that HPF provides the primary mechanism for ribosome preservation during nutrient starvation of *P. aeruginosa* and that ribosome preservation is needed for *P. aeruginosa* cells to resuscitate from dormancy.

Materials and Methods

Bacterial Strains and Growth Conditions. Studies were performed on *P. aeruginosa* strain PAO1 and its Δ*rmf*, Δ*hpf*, and Δ*hpf*Δ*rmf* mutant derivatives and on complemented strains as described in *SI Appendix, SI Materials and Methods*, and previously (9). The stringent response mutant, containing deletions of *relA* and *spoT* (28), was provided by Pradeep Singh, University of Washington, Seattle. Nutrient-starvation studies and the drop-plate method (43) used to quantify cfu's were performed as described in *SI Appendix, SI Materials and Methods*.

RNA Extraction and Determination of Relative rRNA Abundances. RNA was extracted as described previously (44) with modifications described in *SI Appendix, SI Materials and Methods*. RNA was analyzed using the Bioanalyzer 2100 (Agilent Technologies) as described in detail in *SI Appendix, SI Materials and Methods*. Total rRNA and 16S and 23S rRNAs were quantified using the NanoDrop1000 (Thermo Fisher Scientific) and by RT-qPCR as described in *SI Appendix, SI Materials and Methods*.

FISH for Quantification of rRNA. FISH, as described by Brileya et al. (45), and using a Cy3-labeled 16S rRNA probe described by Hogardt et al. (46), was used to quantify the relative amounts of 16S RNA from individual cells. A detailed description of the FISH method and analysis is provided in *SI Appendix, SI Materials and Methods*.

Drop Encapsulation and Monitoring Growth of Single Bacterial Cells. Single bacterial cells were encapsulated into microfluidic drops as described in detail in *SI Appendix, SI Materials and Methods* and in ref. 47. Drop-encapsulated cells were injected into a modified "Dropspots" immobilization device (48). Microscopic and statistical analyses of bacterial growth in drops are provided in *SI Appendix, SI Materials and Methods*.

ACKNOWLEDGMENTS. We thank Phil Stewart, Joanna Borgogna, and Al Parker for their helpful discussions of this work; Geoffrey Zath for microfluidic drop growth rate analysis; Betsy Pitts, Kristen Brileya, and Amanda Richards for microscopy data acquisition; and Dr. Pradeep K. Singh for providing the Δ*relA*/Δ*spoT* mutant. This work was funded by National Institute of Allergy and Infectious Diseases Grant AI113330 (to M.J.F.), National Institute of General Medical Sciences Grant P20GM103474 (to S.P.), and Montana State University's Graduate School (T.A.).

1. Costerton JW, Lewandowski Z, Caldwell DE, Korber DR, Lappin-Scott HM (1995) Microbial biofilms. *Annu Rev Microbiol* 49:711–745.
2. Flemming HC, Wingender J (2010) The biofilm matrix. *Nat Rev Microbiol* 8(9):623–633.
3. Costerton JW, Stewart PS, Greenberg EP (1999) Bacterial biofilms: A common cause of persistent infections. *Science* 284(5418):1318–1322.
4. Stewart PS, Costerton JW (2001) Antibiotic resistance of bacteria in biofilms. *Lancet* 358(9276):135–138.
5. Lyczak JB, Cannon CL, Pier GB (2002) Lung infections associated with cystic fibrosis. *Clin Microbiol Rev* 15(2):194–222.
6. Burns JL, et al. (2001) Longitudinal assessment of *Pseudomonas aeruginosa* in young children with cystic fibrosis. *J Infect Dis* 183(3):444–452.
7. Warren AE, et al. (2011) Genotypic and phenotypic variation in *Pseudomonas aeruginosa* reveals signatures of secondary infection and mutator activity in certain cystic fibrosis patients with chronic lung infections. *Infect Immun* 79(12):4802–4818.
8. Lewis K (2007) Persister cells, dormancy and infectious disease. *Nat Rev Microbiol* 5(1):48–56.
9. Williamson KS, et al. (2012) Heterogeneity in *Pseudomonas aeruginosa* biofilms includes expression of ribosome hibernation factors in the antibiotic-tolerant subpopulation and hypoxia-induced stress response in the metabolically active population. *J Bacteriol* 194(8):2062–2073.
10. Stewart PS, Franklin MJ (2008) Physiological heterogeneity in biofilms. *Nat Rev Microbiol* 6(3):199–210.
11. Ueta M, et al. (2005) Ribosome binding proteins YhbH and YfiA have opposite functions during 100S formation in the stationary phase of *Escherichia coli*. *Genes Cells* 10(12):1103–1112.
12. Polikanov YS, Blaha GM, Steitz TA (2012) How hibernation factors RMF, HPF, and YfiA turn off protein synthesis. *Science* 336(6083):915–918.
13. Wada A, Yamazaki Y, Fujita N, Ishihama A (1990) Structure and probable genetic location of a "ribosome modulation factor" associated with 100S ribosomes in stationary-phase *Escherichia coli* cells. *Proc Natl Acad Sci USA* 87(7):2657–2661.
14. Wada A, Mikkola R, Kurland CG, Ishihama A (2000) Growth phase-coupled changes of the ribosome profile in natural isolates and laboratory strains of *Escherichia coli*. *J Bacteriol* 182(10):2893–2899.
15. Yamagishi M, et al. (1993) Regulation of the *Escherichia coli rmf* gene encoding the ribosome modulation factor: Growth phase- and growth rate-dependent control. *EMBO J* 12(2):625–630.
16. Ueta M, et al. (2008) Role of HPF (hibernation promoting factor) in translational activity in *Escherichia coli*. *J Biochem* 143(3):425–433.
17. Wada A, Igarashi K, Yoshimura S, Aimoto S, Ishihama A (1995) Ribosome modulation factor: Stationary growth phase-specific inhibitor of ribosome functions from *Escherichia coli*. *Biochem Biophys Res Commun* 214(2):410–417.
18. Kato T, et al. (2010) Structure of the 100S ribosome in the hibernation stage revealed by electron cryomicroscopy. *Structure* 18(6):719–724.
19. Ueta M, Wada C, Wada A (2010) Formation of 100S ribosomes in Staphylococcus aureus by the hibernation promoting factor homolog SaHPF. *Genes Cells* 15(1):43–58.
20. Stover CK, et al. (2000) Complete genome sequence of Pseudomonas aeruginosa PAO1, an opportunistic pathogen. *Nature* 406(6799):959–964.
21. Sabharwal D, Song T, Papenfort K, Wai SN (2015) The VrrA sRNA controls a stationary phase survival factor Vrp of *Vibrio cholerae*. *RNA Biol* 12(2):186–196.
22. Kline BC, McKay SL, Tang WW, Portnoy DA (2015) The *Listeria monocytogenes* hibernation-promoting factor is required for the formation of 100S ribosomes, optimal fitness, and pathogenesis. *J Bacteriol* 197(3):581–591.
23. Trauner A, Lougheed KE, Bennett MH, Hingley-Wilson SM, Williams HD (2012) The dormancy regulator DosR controls ribosome stability in hypoxic mycobacteria. *J Biol Chem* 287(28):24053–24063.
24. El-Sharoud WM, Niven GW (2007) The influence of ribosome modulation factor on the survival of stationary-phase *Escherichia coli* during acid stress. *Microbiology* 153(Pt 1):247–253.
25. Garay-Arroyo A, Colmenero-Flores JM, Garciarrubio A, Covarrubias AA (2000) Highly hydrophilic proteins in prokaryotes and eukaryotes are common during conditions of water deficit. *J Biol Chem* 275(8):5668–5674.
26. McKay SL, Portnoy DA (2015) Ribosome hibernation facilitates tolerance of stationary-phase bacteria to aminoglycosides. *Antimicrob Agents Chemother* 59(11):6992–6999.
27. Niven GW (2004) Ribosome modulation factor protects *Escherichia coli* during heat stress, but this may not be dependent on ribosome dimerisation. *Arch Microbiol* 182(1):60–66.
28. Nguyen D, et al. (2011) Active starvation responses mediate antibiotic tolerance in biofilms and nutrient-limited bacteria. *Science* 334(6058):982–986.
29. Hauryliuk V, Atkinson GC, Murakami KS, Tenson T, Gerdes K (2015) Recent functional insights into the role of (p)ppGpp in bacterial physiology. *Nat Rev Microbiol* 13(5):298–309.
30. Durfee T, Hansen AM, Zhi H, Blattner FR, Jin DJ (2008) Transcription profiling of the stringent response in *Escherichia coli*. *J Bacteriol* 190(3):1084–1096.
31. Basturea GN, Zundel MA, Deutscher MP (2011) Degradation of ribosomal RNA during starvation: Comparison to quality control during steady-state growth and a role for RNase PH. *RNA* 17(2):338–345.
32. Petersen C (1990) *Escherichia coli* ribosomal protein L10 is rapidly degraded when synthesized in excess of ribosomal protein L7/L12. *J Bacteriol* 172(1):431–436.
33. Zundel MA, Basturea GN, Deutscher MP (2009) Initiation of ribosome degradation during starvation in *Escherichia coli*. *RNA* 15(5):977–983.
34. Guo MT, Rotem A, Heyman JA, Weitz DA (2012) Droplet microfluidics for high-throughput biological assays. *Lab Chip* 12(12):2146–2155.
35. Nomura M, Gourse R, Baughman G (1984) Regulation of the synthesis of ribosomes and ribosomal components. *Annu Rev Biochem* 53:75–117.
36. Sarmientos P, Cashel M (1983) Carbon starvation and growth rate-dependent regulation of the *Escherichia coli* ribosomal RNA promoters: Differential control of dual promoters. *Proc Natl Acad Sci USA* 80(22):7010–7013.
37. Madar D, et al. (2013) Promoter activity dynamics in the lag phase of *Escherichia coli*. *BMC Syst Biol* 7:136.
38. Folsom JP, et al. (2010) Physiology of *Pseudomonas aeruginosa* in biofilms as revealed by transcriptome analysis. *BMC Microbiol* 10:294.
39. Pérez-Osorio AC, Williamson KS, Franklin MJ (2010) Heterogeneous *rpoS* and *rhlR* mRNA levels and 16S rRNA/rDNA (rRNA gene) ratios within *Pseudomonas aeruginosa* biofilms, sampled by laser capture microdissection. *J Bacteriol* 192(12):2991–3000.
40. Deutscher MP (2003) Degradation of stable RNA in bacteria. *J Biol Chem* 278(46):45041–45044.
41. Vila-Sanjurjo A, Schuwirth BS, Hau CW, Cate JH (2004) Structural basis for the control of translation initiation during stress. *Nat Struct Mol Biol* 11(11):1054–1059.
42. Schmeing TM, Ramakrishnan V (2009) What recent ribosome structures have revealed about the mechanism of translation. *Nature* 461(7268):1234–1242.
43. Herigstad B, Hamilton M, Heersink J (2001) How to optimize the drop plate method for enumerating bacteria. *J Microbiol Methods* 44(2):121–129.
44. Guragain M, et al. (2016) The *Pseudomonas aeruginosa* PAO1 two-component regulator carsr regulates calcium homeostasis and calcium-induced virulence factor production through its regulatory targets CarO and CarP. *J Bacteriol* 198(6):951–963.
45. Brileya KA, Camilleri LB, Fields MW (2014) 3D-fluorescence in situ hybridization of intact, anaerobic biofilm. *Methods Mol Biol* 1151:189–197.
46. Hogardt M, et al. (2000) Specific and rapid detection by fluorescent in situ hybridization of bacteria in clinical samples obtained from cystic fibrosis patients. *J Clin Microbiol* 38(2):818–825.
47. Holtze C, et al. (2008) Biocompatible surfactants for water-in-fluorocarbon emulsions. *Lab Chip* 8(10):1632–1639.
48. Schmitz CH, Rowat AC, Köster S, Weitz DA (2009) Dropspots: A picoliter array in a microfluidic device. *Lab Chip* 9(1):44–49.

MICROBIOLOGY

APPENDIX B

FURTHER DEVELOPMENT OF THE DROPSOAC CAPSULE

Summary

The DropSOAC chamber published in 2019 [1] was fabricated by laser-cutting a port into the base of a lidded, liquid-tight cell culture dish and embedding a PDMS and coverglass microfluidic array device in the port with epoxy (B Figure 1). These devices were effective for housing the microfluidic drop arrays and equilibrium described in the DropSOAC method [1]. Still, the chambers had several limitations. The hand-made single-use DropSOAC chambers were time-intensive to prepare and were rarely optically flat; the resulting skew of chambers complicated microscopy set-up and analysis. Additionally, the epoxy bond deteriorated during the device preprocessing steps of the DropSOAC method, rendering a subset of fabricated chambers useless. Finally, adapting the DropSOAC approach for anaerobic cultivation for future studies, was not feasible because the original chamber could not be made airtight.

To address these issues, I developed a reusable version of the original DropSOAC chamber via computer-aided 3-D design, prototyped the design using laser-cutting and 3-D printing techniques, and prepared these designs as machine drawings for milling out of aluminum. This process aimed to generate a chamber that was: (1) Reusable; (2) Compatible to house disposable PDMS and coverglass microfluidic devices; (3) Autoclavable; (4) Easy to use while wearing thick nitrile gloves (an element of working in anaerobic glove bags); (5) Flat; (6) Compatible with microscope objectives with low working distances, and; (7) Airtight. The following is a brief description of various prototype iterations, as well as the final design. All chambers were 54 mm in diameter for compatibility with existing microscope stage inserts.

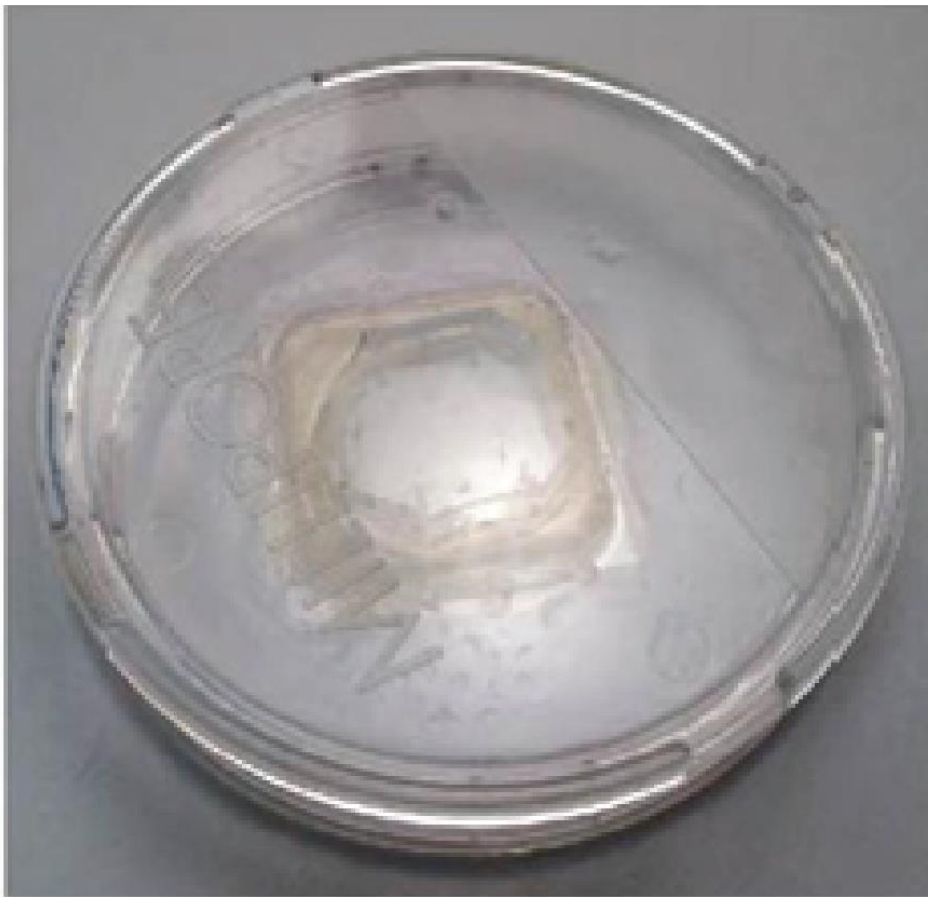

Appendix B Figure 1: The original DropSOAC chamber published in *Frontiers in Microbiology* [1] was fabricated by inserting a PDMS and coverglass microfluidic device in the base of a liquid-tight cell culture dish through a laser-cut port, and bonding the microfluidic device to the dish using 2-component epoxy.

Prototypes

Round-port prototype with rubber slab, silicon o-rings and bolt-and-nut closures

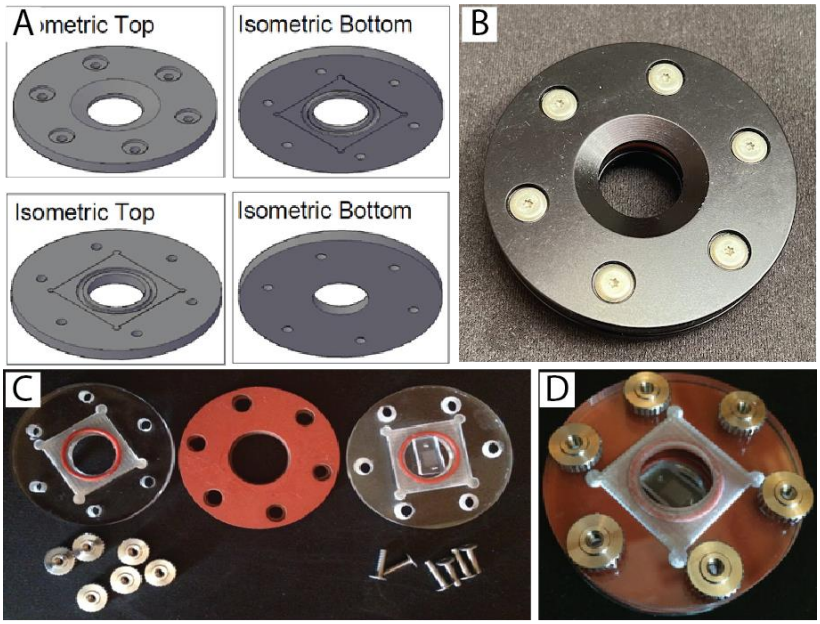

Appendix B Figure 2: (A) CAD drawings of device design. PDMS-coverslip microfluidic device and top sealing coverslip not shown. (B) bottom side of the chamber secured with low-head bolts. (C,D) Prototypes made from laser-cut and laser-etched acrylic. This device was the first reusable DropSOAC chamber design tested, and performed well. The major limitations of this device design were the small viewing port and bulkiness of the thick rubber gasket.

The round-port device was the first reusable DropSOAC chamber design tested, which performed well by being leak-free and facilitated DropSOAC treatment. The major limitations of this device design were the small viewing port and bulkiness of the thick rubber gasket. This device was used for many DropSOAC studies before being replaced by an improved design.

Rectangular-port prototype with o-ring gaskets and bolt-and-nut closures

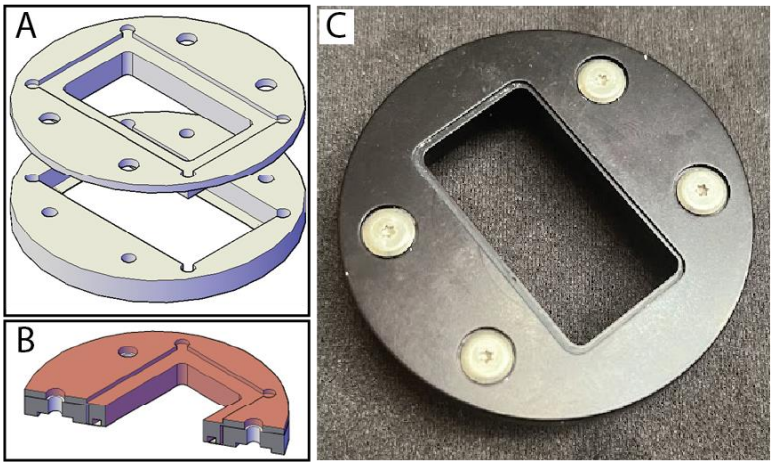

Appendix B Figure 3: (A) CAD designs for the top and bottom device components. PDMS-coverslip microfluidic device and top sealing coverslip not shown. (B) Drawing cutaways showing configuration of assembled device. (C) the bottom side of the finalized device.

This rectangular port chamber improved on the previous design by removing the thick rubber gasket and expanding the viewport. The major limitations of this device design were the hard-to-turn nuts and bolts that complicated the use of this chamber while wearing nitrile gloves, as well as the necessity for vacuum grease to affix the top-sealing coverslip. This device is still used regularly to facilitate DropSOAC studies.

Bayonet closure and knurled edges

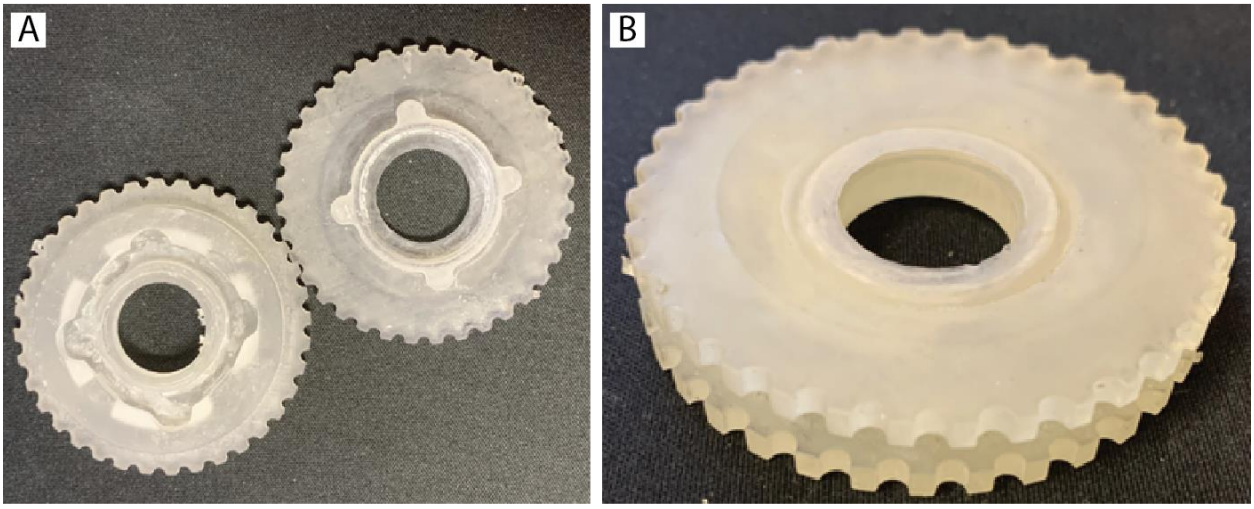

Appendix B Figure 4: SLA printed prototypes of a device with a bayonette closure method and knurled edges. (A) individual device components. (B) The assembled device.

The bayonet closure and knurled edges prototype improved on the previous design replacing nut-and-bolt closure with a bayonet style closure and adding knurled edges to improve dexterity. The major limitation of this prototype was manufacturing complexities, as it required multi-axis milling in tight spaces. Additionally, the knurling was painful to turn, and the viewport was small, which was a necessary design modification to enable the bayonet style closure geometry. For these reasons, this device was never attempted in aluminum.

Hybrid plastic and aluminum device with screw closure

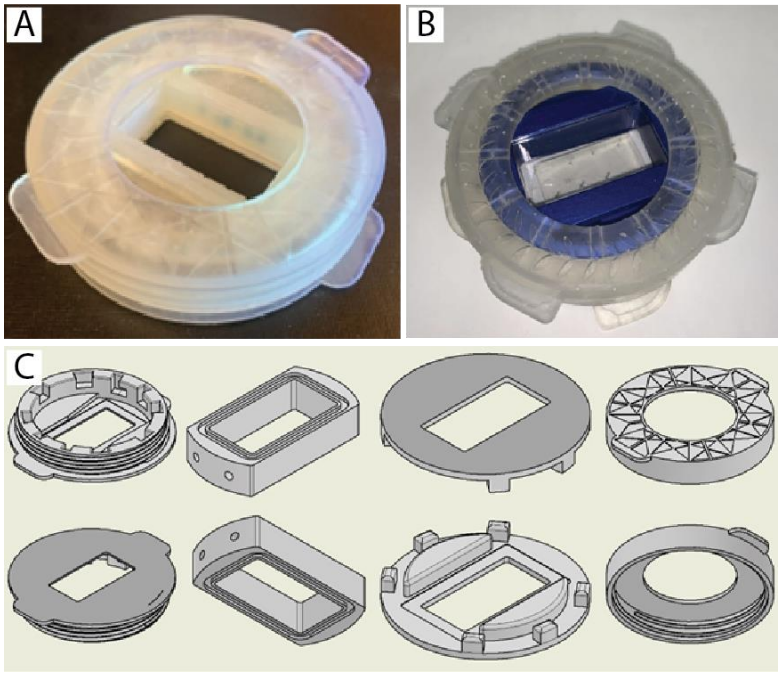

Appendix B Figure 5: A hybrid aluminum and 3-D printed plastic resin chamber. (A) An assembled 3-D printed protype, (B) An assembled device incorporating the aluminum elements, and (C) CAD design for individual components. This device improved on the previous design in being easy and cheaper to manufacture, while maintaining the bolt-and nut free closure. The major limitation of this device were a strength and durability issues in the 3-D printed components, 3-D printing fidelity, and the overly complicated nature of the design.

The hybrid aluminum and 3-D printed resin device improved on the previous design in being easy and cheaper to manufacture, while maintaining the bolt-and nut free closure. The major limitation of this device were a strength and durability issues in the 3-D printed components, 3-D printing fidelity, and the overly complicated nature of the design. While this device was attempted in aluminum, it was never useful for conducting DropSOAC experiments.

Final Chamber

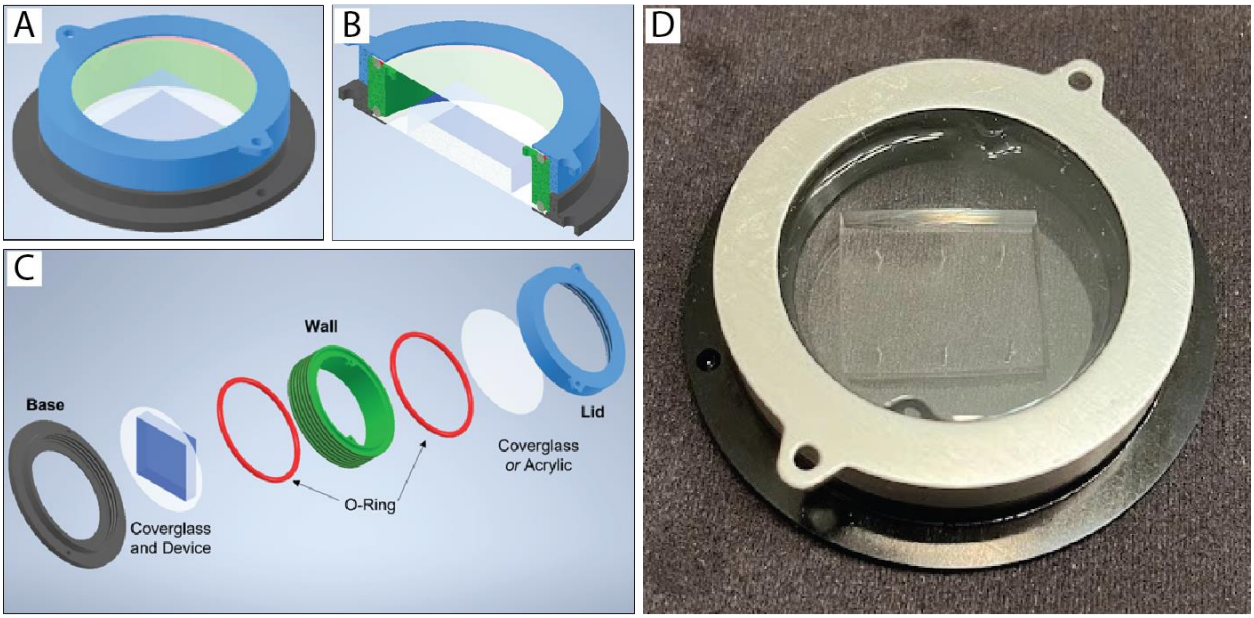

Appendix B Figure 6: The final DropSOAC chamber, currently in use in the Chang lab. (A) CAD design of assembled chamber. (B) Cutaway drawing of the assembled chamber. (C) description of chamber components, and (D) an assembled device housing a DropSOAC prepared drop-array system.

The most recent and successful device design tested improves on previous designs by replacing the rectangular cover glasses for large, circular cover glasses. This allows the device to be closed using a simple, screw type closure. The devices pins inserts (the small holes visualized most clearly in B Figure 6) are easy to hold and turn, and, if necessary, can be fitted with pins to improve handling in the anaerobic glove bag. This device has worked well thus far, but remains untested for anaerobic culture. One minor limitation of this device is the fragility of round cover glasses, which occasionally break during chamber assembly. So far, this device has proven to be

useful for DropSOAC experiments conducted by myself and other Chang Lab members, and testing the device in an anaerobic chamber is planned in future work.

APPENDIX C

CHAPTER 4 SUPPLEMENTARY MATERIALS

Supplementary Tables Supplementary Tables

Supplementary table 1: Capsule Shell Thickness Assay Flow Rates

	Flow rates (µL/h)			
Sample	Core Solution	Shell Solution	Oil Solution	DTT nanoemulsion
1	40	160	400	600
2	100	100	400	600
3	120	80	400	600
4	140	60	400	600
5	160	40	400	600
6	180	20	400	600

Core solution composition:		260 mg/mL 10kDa dextran in PBS with 10kDa FITC-dextran		
Shell solution composition:		200 mg/mL 10kDa 4-arm PEG-mal in PBS with Cy5.5-maleimide		
Oil solution composition:		5wt/wt% Span 80 in light mineral oil		
DTT nanoemulsion composition:		50mg/mL DTT solution nano emulsified 1:15 in 5wt/wt% Span 80 in light mineral oil		

Supplementary table 2: Capsule Diameter Assay Flow Rates

	Flow rates (µL/h)			
Sample	Core Solution	Shell Solution	Oil Solution	DTT nanoemulsion
1	100	100	400	600
2	65	65	600	900
3	30	30	800	1200

Core solution composition:	260 mg/mL 10kDa dextran in PBS with 10kDa FITC-dextran
Shell solution composition:	200 mg/mL 10kDa 4-arm PEG-mal in PBS with Cy5.5-maleimide
Oil solution composition:	5wt/wt% Span 80 in light mineral oil
DTT nanoemulsion composition:	50mg/mL DTT solution nano emulsified 1:15 in 5wt/wt% Span 80 in light mineral oil

Supplementary table 3: Biological Experiment Flow Rates

	Flow rates (µL/h)			
Sample	Core Solution	Shell Solution	Oil Solution	DTT nanoemulsion
TSB Capsule Growth	100	100	400	600
Time Varied Growth	50	50	400	400

Core solution composition:	260 mg/mL 10kDa dextran in PBS
Shell solution composition:	200 mg/mL 10kDa 4-arm PEG-mal in PBS with Cy5.5-maleimide
Oil solution composition:	5wt/wt% Span 80 in light mineral oil
DTT nanoemulsion composition:	50mg/mL DTT solution nano emulsified 1:15 in 5wt/wt% Span 80 in light mineral oil

Supplementary table 4: Comparison of Means for Antibiotic Assay

Two Sample Comparison of Means (2 tailed T-Test) P values				
Treatment	T0 vs. Tmax	T0 vs. Tf	Tmax vs. Tf	Sample Size
0 h	<2.2e-16	3.1E-08	<2.2e-16	132
4 h	<2.2e-16	0.011	<2.2e-16	182
7 h	<2.2e-16	<2.2e-16	<2.2e-16	189
10 h	<2.2e-16	<2.2e-16	2.1E-05	62
untreated	NA	<2.2e-16	NA	173

Supplementary Figures

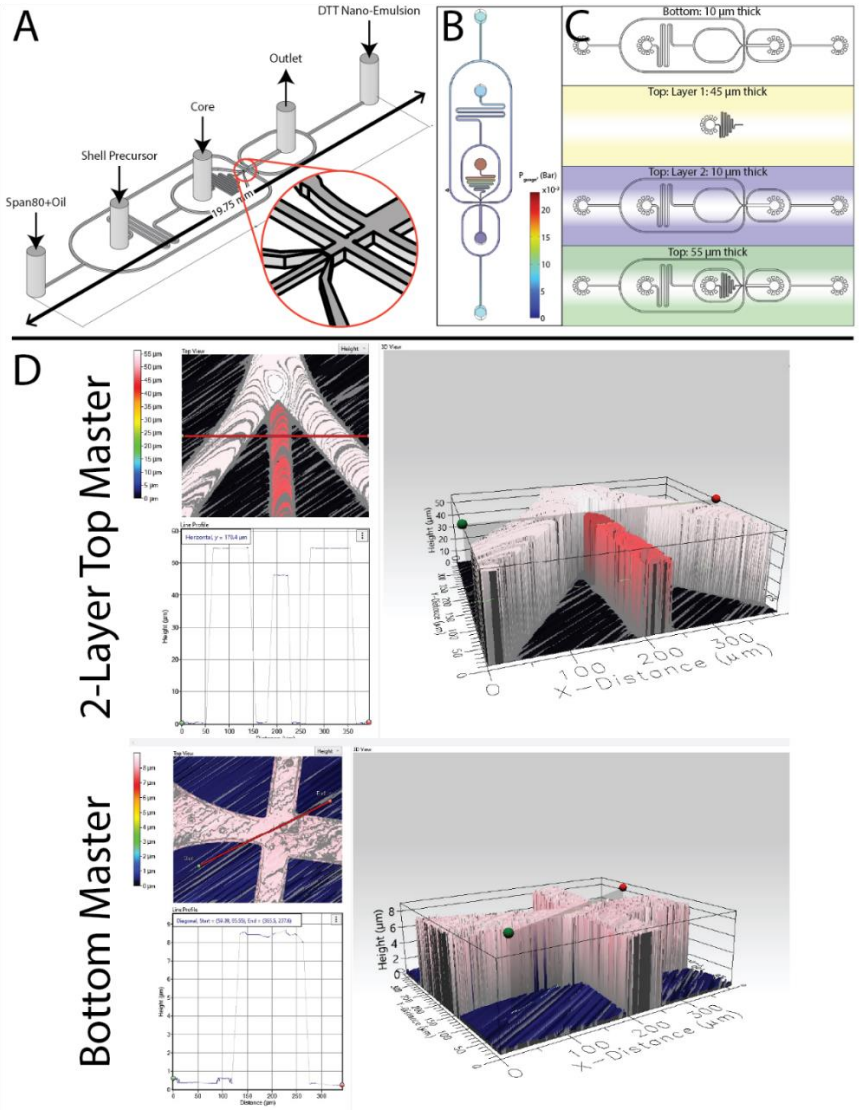

Supplementary Figure 1: BioFlex capsule generation device design and fabrication notes. (A) The capsule generation device is a flow-focusing drop generation device with non-planar geometry at the junction of the core and sheath precursor channels. (B) A snapshot of pressure drop across the device for STP water at capsule-generation flow rates. Color gradient indicates pressure. (C) Non-planar geometry is achieved using multi-layered PDMS molds. The molds are made on silica wafers using 2 layers of photoresist on the top mold and a single layer on the bottom mold. (D) Profilometry was used to ensure mold features are high fidelity and the desired height.

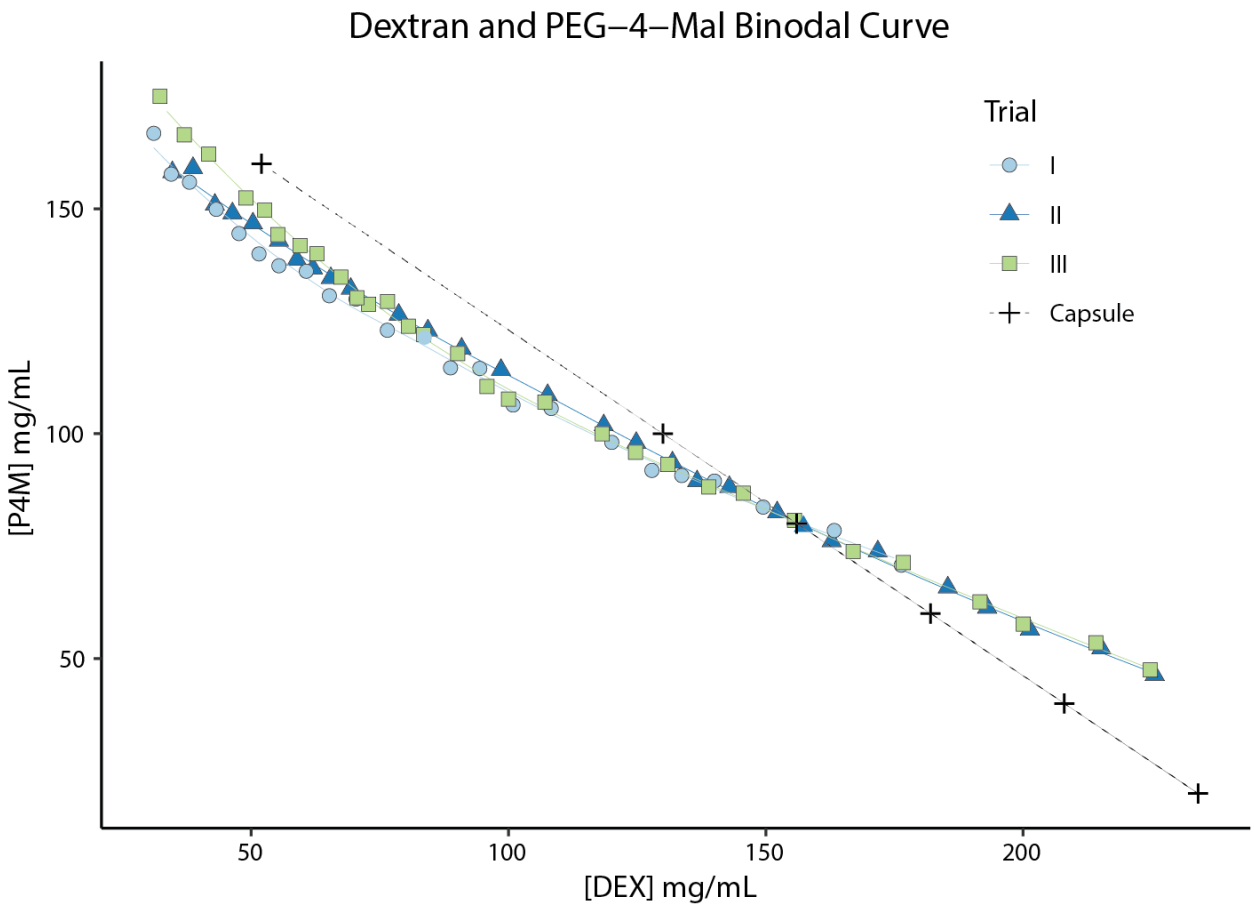

Supplementary Figure 2: Individual cloud point titration trials used to determine the binodal curve of 4-arm PEG-mal / dextran ATPS used in the BioFlex capsules. Dashed line with + symbols represents the concentrations tested during the shell thickness variation experiment.

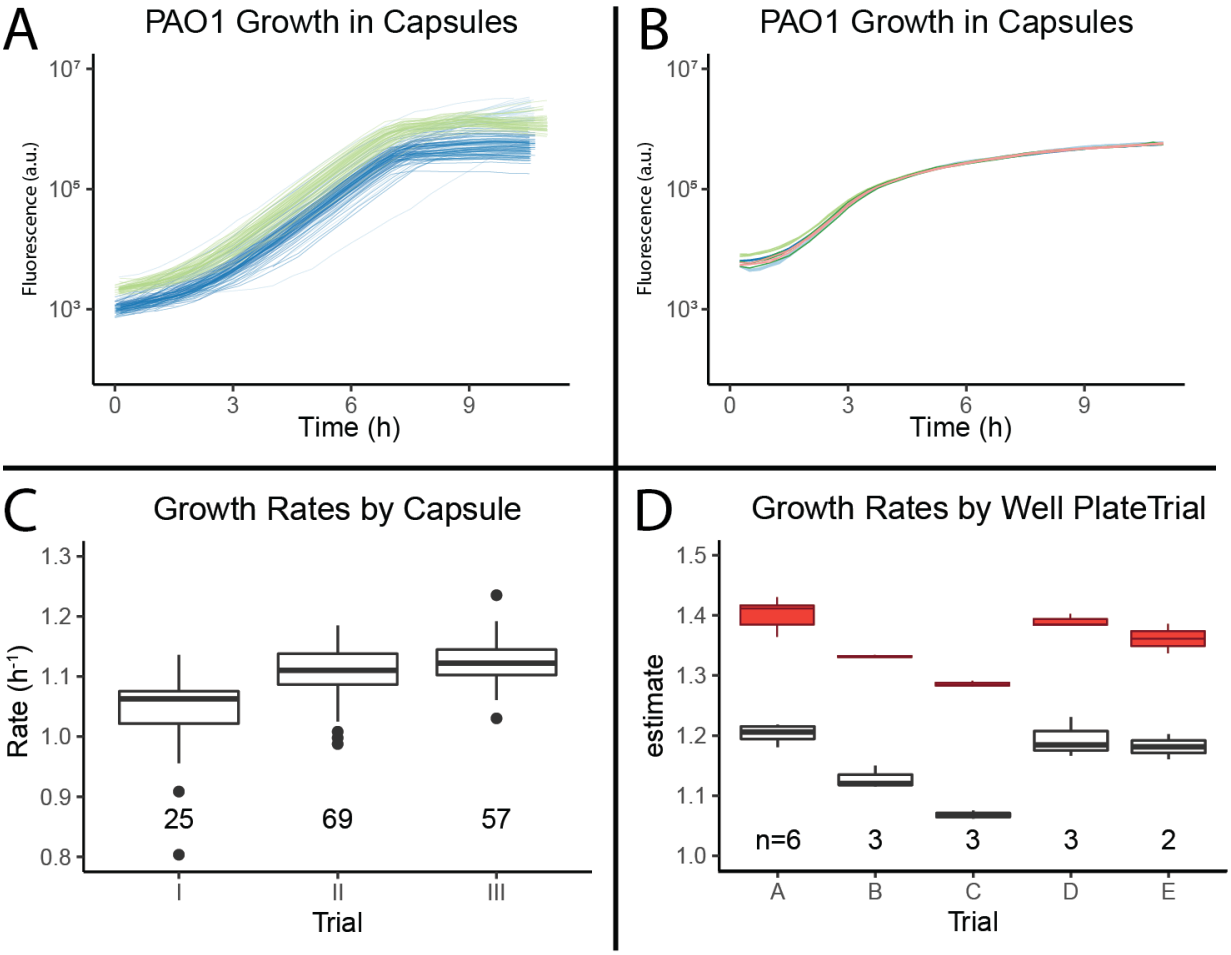

Supplementary Figure 3: Summary of growth in capsules vs. bulk experiments. (A, B) Growth curves for bacteria in individual capsules or individual well of a 96-well plate. (C) Growth rates based on fluorescence increase for capsule trials. (D) Growth rates based on OD (red) and fluorescence (black) for the 96-well plate trials.

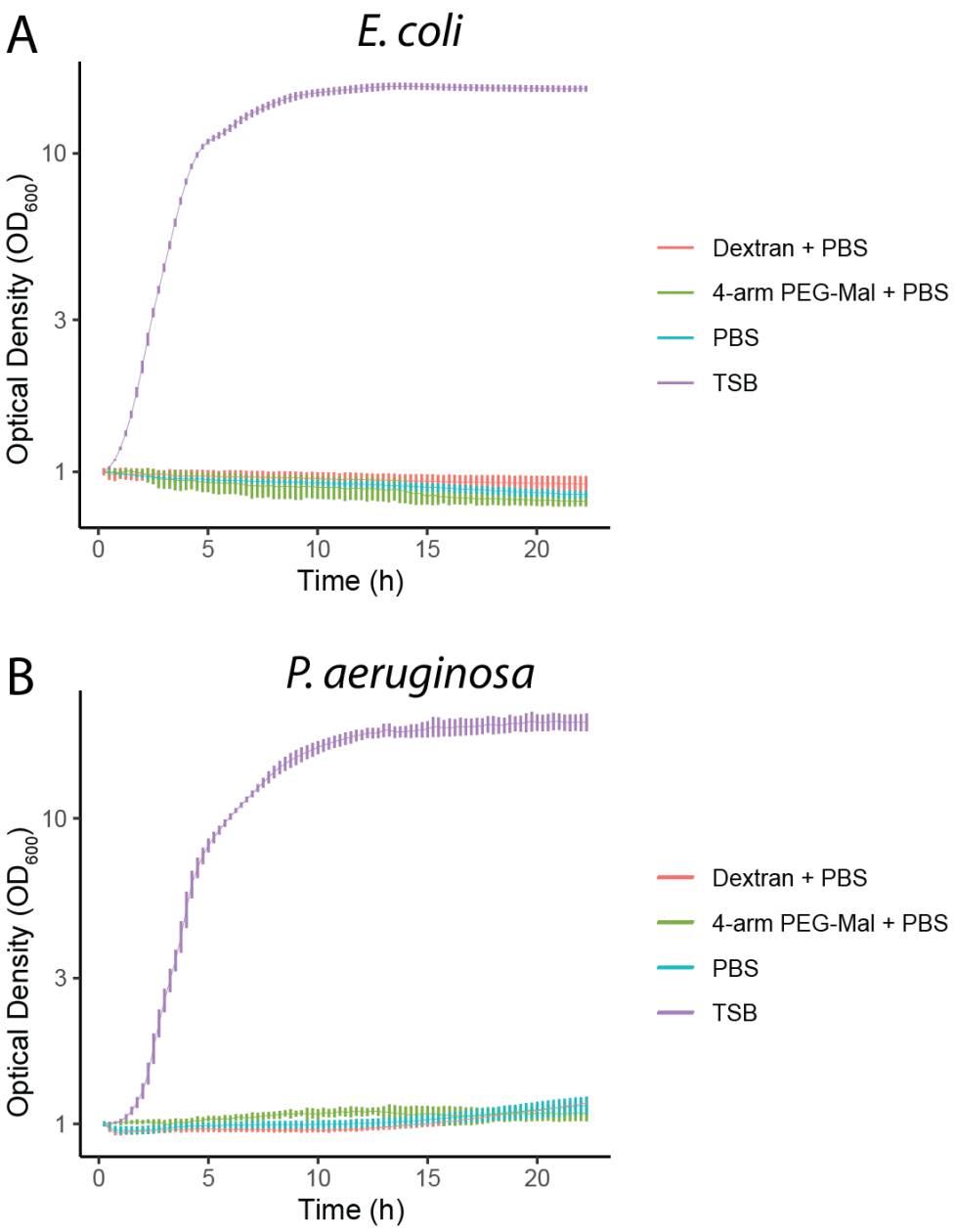

Supplementary figure 4: Optical density based analysis of growth on Dextran or 4-arm PEG-mal for (A) *E. coli* HB101 (pMF 230) and (B) *P. aeruginosa* PAO1 (pMF230), assessed via 96-well plate culture monitored in a plate-reader.

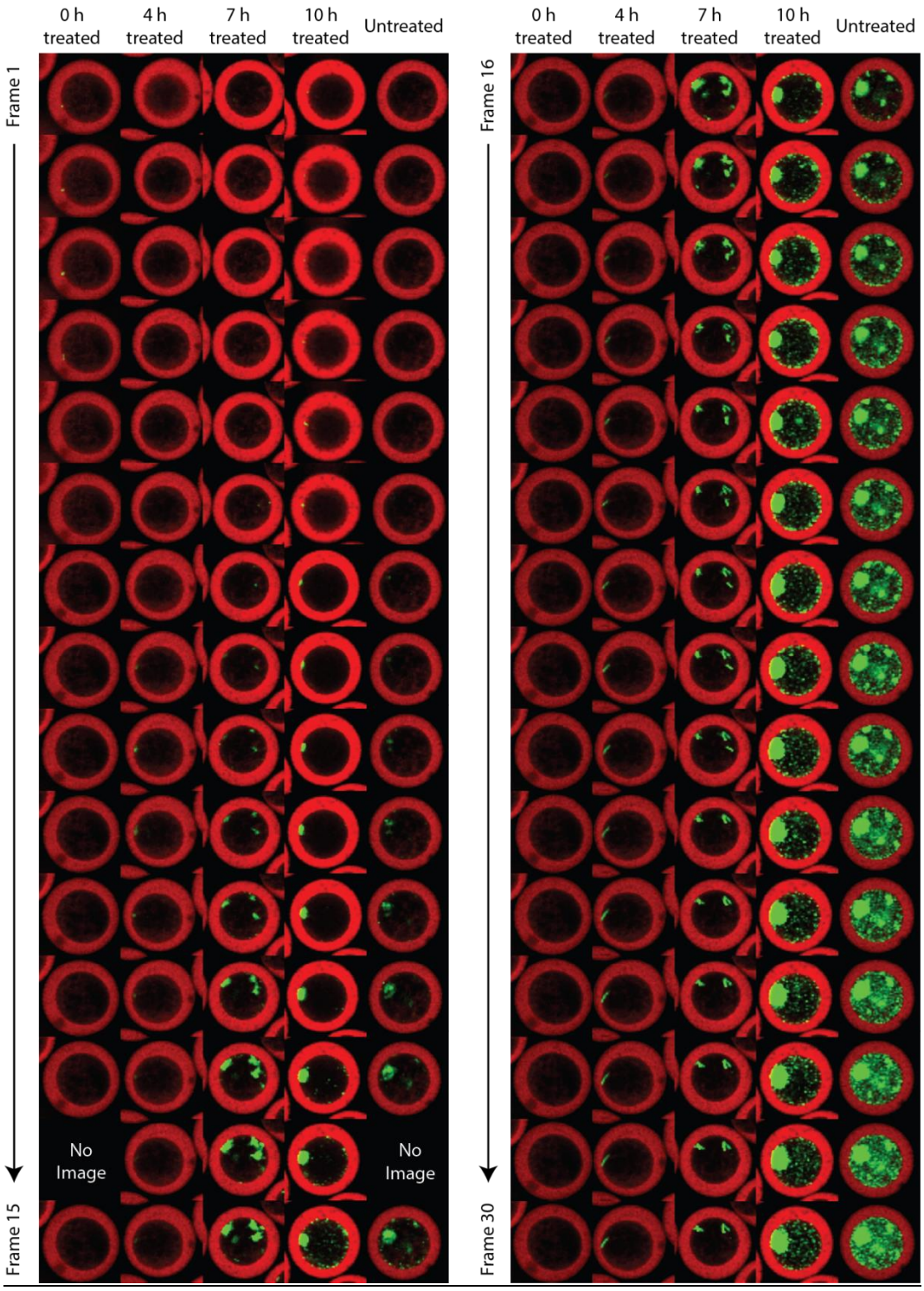

Supplementary Figure 5: Representative capsule from each antibiotic treatment schedule shown for each individual imaging frame. Images represent a single slice taken at the capsule middle-plane via iCLSM. Capsule shells are shown in red (Cy5.5) and *P. aeruginosa* is in green (GFP). Capsule diameters: approx. 80 µm.

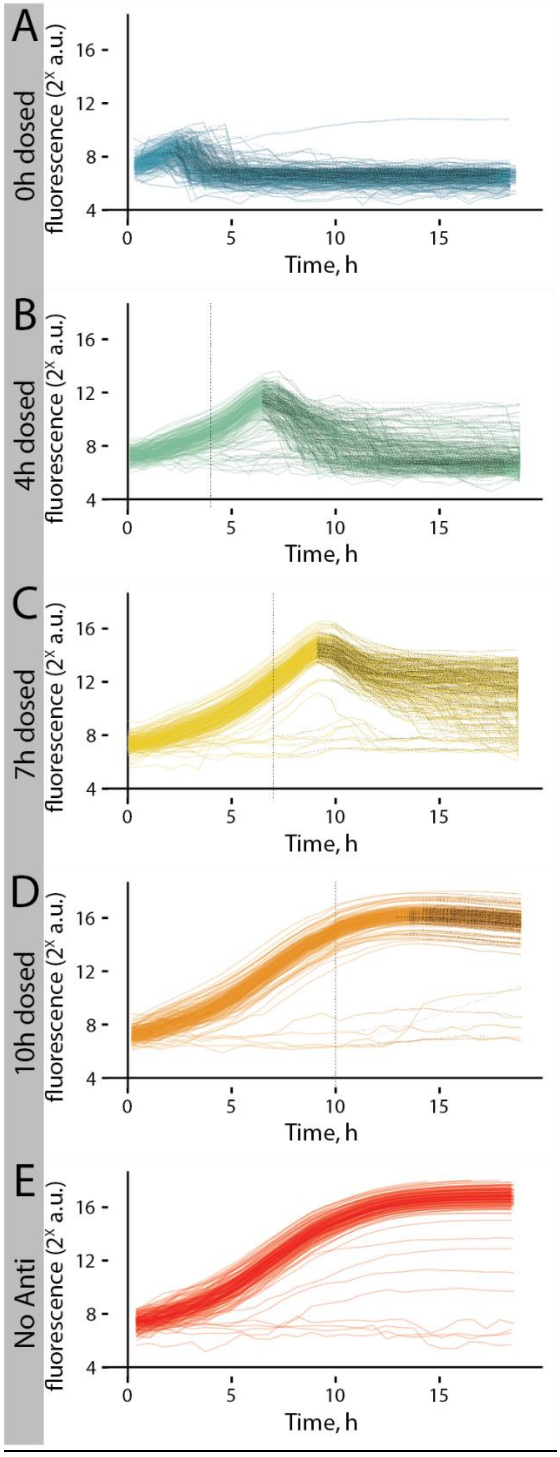

Supplementary Figure 6: All individual capsule growth curves from each antibiotic treatment schedule tested. Black dashed lines overlay portions of each curve with a negative slope, representing decreased fluorescence.

APPENDIX D

ALGINATE DISSINTEGRATION VIA ELECTROPHORESIS

Summary

While investigating the properties of alginate hydrogels, it was discovered that alginate hydrogels disintegrate during electrophoresis. Following this discovery, I embarked on work to characterize this phenomenon and explore the application of electrophoresis-driven alginate disintegration to make higher-order solid hydrogel structures with liquid inclusions. This process was deemed Alginate Reversible Templating, or ART. While conducting this research, I developed a series of specialized electrophoresis chambers, designed and generated composite alginate particles, and conducted experiments to test the effect of electrophoresis on alginate. The results of this work show that subjecting alginate to electrophoresis causes alginate disintegration, and that the degree of disintegration increases with the strength of electric field. Here, I present an abbreviated summary of those efforts. Dr. Dmitri Bikos contributed to the design of this work.

Background

Before developing the hydrogel capsules described in Chapter 4, I explored the possibility of using solid alginate microspheres as a bacterial-cell cultivation platform. Like the BioFlex capsules, the use of alginate microspheres was based on techniques developed for mammalian cell culture [144]. After observing microbial escape from alginate microspheres during in-microsphere bacterial culture, signified by repeated significant contamination of the bulk media surrounding the microspheres (C Figure 1), I sought to confirm that bacterial escape was caused by disruption of the alginate hydrogel structure. To do this, I needed to rule out the possibility that bacteria might be able to move through the pores of alginate hydrogels. The pore

sizes in polyacrylamide and agarose hydrogels can be evaluated by measuring the electrophoretic mobility of charged particles of a known size through the bulk hydrogel substrate [145, 146]. In collaboration with Dr. Dmitri Bikos, I attempted to apply this method to measure the pore size of alginate hydrogels. While conducting these studies, it was observed that the alginate samples had disintegrated, leaving behind a fully liquid solution, which inspired the investigations described in the following report.

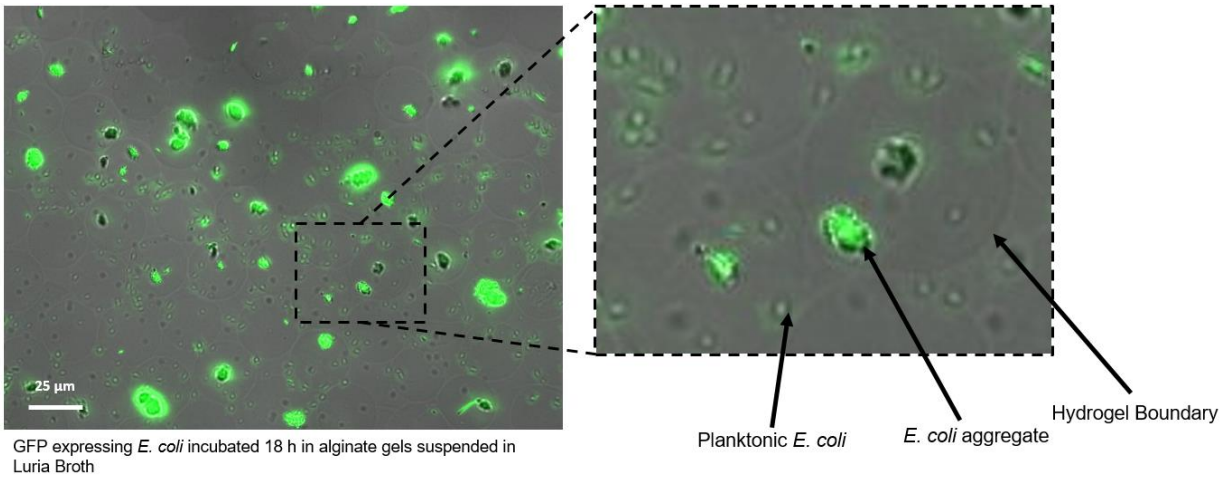

Appendix C Figure 1: *Escherichia coli* incubated for 18 hours after encapsulation in CLEX alginate hydrogels.

Investigations

Alginate description:

Alginates are block copolymers consisting of alternating segments of repeated β-d-mannuronate (M) or repeated α-l-guluronate (G) residues [147]. Alginic acid solutions are crosslinked into solid alginate hydrogels by adding multivalent metal cations, most-often calcium

(Ca^{2+}). These cations associate between alginate G domains, forming a characteristic "egg-carton" crosslinking of alginate polymer [148] (C Figure 2). Alginate hydrogels used in this work were generated using competitive ligand exchange (CLEX)[144] and by Ca^{2+}bath [149] cation-introduction (i.e., crosslinking) strategies. The CLEX crosslinking approach is designed explicitly for alginate manipulation in microfluidic devices, and the Ca^{2+}bath approach is commonly used in molecular gastronomy in a process called "spherification." CLEX was used when the experimental goals required casting macroscale gels, and Ca^{2+}baths were used to form millifluidic alginate spheres.

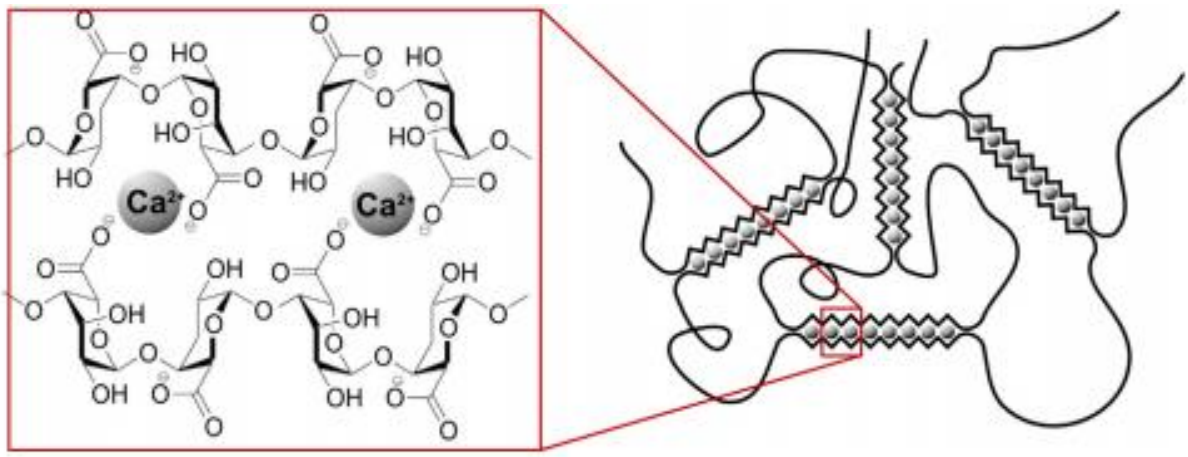

Appendix C Figure 2: Microscale structure of crosslinked alginate, taken from *Fabrication of patterned calcium cross-linked alginate hydrogel films and coatings through reductive cation exchange* by Bruchet and Melman [148]. Alginates crosslink by incorporating multivalent cation bridges between G blocks of the alginate polymer, forming an "egg-carton" structure.

Initial observations of alginate during electrophoresis

The phenomenon of alginate disintegration during electrophoresis was replicated by casting an alginate disk and encapsulating the disk in a slab of low melt agarose, a hydrogel commonly used in gel-electrophoresis[150], and subjecting the composite, macroscale hydrogel

to electrophoresis in Tris-borate-EDTA (TBE) buffer for 1 h. At the end of this hour, the hydrogel composite was removed from the electrophoresis chamber. After electrophoresis, there was a void in the agarose where the alginate had once been (C Figure 3.) Similar experiments were conducted with various macroscale (larger than 1 cm^3) alginate-in-agarose constructs in varied electric field strengths, all with the same result of alginate disintegration.

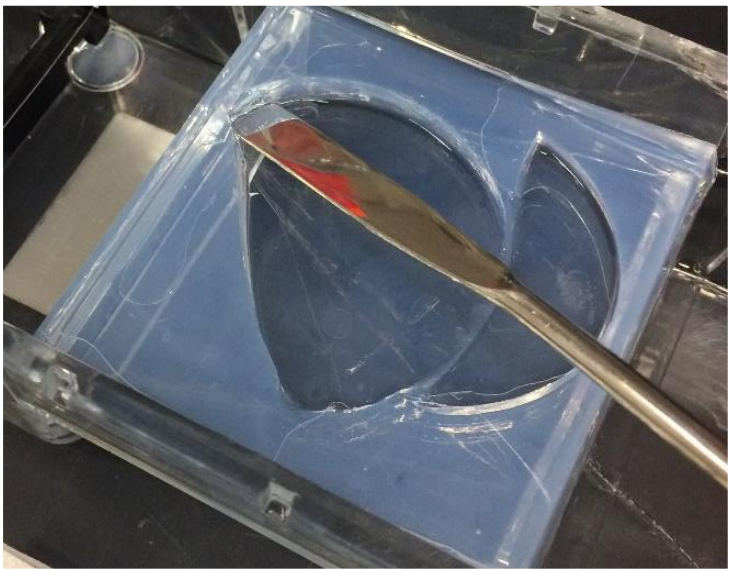

Appendix C Figure 2: Electrophoresis of alginate in agarose composite hydrogels revealed alginate disintegration, evident from a void in the composite hydrogel corresponding to the initial alginate location.

2-D electrophoresis of millifluidic hydrogel composites

To characterize the time-dynamics of alginate disintegration via electrophoresis, I designed and fabricated a miniaturized electrophoresis chamber for time-lapse monitored 2-D electrophoresis of millifluidic alginate-in-agarose hydrogel composites (C Figure 3). The miniaturized electrophoresis chamber consisted of an extrusion 3D printed chamber body for

containing buffer and the gel samples, platinum and nichrome pins for delivering current from the electrophoresis power supplies, and filter papers for containing foam and bubbles generated during electrophoretic hydrolysis. Millifluidic hydrogel microspheres were generated via a Ca^{2+} bath spherification and agarose coating process (C Figure 4). Colloidal silica was included in the alginate formulation to make the alginate millispheres white and thus improve visualization.

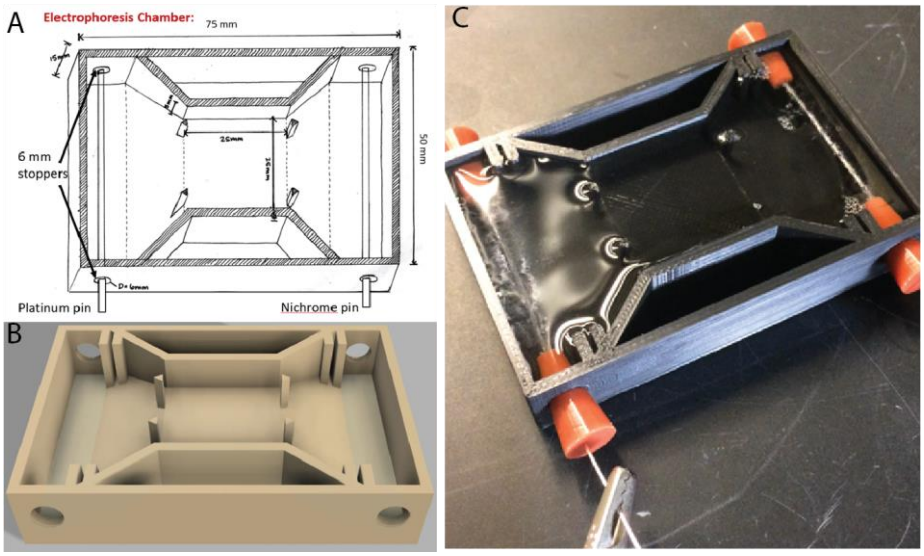

Appendix C Figure 3: The design-to-production process for the 2D miniaturized electrophoresis chamber. An iterative prototyping process including (A.) chamber design, (B.) computer-aided 3-D modeling, extrusion-based 3-D printing and device assembly (not shown), and (C.) testing.

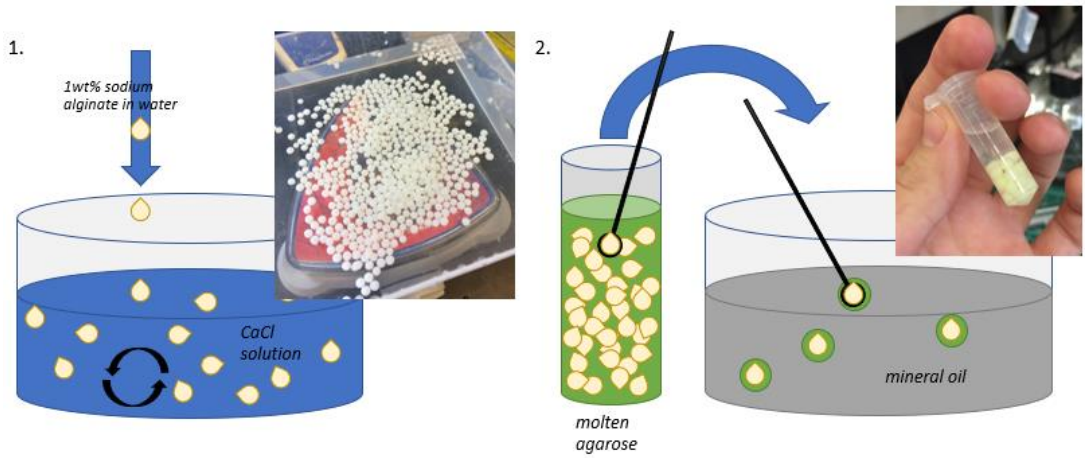

Appendix C Figure 4: Production of millifluidic alginate-in-agarose composites. (1) Spherification was used to produce alginate beads, which were then (2) coated in molten agarose. Coated alginate beads were dropped into a mineral oil bath to enable agarose solidification.

The millifluidic alginate-in-agarose composites were subjected to electrophoresis in TBE buffer in the 2-D miniature electrophoresis chamber, and the process was imaged via time-lapse digital photography. During these studies, the encapsulated alginate millisphere swelled, tearing the outer agarose membrane. The swollen alginate moved in the electric field, leaving behind an agarose husk. As the alginate swelled, large cracks developed and the alginate surface. The swollen alginate then started disappearing, disintegrating into the TEA buffer and leaving behind a silica trail.

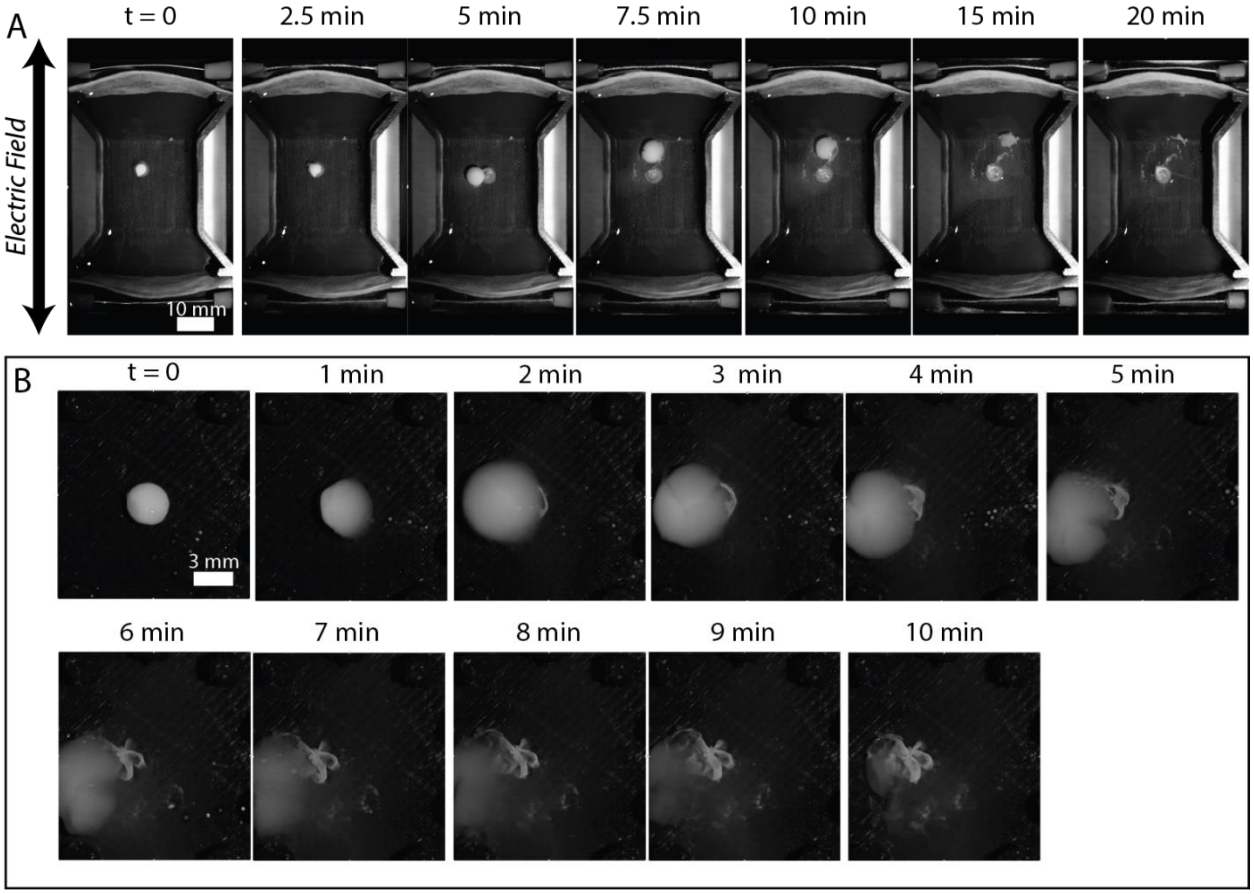

Appendix C Figure 5: Electrophoresis of alginate-in-agarose millifluidic spheres in TBE. (A) Visualization of the entire 2D electrophoresis chamber. (30±2 mAmps). (B) Closeup of a single composite hydrogel (60±2 mAmps).

3-D electrophoresis in a custom-made cylindrical electrophoresis chamber

Additional electrophoresis experiments revealed that the disintegration of alginate via electrophoretic current occurred in a front corresponding to the direction of current (from anodic to cathodic). This was most clearly demonstrated in a macroscale electrophoresis experiment in which alginate millispheres were embedded in an agar gel and electrophoresed for a short time prior to complete disintegration of embedded millispheres (C Figure 6). At the end point of this experiment, millispheres closest to the electrophoresis chamber's anode were wholly

disintegrated, while millispheres closest to the cathode were unaffected. Millispheres located between these two regions were at some intermediate phase of disintegration, ranging from swollen and partially disintegrated to swollen and intact.

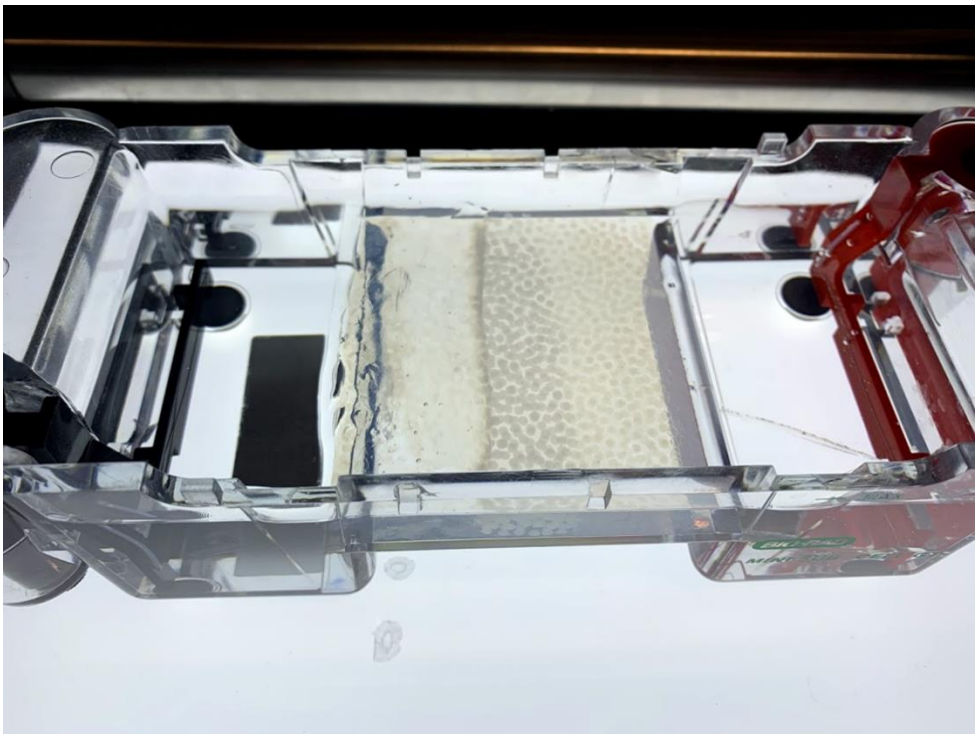

Appendix C Figure 6: Incomplete electrophoresis of alginate millispheres embedded in an agar pad demonstrate a dissintegration front in line with the electric field (moving from the anode to cathode).

Based on the observation of a disintegration front, a new, cylindrical electrophoresis chamber and sample holder were designed to apply a uniform electric field that passed through the z-direction of a thin alginate disk. This device was constructed from rigid acrylic tubing and laser-cut acrylic sheets that were solvent welded together (C Figure 7).

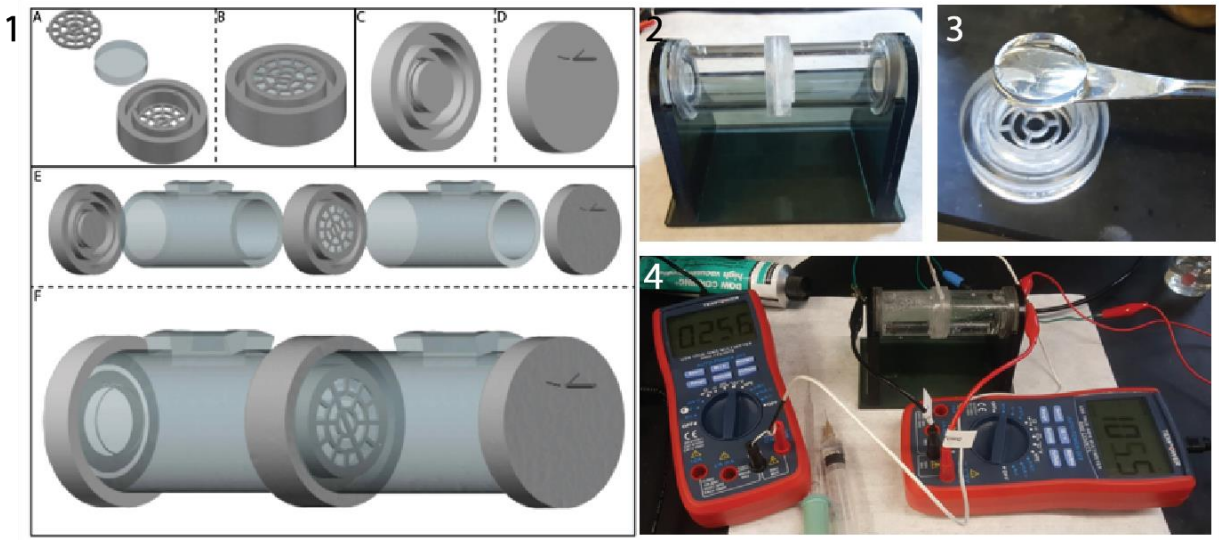

Appendix C Figure 7: Cylindrical electrophoresis chamber for conducting electrophoresis on alginate disks. (1) Chamber components modeled in 3D design software. (2) Cylindrical electrophoresis chamber assembled and cradled in the chamber stand. (3) An alginate disk ready to deposit into the sample holder, which is placed at the midpoint of the cylindrical electrophoresis chamber length. (4) The assembled device with electrical hookups and multimeters for characterizing the electric field across the chamber.

The cylindrical electrophoresis chamber was used in an attempt to quantify the extent of degradation as a factor of time for a given field strength (C Figure 8). Images taken from samples were informative for qualitative comparison but did not provide the desired quantifiable data. The most significant factor preventing the quantification of results from these experiments was the fragility of alginate, which only increased with disintegration and meant that pieces of alginate were unretrievable within the chamber.

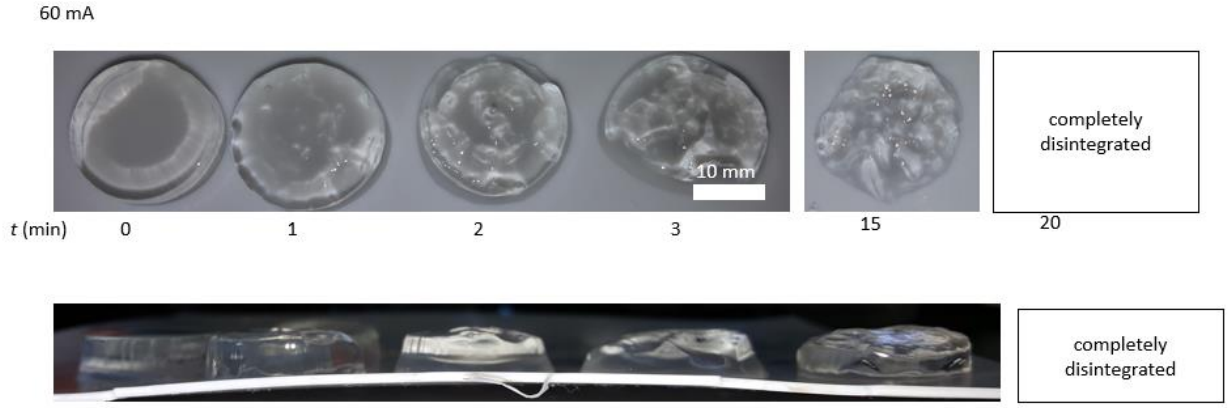

Appendix C Figure 8: Cylindrical electrophoresis chamber for conducting electrophoresis on alginate disks. (1) Chamber components modeled in 3D design software. (2) Cylindrical electrophoresis chamber assembled and cradled in the chamber stand. (3) An alginate disk ready to deposit into the sample holder, which is placed at the midpoint of the cylindrical electrophoresis chamber length. (4) The assembled device with electrical hookups and multimeters for characterizing the electric field across the chamber.

Quantification of alginate degradation via bulk electrophoresis

Ultimately, a traditional electrophoresis format in a standard electrophoresis chamber was used to quantify the extent of electrophoretic degradation as a factor of field strength. The electrophoresis chamber was equipped with multimeters to monitor voltage and current, a constant flow system to continuously replace the electrophoresis buffer, a conductivity meter to verify that the electrophoresis buffer was replaced at a rate sufficient to maintain constant conductivity of the electrophoresis buffer, and a constant-voltage power supply (C Figure 9). To conduct the electrophoresis studies, alginate cubes were cast and placed in a hand-sewn fiber-glass mesh basket lined with filter paper, and the mass of the alginate in the baskets was recorded. The baskets were placed in the electrophoresis chamber and exposed to constant voltage electrophoresis for 60 min.

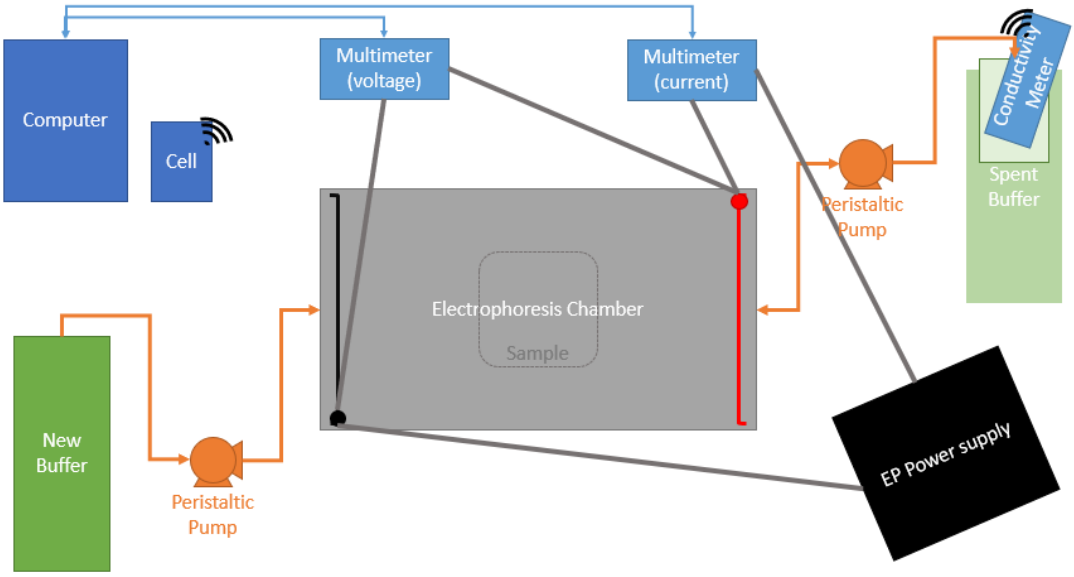

Appendix C Figure 9: Design of the electrophoresis system used to measure alginate disintegration vs. voltage for a set length of time.

After exposing the alginate samples to electrophoresis at varying voltages for 1 h, the sample baskets were removed from the electrophoresis chamber and the samples were imaged then transferred to an oven at 95°C for dehydration. Completely dehydrated samples were removed after 3 d and massed, and the mass was compared to the pre-electrophoresis mass. These results revealed that the degree of alginate mass loss varied with voltage maintained during electrophoresis (C Figure 10), with the degree of alginate mass loss increasing with voltage. Wet masses were not used for both the initial and final alginate measurements as it was not possible to control for the amount of water absorbed as a result of alginate swelling in these preliminary experiments.

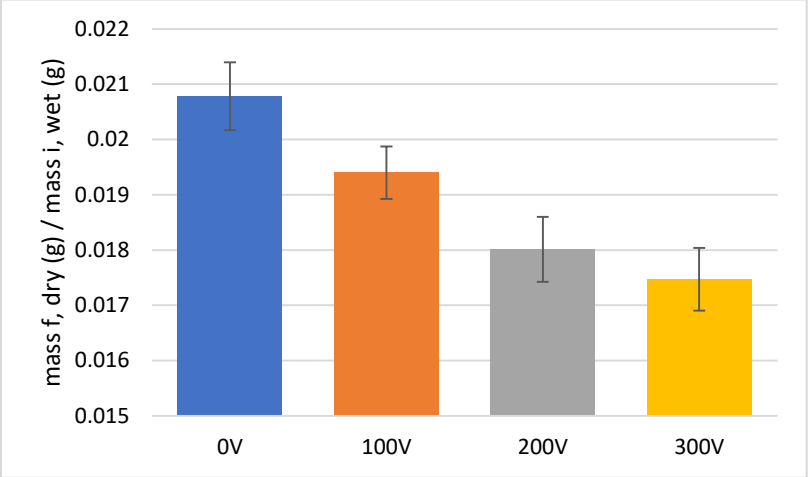

Appendix C Figure 10: Post-electrophoresis dried mass vs. pre-electrophoresis initial wet mass of alginate samples.

Preliminary Results and Prospectus

These results demonstrate that Ca-alginate hydrogels deteriorate and disintegrate when submitted to an electric field. This deterioration is spatially heterogenous throughout the alginate volume, moving in a front from the side of the alginate volume closest to the anode to the side closest to the cathode. We hypothesize that this occurs due to the removal of Ca^{2+} from the alginate due to transport in the imposed electric field, though additional testing, including characterization of the alginate polymers post-disintegration, is required to assert this mechanism of disintegration.

One large, unanswered question arising from these studies is the cause of alginate swelling. During the design of this project, the prospect of non-invasively dissolving solid alginate from inside hydrogel composites was a major motivation. The significant swelling observed during alginate electrophoresis suggests that any attempts to template liquid inclusions

within other hydrogels will require accommodations for the swelling that may or may not be possible within the existing hydrogel formulation options.

REFERENCES CITED

1. Pratt, S.L., et al., *DropSOAC: stabilizing microfluidic drops for time-lapse quantification of single-cell bacterial physiology.* Frontiers in Microbiology, 2019. **10**: p. 2112.

2. Høiby, N., et al., *The clinical impact of bacterial biofilms.* International journal of oral science, 2011. **3**(2): p. 55-65.

3. Falanga, V., et al., *Chronic wounds.* Nature Reviews Disease Primers, 2022. **8**(1): p. 50.

4. Cookson, W.O., M.J. Cox, and M.F. Moffatt, *New opportunities for managing acute and chronic lung infections.* Nature Reviews Microbiology, 2018. **16**(2): p. 111-120.

5. Dlugaszewska, J., et al., *The pathophysiological role of bacterial biofilms in chronic sinusitis.* European Archives of Oto-Rhino-Laryngology, 2016. **273**: p. 1989-1994.

6. Arciola, C.R., D. Campoccia, and L. Montanaro, *Implant infections: adhesion, biofilm formation and immune evasion.* Nature reviews microbiology, 2018. **16**(7): p. 397-409.

7. Kapadia, B.H., et al., *Periprosthetic joint infection.* The Lancet, 2016. **387**(10016): p. 386-394.

8. Olsson, M., et al., *The humanistic and economic burden of chronic wounds: a systematic review.* Wound Repair and Regeneration, 2019. **27**(1): p. 114-125.

9. Powers, J.G., et al., *Wound healing and treating wounds: Chronic wound care and management.* Journal of the American Academy of Dermatology, 2016. **74**(4): p. 607-625.

10. Rodrigo-Troyano, A., et al., *Pseudomonas aeruginosa resistance patterns and clinical outcomes in hospitalized exacerbations of COPD.* Respirology, 2016. **21**(7): p. 1235-1242.

11. Nussbaum, S.R., et al., *An economic evaluation of the impact, cost, and medicare policy implications of chronic nonhealing wounds.* Value in Health, 2018. **21**(1): p. 27-32.

12. Cierny III, G. and D. DiPasquale, *Treatment of chronic infection.* JAAOS-Journal of the American Academy of Orthopaedic Surgeons, 2006. **14**(10): p. S105-S110.

13. Brandl, M., et al., *Factors associated with generic health-related quality of life (HRQOL) in patients with chronic obstructive pulmonary disease (COPD): a cross-sectional study.* Journal of thoracic disease, 2018. **10**(2): p. 766.

14. Sajobi, T.T., et al., *Trajectories of health-related quality of life in coronary artery disease.* Circulation: Cardiovascular Quality and Outcomes, 2018. **11**(3): p. e003661.

15. Roberts, A.E., et al., *The limitations of in vitro experimentation in understanding biofilms and chronic infection.* Journal of Molecular Biology, 2015. **427**(23): p. 3646-3661.

16. Jackson, L. and V. Waters, *Factors influencing the acquisition and eradication of early Pseudomonas aeruginosa infection in cystic fibrosis.* Journal of Cystic Fibrosis, 2021. **20**(1): p. 8-16.

17. Jindal, A., K. Pandya, and I. Khan, *Antimicrobial resistance: A public health challenge.* Medical journal armed forces India, 2015. **71**(2): p. 178-181.

18. Pettygrove, B.A., et al., *Delayed neutrophil recruitment allows nascent Staphylococcus aureus biofilm formation and immune evasion.* Biomaterials, 2021. **275**: p. 120775.

19. Stewart, P.S. and M.J. Franklin, *Physiological heterogeneity in biofilms.* Nature Reviews Microbiology, 2008. **6**(3): p. 199-210.

20. Vaughn Cooper, M.F., Garth James, Chris Jones, Darla Goeres. *Panel Discussion: Defining a Biofilm*. in *Montana Biofilm Meeting*. 2022. Bozeman, MT: Center for Biofilm Engineering.

21. Bjarnsholt, T., et al., *The importance of understanding the infectious microenvironment.* The Lancet Infectious Diseases, 2022. **22**(3): p. e88-e92.

22. Wolcott, R.D. and G.D. Ehrlich, *Biofilms and chronic infections.* Jama, 2008. **299**(22): p. 2682-2684.

23. DeLeon, S., et al., *Synergistic interactions of Pseudomonas aeruginosa and Staphylococcus aureus in an in vitro wound model.* Infection and immunity, 2014. **82**(11): p. 4718-4728.

24. Pastar, I., et al., *Interactions of methicillin resistant Staphylococcus aureus USA300 and Pseudomonas aeruginosa in polymicrobial wound infection.* PloS one, 2013. **8**(2): p. e56846.

25. CDC, *Antibiotic Resistance Threats in the United States, 2019.*, C. U.S. Department of Health and Human Services, Editor. 2019, U.S. Centers for Disease Control and Prevention: Online. p. 97-98.

26. Valderrey, A.D., et al., *Chronic colonization by Pseudomonas aeruginosa of patients with obstructive lung diseases: cystic fibrosis, bronchiectasis, and chronic obstructive pulmonary disease.* Diagnostic microbiology and infectious disease, 2010. **68**(1): p. 20-27.

27. Frimmersdorf, E., et al., *How Pseudomonas aeruginosa adapts to various environments: a metabolomic approach.* Environmental microbiology, 2010. **12**(6): p. 1734-1747.

28. Moore, N.M. and M.L. Flaws, *Introduction: pseudomonas aeruginosa.* Clinical laboratory science, 2011. **24**(1): p. 41.

29. McGill, S.L., et al., *Pseudomonas aeruginosa reverse diauxie is a multidimensional, optimized, resource utilization strategy.* Scientific reports, 2021. **11**(1): p. 1-16.

30. Laborda, P., et al., *Pseudomonas aeruginosa: An antibiotic resilient pathogen with environmental origin.* Current Opinion in Microbiology, 2021. **64**: p. 125-132.

31. O'Toole, G.A. and R. Kolter, *Flagellar and twitching motility are necessary for Pseudomonas aeruginosa biofilm development.* Molecular microbiology, 1998. **30**(2): p. 295-304.

32. Bonomo, R.A. and D. Szabo, *Mechanisms of multidrug resistance in Acinetobacter species and Pseudomonas aeruginosa.* Clinical infectious diseases, 2006. **43**(Supplement_2): p. S49-S56.

33. Davies, O., *WHO publishes list of bacteria for which new antibiotics are urgently needed* 2017, World Health Organization: Online.

34. Lebeaux, D., J.-M. Ghigo, and C. Beloin, *Biofilm-related infections: bridging the gap between clinical management and fundamental aspects of recalcitrance toward antibiotics.* Microbiology and Molecular Biology Reviews, 2014. **78**(3): p. 510-543.

35. Lewis, K., *Persister cells.* Annual review of microbiology, 2010. **64**: p. 357-372.

36. Evans, C.R., et al., *Metabolic heterogeneity and cross-feeding in bacterial multicellular systems.* Trends in microbiology, 2020. **28**(9): p. 732-743.

37. Beaumont, H.J., et al., *Experimental evolution of bet hedging.* Nature, 2009. **462**(7269): p. 90-93.

38. García-Betancur, J.-C., et al., *Cell differentiation defines acute and chronic infection cell types in Staphylococcus aureus.* Elife, 2017. **6**: p. e28023.

39. Cullen, L. and S. McClean, *Bacterial adaptation during chronic respiratory infections.* Pathogens, 2015. **4**(1): p. 66-89.

40. Köster, S., et al., *Drop-based microfluidic devices for encapsulation of single cells.* Lab on a Chip, 2008. **8**(7): p. 1110-1115.

41. Rakszewska, A., et al., *One drop at a time: toward droplet microfluidics as a versatile tool for single-cell analysis.* NPG Asia Materials, 2014. **6**(10): p. e133-e133.

42. Mazutis, L., et al., *Single-cell analysis and sorting using droplet-based microfluidics.* Nature protocols, 2013. **8**(5): p. 870-891.

43. Akiyama, T., et al., *Resuscitation of Pseudomonas aeruginosa from dormancy requires hibernation promoting factor (PA4463) for ribosome preservation.* Proceedings of the National Academy of Sciences, 2017. **114**(12): p. 3204-3209.

44. van Zee, M., et al., *High-throughput selection of cells based on accumulated growth and division using PicoShell particles.* Proceedings of the National Academy of Sciences, 2022. **119**(4): p. e2109430119.

45. Agresti, J.J., et al., *Ultrahigh-throughput screening in drop-based microfluidics for directed evolution.* Proceedings of the National Academy of Sciences, 2010. **107**(9): p. 4004-4009.

46. Zath, G.K., et al., *Rapid parallel generation of a fluorescently barcoded drop library from a microtiter plate using the plate-interfacing parallel encapsulation (PIPE) chip.* Lab on a Chip, 2022. **22**(23): p. 4735-4745.

47. Ding, Y., J. Choo, and A.J. DeMello, *From single-molecule detection to next-generation sequencing: microfluidic droplets for high-throughput nucleic acid analysis.* Microfluidics and nanofluidics, 2017. **21**: p. 1-20.

48. Zhang, W., et al., *PMMA/PDMS valves and pumps for disposable microfluidics.* Lab on a Chip, 2009. **9**(21): p. 3088-3094.

49. Niculescu, A.-G., et al., *Fabrication and applications of microfluidic devices: A review.* International Journal of Molecular Sciences, 2021. **22**(4): p. 2011.

50. Whitesides, G.M. and A.D. Stroock, *Flexible methods for microfluidics.* Phys. Today, 2001. **54**(6): p. 42-48.

51. Stone, H.A. and S. Kim, *Microfluidics: basic issues, applications, and challenges.* American Institute of Chemical Engineers. AIChE Journal, 2001. **47**(6): p. 1250.

52. Lashkaripour, A., et al., *Performance tuning of microfluidic flow-focusing droplet generators.* Lab on a Chip, 2019. **19**(6): p. 1041-1053.

53. Ibrahim, A.M., et al., *Modeling of droplet generation in a microfluidic flow-focusing junction for droplet size control.* Micromachines, 2021. **12**(6): p. 590.

54. Utada, A.S., et al., *Dripping to jetting transitions in coflowing liquid streams.* Physical review letters, 2007. **99**(9): p. 094502.

55. Shah, R.K., et al., *Designer emulsions using microfluidics.* Materials Today, 2008. **11**(4): p. 18-27.

56. Rotem, A., et al., *Drop formation in non-planar microfluidic devices.* Lab on a Chip, 2012. **12**(21): p. 4263-4268.

57. Kovalchuk, N.M. and M.J. Simmons, *Review of the role of surfactant dynamics in drop microfluidics.* Advances in Colloid and Interface Science, 2023: p. 102844.

58. Sart, S., et al., *Cell culture in microfluidic droplets.* Chemical Reviews, 2022. **122**(7): p. 7061-7096.

59. Caldwell, A.S., B.A. Aguado, and K.S. Anseth, *Designing microgels for cell culture and controlled assembly of tissue microenvironments.* Advanced functional materials, 2020. **30**(37): p. 1907670.

60. Xu, Y., et al., *Recent advances in microgels: from biomolecules to functionality.* Small, 2022. **18**(34): p. 2200180.

61. Huang, H., et al., *Generation and manipulation of hydrogel microcapsules by droplet-based microfluidics for mammalian cell culture.* Lab on a Chip, 2017. **17**(11): p. 1913-1932.

62. Tibbitt, M.W. and K.S. Anseth, *Hydrogels as extracellular matrix mimics for 3D cell culture.* Biotechnology and bioengineering, 2009. **103**(4): p. 655-663.

63. Ruedinger, F., et al., *Hydrogels for 3D mammalian cell culture: a starting guide for laboratory practice.* Applied microbiology and biotechnology, 2015. **99**: p. 623-636.

64. Mahdieh, Z., et al., *Granular Matrigel: restructuring a trusted extracellular matrix material for improved permeability.* Biomedical Materials, 2022. **17**(4): p. 045020.

65. Fattahi, P., et al., *Core–shell hydrogel microcapsules enable formation of human pluripotent stem cell spheroids and their cultivation in a stirred bioreactor.* Scientific reports, 2021. **11**(1): p. 1-13.

66. Leonaviciene, G., et al., *Multi-step processing of single cells using semi-permeable capsules.* Lab on a Chip, 2020. **20**(21): p. 4052-4062.

67. Michielin, G. and S.J. Maerkl, *Direct encapsulation of biomolecules in semi-permeable microcapsules produced with double-emulsions.* Scientific Reports, 2022. **12**(1): p. 1-9.

68. Mytnyk, S., et al., *Microcapsules with a permeable hydrogel shell and an aqueous core continuously produced in a 3D microdevice by all-aqueous microfluidics.* RSC advances, 2017. **7**(19): p. 11331-11337.

69. Siltanen, C., et al., *One step fabrication of hydrogel microcapsules with hollow core for assembly and cultivation of hepatocyte spheroids.* Acta biomaterialia, 2017. **50**: p. 428-436.

70. Watanabe, T., I. Motohiro, and T. Ono, *Microfluidic formation of hydrogel microcapsules with a single aqueous core by spontaneous cross-linking in aqueous two-phase system droplets.* Langmuir, 2019. **35**(6): p. 2358-2367.

71. Fredrikson, J.P., et al., *Metabolomic Profiling and Mechanotransduction of Single Chondrocytes Encapsulated in Alginate Microgels.* Cells, 2022. **11**(5): p. 900.

72. Malhotra, S., D. Hayes Jr, and D.J. Wozniak, *Cystic fibrosis and Pseudomonas aeruginosa: the host-microbe interface.* Clinical microbiology reviews, 2019. **32**(3): p. e00138-18.

73. Lyczak, J.B., C.L. Cannon, and G.B. Pier, *Lung infections associated with cystic fibrosis.* Clinical microbiology reviews, 2002. **15**(2): p. 194-222.

74. Davis, K.M. and R.R. Isberg, *Defining heterogeneity within bacterial populations via single cell approaches.* Bioessays, 2016. **38**(8): p. 782-790.

75. Hatzenpichler, R. and V.J. Orphan, *Detection of protein-synthesizing microorganisms in the environment via bioorthogonal noncanonical amino acid tagging (BONCAT).* Hydrocarbon and lipid microbiology protocols: Single-cell and single-molecule methods, 2016: p. 145-157.

76. Lindivat, M., et al., *Bioorthogonal non-canonical amino acid tagging combined with flow cytometry for determination of activity in aquatic microorganisms.* Frontiers in Microbiology, 2020. **11**: p. 1929.

77. Amann, R. and B.M. Fuchs, *Single-cell identification in microbial communities by improved fluorescence in situ hybridization techniques.* Nature Reviews Microbiology, 2008. **6**(5): p. 339-348.

78. Moffitt, J.R., et al., *High-throughput single-cell gene-expression profiling with multiplexed error-robust fluorescence in situ hybridization.* Proceedings of the National Academy of Sciences, 2016. **113**(39): p. 11046-11051.

79. Basu, S., et al., *Purification of specific cell population by fluorescence activated cell sorting (FACS).* Journal of visualized experiments: JoVE, 2010(41).

80. Song, Y., H. Yin, and W.E. Huang, *Raman activated cell sorting.* Current opinion in chemical biology, 2016. **33**: p. 1-8.

81. Kashima, Y., et al., *Single-cell sequencing techniques from individual to multiomics analyses.* Experimental & Molecular Medicine, 2020. **52**(9): p. 1419-1427.

82. Hartmann, R., et al., *Quantitative image analysis of microbial communities with BiofilmQ.* Nature microbiology, 2021. **6**(2): p. 151-156.

83. Vidakovic, L., et al., *Dynamic biofilm architecture confers individual and collective mechanisms of viral protection.* Nature microbiology, 2018. **3**(1): p. 26-31.

84. Connell, J.L., et al., *Probing prokaryotic social behaviors with bacterial "lobster traps".* MBio, 2010. **1**(4): p. e00202-10.

85. Wessel, A.K., et al., *Going local: technologies for exploring bacterial microenvironments.* Nature Reviews Microbiology, 2013. **11**(5): p. 337-348.

86. Anggraini, D., et al., *Recent advances in microfluidic devices for single-cell cultivation: methods and applications.* Lab on a Chip, 2022.

87. Tao, Y., et al., *Rapid, targeted and culture-free viral infectivity assay in drop-based microfluidics.* Lab on a Chip, 2015. **15**(19): p. 3934-3940.

88. Rotem, A., et al., *High-throughput single-cell labeling (Hi-SCL) for RNA-Seq using drop-based microfluidics.* PloS one, 2015. **10**(5): p. e0116328.

89. Jansen, L.E., et al., *Control of thiol-maleimide reaction kinetics in PEG hydrogel networks.* Acta biomaterialia, 2018. **70**: p. 120-128.

90. Nair, D.P., et al., *The thiol-Michael addition click reaction: a powerful and widely used tool in materials chemistry.* Chemistry of Materials, 2014. **26**(1): p. 724-744.

91. Kim, J., et al., *Characterization of the crosslinking kinetics of multi-arm poly (ethylene glycol) hydrogels formed via Michael-type addition.* Soft matter, 2016. **12**(7): p. 2076-2085.

92. Pistori, H., J. Pistori, and E.R. Costa. *Hough-circles: Um módulo de detecçao de circunferências para o imagej*. in *Workshop Software Livre, Porto Alegre. Anais do 6o Workshop de Software Livre*. 2005.

93. Ferreira, L.A. and J.A. Teixeira, *Salt effect on the aqueous two-phase system PEG 8000− Sodium sulfate.* Journal of Chemical & Engineering Data, 2011. **56**(1): p. 133-137.

94. Nivens, D.E., et al., *Role of alginate and its O acetylation in formation of Pseudomonas aeruginosa microcolonies and biofilms.* Journal of bacteriology, 2001. **183**(3): p. 1047-1057.

95. Schindelin, J., et al., *Fiji: an open-source platform for biological-image analysis.* Nature methods, 2012. **9**(7): p. 676-682.

96. Ershov, D., et al., *TrackMate 7: integrating state-of-the-art segmentation algorithms into tracking pipelines.* Nature methods, 2022. **19**(7): p. 829-832.

97. Allaire, J., *RStudio: integrated development environment for R.* Boston, MA, 2012. **770**(394): p. 165-171.

98. Ihaka, R. and R. Gentleman, *R: a language for data analysis and graphics.* Journal of computational and graphical statistics, 1996. **5**(3): p. 299-314.

99. Wickham, H. and M.H. Wickham, *Package tidyverse.* Easily Install and Load the 'Tidyverse, 2017.

100. Wickham, H., W. Chang, and M.H. Wickham, *Package 'ggplot2'.* Create elegant data visualisations using the grammar of graphics. Version, 2016. **2**(1): p. 1-189.

101. Jockers, M.L., et al., *Introduction to dplyr.* Text Analysis with R: For Students of Literature, 2020: p. 121-132.

102. Robinson, D., et al., *Package 'broom'.* 2015.

103. Sánchez-Tapia, A., et al. *Model-R: a framework for scalable and reproducible ecological niche modeling*. in *High Performance Computing: 4th Latin American Conference, CARLA 2017, Buenos Aires, Argentina, and Colonia del Sacramento, Uruguay, September 20-22, 2017, Revised Selected Papers 4*. 2018. Springer.

104. Wickham, H., M.H. Wickham, and I. RColorBrewer, *Package 'scales'.* R package version, 2016. **1**(0).

105. Bates, D., et al., *Package 'lme4'.* URL http://lme4. r-forge. r-project. org, 2009.

106. Kuznetsova, A., P.B. Brockhoff, and R.H.B. Christensen, *Package 'lmertest'.* R package version, 2015. **2**(0): p. 734.

107. Cheng, Q., et al., *Tunable Janus geometric morphology from aqueous two-phase systems on a superhydrophobic substrate.* Journal of Materials Chemistry A, 2023. **11**(8): p. 4155-4161.

108. Headen, D.M., et al., *Microfluidic-based generation of size-controlled, biofunctionalized synthetic polymer microgels for cell encapsulation.* Advanced materials, 2014. **26**(19): p. 3003-3008.

109. Park, H., et al., *Pseudomonad reverse carbon catabolite repression, interspecies metabolite exchange, and consortial division of labor.* Cellular and Molecular Life Sciences, 2020. **77**: p. 395-413.

110. Diver, J. and R. Wise, *Morphological and biochemical changes in Escherichia coli after exposure to ciprofloxacin.* Journal of Antimicrobial Chemotherapy, 1986. **18**(Supplement_D): p. 31-41.

111. Wang, X., et al., *Proliferation and differentiation of mouse embryonic stem cells in APA microcapsule: A model for studying the interaction between stem cells and their niche.* Biotechnology progress, 2006. **22**(3): p. 791-800.

112. Zhang, W., et al., *A novel core–shell microcapsule for encapsulation and 3D culture of embryonic stem cells.* Journal of materials chemistry B, 2013. **1**(7): p. 1002-1009.

113. Agarwal, P., et al., *One-step microfluidic generation of pre-hatching embryo-like core–shell microcapsules for miniaturized 3D culture of pluripotent stem cells.* Lab on a Chip, 2013. **13**(23): p. 4525-4533.

114. Phelps, E.A., et al., *Maleimide cross-linked bioactive peg hydrogel exhibits improved reaction kinetics and cross-linking for cell encapsulation and in situ delivery.* Advanced materials, 2012. **24**(1): p. 64-70.

115. Tang, T.-C., et al., *Hydrogel-based biocontainment of bacteria for continuous sensing and computation.* Nature chemical biology, 2021. **17**(6): p. 724-731.

116. Li, Y., et al., *Construction of multilayer alginate hydrogel beads for oral delivery of probiotics cells.* International journal of biological macromolecules, 2017. **105**: p. 924-930.

117. Patini, R., et al., *The effect of different antibiotic regimens on bacterial resistance: a systematic review.* Antibiotics, 2020. **9**(1): p. 22.

118. Wicha, S.G., et al., *From therapeutic drug monitoring to model-informed precision dosing for antibiotics.* Clinical Pharmacology & Therapeutics, 2021. **109**(4): p. 928-941.

119. Krismer, B., et al., *Nutrient limitation governs Staphylococcus aureus metabolism and niche adaptation in the human nose.* PLoS pathogens, 2014. **10**(1): p. e1003862.

120. Quinn, R.A., et al., *A Winogradsky-based culture system shows an association between microbial fermentation and cystic fibrosis exacerbation.* The ISME journal, 2015. **9**(4): p. 1024-1038.

121. Li, Y., et al., *Effect of Tryptophan Metabolites on Cell Damage Revealed by Bacteria–Cell Interactions in Hydrogel Microspheres.* Analytical Chemistry, 2023.

122. Pérez-Rodríguez, S., J.M. García-Aznar, and J. Gonzalo-Asensio, *Microfluidic devices for studying bacterial taxis, drug testing and biofilm formation.* Microbial Biotechnology, 2022. **15**(2): p. 395-414.

123. Arvaniti, M. and P.N. Skandamis, *Defining bacterial heterogeneity and dormancy with the parallel use of single-cell and population level approaches.* Current Opinion in Food Science, 2022. **44**: p. 100808.

124. Hare, P.J., et al., *Single-cell technologies to study phenotypic heterogeneity and bacterial persisters.* Microorganisms, 2021. **9**(11): p. 2277.

125. Shi, H., et al., *Recent advances of integrated microfluidic systems for fungal and bacterial analysis.* TrAC Trends in Analytical Chemistry, 2022: p. 116850.

126. Uzoukwu, E.U., et al., *Droplet-based microsystems as novel assessment tools for oral microbial dynamics.* Biotechnology Advances, 2022: p. 107903.

127. Hattori, K., et al., *Droplet array-based platform for parallel optical analysis of dynamic extracellular vesicle secretion from single cells.* Analytical Chemistry, 2022. **94**(32): p. 11209-11215.

128. Zambare, N.M., et al., *Mineralogy of microbially induced calcium carbonate precipitates formed using single cell drop-based microfluidics.* Scientific reports, 2020. **10**(1): p. 1-11.

129. Szulwach, K.E., et al., *Single-cell genetic analysis using automated microfluidics to resolve somatic mosaicism.* PloS one, 2015. **10**(8): p. e0135007.

130. Amselem, G., et al., *Universal microfluidic platform for bioassays in anchored droplets.* Lab on a Chip, 2016. **16**(21): p. 4200-4211.

131. Dewan, A., et al., *Growth kinetics of microalgae in microfluidic static droplet arrays.* Biotechnology and bioengineering, 2012. **109**(12): p. 2987-2996.

132. Pan, J., et al., *Quantitative tracking of the growth of individual algal cells in microdroplet compartments.* Integrative Biology, 2011. **3**(10): p. 1043-1051.

133. Schmitz, C.H., et al., *Dropspots: a picoliter array in a microfluidic device.* Lab on a Chip, 2009. **9**(1): p. 44-49.

134. Huebner, A., et al., *Static microdroplet arrays: a microfluidic device for droplet trapping, incubation and release for enzymatic and cell-based assays.* Lab on a Chip, 2009. **9**(5): p. 692-698.

135. Shim, J.-u., et al., *Simultaneous determination of gene expression and enzymatic activity in individual bacterial cells in microdroplet compartments.* Journal of the American Chemical Society, 2009. **131**(42): p. 15251-15256.

136. Shim, J.-u., et al., *Control and measurement of the phase behavior of aqueous solutions using microfluidics.* Journal of the American Chemical Society, 2007. **129**(28): p. 8825-8835.

137. Hindson, B.J., et al., *High-throughput droplet digital PCR system for absolute quantitation of DNA copy number.* Analytical chemistry, 2011. **83**(22): p. 8604-8610.

138. O'Neal, L., et al., *The Wsp system of Pseudomonas aeruginosa links surface sensing and cell envelope stress.* Proceedings of the National Academy of Sciences, 2022. **119**(18): p. e2117633119.

139. Rojas, E.R. and K.C. Huang, *Regulation of microbial growth by turgor pressure.* Current Opinion in Microbiology, 2018. **42**: p. 62-70.

140. Li, R.H., D.H. Altreuter, and F.T. Gentile, *Transport characterization of hydrogel matrices for cell encapsulation.* Biotechnology and bioengineering, 1996. **50**(4): p. 365-373.

141. Schmidt, J.J., J. Rowley, and H.J. Kong, *Hydrogels used for cell-based drug delivery.* Journal of Biomedical Materials Research Part A: An Official Journal of The Society for Biomaterials, The Japanese Society for Biomaterials, and The Australian Society for Biomaterials and the Korean Society for Biomaterials, 2008. **87**(4): p. 1113-1122.

142. Witten, J. and K. Ribbeck, *The particle in the spider's web: transport through biological hydrogels.* Nanoscale, 2017. **9**(24): p. 8080-8095.

143. De Maio, F.G., *Income inequality measures.* Journal of Epidemiology & Community Health, 2007. **61**(10): p. 849-852.

144. Håti, A.G., et al., *Versatile, cell and chip friendly method to gel alginate in microfluidic devices.* Lab on a Chip, 2016. **16**(19): p. 3718-3727.

145. Hanauer, M., et al., *Separation of nanoparticles by gel electrophoresis according to size and shape.* Nano letters, 2007. **7**(9): p. 2881-2885.

146. Holmes, D.L. and N.C. Stellwagen, *The electric field dependence of DNA mobilities in agarose gels: A reinvestigation.* Electrophoresis, 1990. **11**(1): p. 5-15.

147. Lee, K.Y. and D.J. Mooney, *Alginate: properties and biomedical applications.* Progress in polymer science, 2012. **37**(1): p. 106-126.

148. Bruchet, M. and A. Melman, *Fabrication of patterned calcium cross-linked alginate hydrogel films and coatings through reductive cation exchange.* Carbohydrate polymers, 2015. **131**: p. 57-64.

149. Lee, P. and M. Rogers, *Effect of calcium source and exposure-time on basic caviar spherification using sodium alginate.* International Journal of Gastronomy and Food Science, 2012. **1**(2): p. 96-100.

150. Voytas, D., *Agarose gel electrophoresis.* Current protocols in molecular biology, 2000. **51**(1): p. 2.5 A. 1-2.5 A. 9.